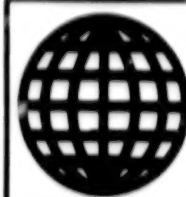


JPRS-UMS-93-001

12 January 1993



FOREIGN
BROADCAST
INFORMATION
SERVICE

JPRS Report—

Science & Technology

***Central Eurasia:
Materials Science***

Science & Technology

Central Eurasia: Materials Science

JPRS-UMS-93-001

CONTENTS

12 January 1993

Analysis, Testing

Physical and Mechanical Properties and Microstructure of Fe-Mo-W Powder Master Alloy [P. N. Ostrik, M. M. Gasik, et al.; <i>IZVESTIYA VYSSHIKH UCHEBNYKH ZAVEDENIY: CHERNAYA METALLURGIYA</i> , No 6, Jun 92]	1
Composition and Physical-Mechanical Properties of Silicon Fly Ash From Ferroalloy Production [G. V. Galevskiy, V. V. Rudneva, et al.; <i>IZVESTIYA VYSSHIKH UCHEBNYKH ZAVEDENIY: CHERNAYA METALLURGIYA</i> , No 6, Jun 92]	1
Crack Resistance of Heat-Treated High-Speed and Tool Steels [V. I. Petrov, V. A. Kuznetsova, et al.; <i>IZVESTIYA VYSSHIKH UCHEBNYKH ZAVEDENIY: CHERNAYA METALLURGIYA</i> , No 6, Jun 92]	1
Dynamics of Atoms in Rapidly Quenched Nb- ⁵⁷ Fe Alloy Formed During Laser Melting [M. M. Nishchenko; <i>METALLOFIZIKA</i> , Vol 14 No 5, May 92]	1
Roentgenographic Studies of Surface Relief and Structural Defects of Thin Surface Layers of Single Crystals [I. M. Fodchuk, O. S. Kshevetskiy; <i>METALLOFIZIKA</i> , Vol 14 No 5, May 92]	2
Substructure of Single Crystals of the W-Ta System and Their Microhardness [I. K. Zasimchuk, V. B. Kiselev, et al.; <i>METALLOFIZIKA</i> , Vol 14 No 5, May 92]	2
The Electric Conduction, Heat Resistance, and Temperature Coefficient of Linear Expansion of Dispersion-Strengthened Cu-Y-Mo Materials. Communication 2 [B.A. Movchan, N.I. Grechanyuk, et al.; <i>PROBLEMY SPETSIALNOY ELEKTROMETALLURGII</i> , No 1, Jan-Feb-Mar 92]	2
Radiation Resistance of Condensed Dispersion-Strengthened Cu-Y-Mo Materials. Communication 3 [B.A. Movchan, S.A. Fabritsiyev, et al.; <i>PROBLEMY SPETSIALNOY ELEKTROMETALLURGII</i> , No 1, Jan-Feb-Mar 92]	3
Diagnosis of Wear and Fracture of Cutting Tool Made of Polycrystalline Superhard Materials [N.V. Novikov, L.N. Devin, et al.; <i>TEKHNICHESKAYA DIAGNOSTIKA I NERAZRUSHAYUSHCHIY KONTROL</i> , No 3, Jul-Aug 92]	3
Auxiliary Materials for Diagnostic Testing of Pipelines and Other Welded Structures [A.S. Leshchenko; <i>TEKHNICHESKAYA DIAGNOSTIKA I NERAZRUSHAYUSHCHIY KONTROL</i> , No 3, Jul-Aug 92]	3
Inspection of Particles in Hot Gas Jet by Acoustic Emission Method [V.V. Vaynberg, M.M. Shpiner; <i>TEKHNICHESKAYA DIAGNOSTIKA I NERAZRUSHAYUSHCHIY KONTROL</i> , No 3, Jul-Aug 92]	4
Amplification of Shock Wave in Condensed Medium Under Explosion Load [A.V. Attetkov, V.V. Lazarev, et al.; <i>PROBLEMY PROCHNOSTI</i> , No 8, Aug 92]	4
Low-Temperature Strength of Welded Structural-Steel Joints After Impact Loading [G.N. Nadezhdin, S.N. Smirnova, et al.; <i>PROBLEMY PROCHNOSTI</i> , No 8, Aug 92]	5
Resistance of Perforated Plates to Cracking Due to Interaction of Holes With Jagged Contours [Yu.A. Vedernikov, I.D. Suzdalnitskiy; <i>PROBLEMY PROCHNOSTI</i> , No 8, Aug 92]	5
Fracture of Brittle Plate Upon Collision With Plastic Striker [A.I. Sadyrin; <i>PROBLEMY PROCHNOSTI</i> , No 8, Aug 92]	5
Penetration of Thin Plate Into Metal Strip at High Velocity [G.G. Savenkov; <i>PROBLEMY PROCHNOSTI</i> , No 8, Aug 92]	6
Pressure Distribution Over Contact Surface After Impact of Deformable Cylinder Against Rigid Barrier [Yu.A. Yemelyanov, A.I. Kozachuk, et al.; <i>PROBLEMY PROCHNOSTI</i> , No 8, Aug 92]	6
Review of Monograph "Strength of Cryoengineering Alloys Under Electromagnetic Action" by V.A. Strizhalo, L.S. Novogradskiy, and Ye.V. Vorobyeva [O.A. Troitskiy; <i>PROBLEMY PROCHNOSTI</i> , No 8, Aug 92]	6
Dynamic Strength and Crack Resistance of Cryogenic Alloys [V. V. Naumenko and A. V. Shiyani; <i>PROBLEMY PROCHNOSTI</i> , No 9, Sep 92]	7
Estimating the Survivability of a Coupling Bolt in a Gas Turbine [V. M. Stepkov and V. T. Krangach; <i>PROBLEMY PROCHNOSTI</i> , No 9, Sep 92]	7
Relationships Between Temperature and the Elastic Properties of Capacitor-Grade Ceramics [V. A. Borisenko and A. I. Troyanskiy; <i>PROBLEMY PROCHNOSTI</i> , No 9, Sep 1992]	8

Domain Structure and Hysteretic Properties of Fine-Grain High-Anisotropy Rare Earth Magnetic Alloys [N.A. Manakov, G.F. Korzinnikova, et al.; <i>FIZIKA METALLOV I METALLOVEDENIYE</i> , No 2, Feb 92]	8
Temperature and Electromagnetic Wave Amplitude Relaxation in Tungsten Under Static Skin Effect Conditions [A.B. Rinkevich; <i>FIZIKA METALLOV I METALLOVEDENIYE</i> , No 2, Feb 92]	8

Coatings

Electron Microscope Studies of Sputtered Niobium Films [J. D. Voytovich, V. A. Lobodyuk, et al.; <i>METALLY</i> , No 3, May-Jun 92]	10
Wear Resistance of Titanium Nitride Coating Deposited by the PVD Method on the Surface of Low-Alloy Steel Subjected to Plasma Nitriding [T. Bell, Y. Sun; <i>METALLY</i> , No 3, May-Jun 92]	10
The Protective Properties of Co-Cr-Al-Y Coatings [Yu.G. Veksler, O.V. Repina, et al.; <i>PROBLEMY SPETSIALNOY ELEKTROMETALLURGII</i> , No 1, Jan-Feb-Mar 92]	10
Absorption of Electromagnetic Radiation by a Layer of Adsorbed Molecules [A. F. Zhuravlev, V. Z. Lozovskiy, et al.; <i>UKRAINSKIY FIZICHESKIY ZHURNAL</i> , Vol 37 No 8, Aug 92]	10
Vacuum-Plasma Coating Apparatus [A.N. Doroshenko; <i>TYAZHELOYE MASHINOSTROYENIYE</i> , No 7, Jul 92]	11
Inspection of Galvanic Nickel Coatings by Magnetomechanical Method of Acoustic Emission [S.A. Novikov, G.I. Khilko; <i>TEKHNICHESKAYA DIAGNOSTIKA I NERAZRUSHAYUSHCHIY KONTROL</i> , No 3, Jul-Aug 92]	11
Optimizing the Composition of Deposited Metal and Parameters of Wear-Resistant Buildup Techniques [L. S. Livshits, O. Yu. Yelagina; <i>SVAROCHNOYE PROIZVODSTVO</i> , No 8, Aug 92]	11
Laser Technology for Imparting Tribotechnical Characteristics to Friction Surfaces [V. S. Avanesov; <i>SVAROCHNOYE PROIZVODSTVO</i> , No 8, Aug 92]	12
Modification of the Surface Layer of Parts by Micro-Arc Oxidation [V. A. Fedorov; <i>SVAROCHNOYE PROIZVODSTVO</i> , No 8, Aug 92]	12
Wear Resistance of Coatings Based on Metalide Alloys [V. A. Neuymin, S. A. Shelukha, et al.; <i>SVAROCHNOYE PROIZVODSTVO</i> , No 8, Aug 92]	12
Effect of Annealing and Ion Bombardment on Hydrogen Content and Properties of Adamantine Films [S.M. Klotsman, S.A. Plotnikov, et al.; <i>FIZIKA I KHIMIYA OBRABOTKI MATERIALOV</i> , No 5, Sep-Oct 92]	13
Effect of Ion-Plasma Rhenium Coating on Mechanical Properties of Molybdenum Wire [A.G. Kolmakov, V.F. Terentyev, et al.; <i>FIZIKA I KHIMIYA OBRABOTKI MATERIALOV</i> , No 5, Sep-Oct 92]	13
Plasma Chemical Deposition of Colored Coats on Polymer and Inorganic Materials [V.F. Sokolov, Yu.A. Sokolova, et al.; <i>FIZIKA I KHIMIYA OBRABOTKI MATERIALOV</i> , No 5, Sep-Oct 92]	13
Ni-Based Alloy Powders With Laves Phases for Gas Thermal Spraying [J.N. Gorbatov, L.K. Shvedova, et al.; <i>FIZIKA I KHIMIYA OBRABOTKI MATERIALOV</i> , No 5, Sep-Oct 92]	14
Composite Structure and Properties Under Laser Modification of Plasma-Sprayed Coats on Powder Materials [A.M. Shmakov, N.N. Ivshina; <i>FIZIKA I KHIMIYA OBRABOTKI MATERIALOV</i> , No 5, Sep-Oct 92]	14
Damage Probability Assessment for Enamel-Coated Chemical Reactors [V. M. Plastinin; Kiev <i>PROBLEMY PROCHNOSTI</i> No 9, Sep 1992]	14
Structure and Electric Properties of Ag-W Films in Metastable States [B.F. Bashev, F.F. Dotsenko, et al.; <i>FIZIKA METALLOV I METALLOVEDENIYE</i> , No 2, Feb 92]	15

Composite Materials

High-Temperature Metal-Matrix Composite [O. A. Bannykh, K. B. Povarova, et al.; <i>METALLY</i> , No 3, May-Jun 92]	16
Changes in the Structure of Polyphosphazene Film Under Biaxial Tension [A.Kh. Kurzennieks, V.M. Parfeyev, et al.; <i>MEKHANIKA KOMPOZITNYKH MATERIALOV</i> , No 4, Jul-Aug 92]	16
The Rational Design of Curved Cross-Ply Fiberglass-Reinforced Plastic Pipes [G.P. Zaytsev, V.N. Tyshevich; <i>MEKHANIKA KOMPOZITNYKH MATERIALOV</i> , No 4, Jul-Aug 92]	16

Laser Interferometry Investigation of the Size Stability of Graphite-Epoxy Resin Composite [Zh. Zhelkobayev, S.S. Sobolev, et al.; MEKHANIKA KOMPOZITNYKH MATERIALOV, No 4, Jul-Aug 92]	16
Forecasting the Life of Hot-Pressed Ceramic Nozzles of Closed-Drift Thrusters by Comprehensive Nondestructive Tests [Ya.I. Bulbik; MEKHANIKA KOMPOZITNYKH MATERIALOV, No 4, Jul-Aug 92]	17
Flash Nondestructive Testing of Materials' Thermophysical Characteristics [O.Yu. Troitskiy; MEKHANIKA KOMPOZITNYKH MATERIALOV, No 4, Jul-Aug 92]	17
Casting of Aluminum Composites With Crystallization Under Pressure [N.N. Belousov; LITEYNOYE PROIZVODSTVO, No 6, Jun 92]	18
Producing Cast Composites With Metal Base [V.G. Borisov; LITEYNOYE PROIZVODSTVO, No 6, Jun 92]	18
Predicting Ultimate Strength of Unidirectionally Oriented Composite Material by Acoustic Emission [Ye.S. Pereverzey, D.G. Borshchevskaya, et al.; TEKHNICHESKAYA DIAGNOSTIKA I NERAZRUSHAYUSHCHIY KONTROL, No 3, Jul-Aug 92]	18
High-Temperature Kinetic Properties of the Contact Zones in Explosive-Welded Titanium-Based Bimetals [I. G. Korshchunov; TEPLOFIZIKA VYSOKIKH TEMPERATUR, Vol 30 No 5, Sep-Oct 92]	19
Physical Properties of Zirconium-Barium Titanate-Lead/Nickel Ferrite Composite Ceramic [V. M. Laletin; PISMA V ZHURNAL TEKHNICHESKOY FIZIKI, Vol 18 No 15, 12 Aug 92]	19
Effects of Radiation on the Physical Properties of Ferrite-Piezoelectric Composite Ceramics [N. F. Kurilovich, V. M. Laletin, et al.; PISMA V ZHURNAL TEKHNICHESKOY FIZIKI, Vol 18 No 15, 12 Aug 92]	20
Thermoelectric Materials for Temperatures Below 150 K [V. A. Kutasov, M. V. Vedernikov, et al.; PISMA V ZHURNAL TEKHNICHESKOY FIZIKI, Vol 18 No 15, 12 Aug 92]	20
The Physicochemical Basis of Creating Composite Ceramic Materials Based on Refractor Compounds [S.S. Ordanyan; OGNEUPORY, No 9-10, Sep-Oct 92]	20

Ferrous Metals

Failure of Carbon Tool Steel During Heat Treatment [V. S. Starikov; IZVESTIYA VYSSHIKH UCHEBNYKH ZAVEDENIY: CHERNAYA METALLURGIYA, No 6, Jun 92]	22
Formation of and Adsorbed Impurity Film at Its Boundary With a Fine Solid Solution Layer [E. L. Feldman, T. N. Fursov, et al.; METALLOFIZIKA, Vol 14 No 4, Apr 92]	22
Characteristics of Martensitic Transformation and the Shape Memory Effect on TiNi Alloys Microalloyed With Cr and Cu [V. A. Lobodyuk and M. M. Medyukh; METALLOFIZIKA, Vol 14 No 4, Apr 92]	22
Studying the Effect of the Cooling Rate on the Structure of Chromium Alloys With Zirconium Carbide [V. G. Ivanchenko, V. V. Pogorelaya, et al.; METALLOFIZIKA Vol 14, No 4, Apr 92]	23
Effect of the Composition of Amorphous Iron and Cobalt-Based Metal Alloys on Their Electron Structure [V. L. Karbovskiy, A. P. Shpak, et al.; METALLOFIZIKA Vol 14, No 4, Apr 92]	23
Effect of Annealed VT16 Titanium Alloy Structure on Its Resistance to Brittle Failure and Toughness Reserve [O. M. Ivasishin, P. Ye. Markovskiy, et al.; METALLOFIZIKA Vol 14, No 4, Apr 92]	23
Properties of and Possible Applications for Superferritic Steel EP882 [S.P. Tomina, V.I. Gerasimov, et al.; TYAZHELOYE MASHINOSTROYENIYE, No 7, Jul 92]	24
Effect of Spheroidizing Modification on Mechanical Properties of Cast Irons With Spheroidal Graphite [G.A. Kosnikov, E.N. Korniyenko, et al.; LITEYNOYE PROIZVODSTVO, No 6, Jun 92]	24
On Steel-Hydrogen Interaction Mechanisms at High Temperatures and Pressures [M.I. Kaplan; METALLY, No 5, Sep-Oct 92]	24
On Cerium's Gaseous Hydrogen Removal Ability in Liquid Fe-C Melts [L.P. Vladimirov, T.G. Sabiryanov, et al.; METALLY, No 5, Sep-Oct 92]	25

Nonferrous Metals, Alloys, Brazes, Solders

Phase Transitions in Reduction of Magnesioferrous Ilmenites [N. I. Talmud, M. S. Model, et al.; METALLY, No 3, May-Jun 92]	26
Mechanism of Formation of Titanium Carbide in the Process of Carbothermic Reduction of Titanium Dioxide [V. D. Lyubimov, T. A. Timoshchuk, et al.; METALLY, No 3, May-Jun 92]	26
Aluminum-Lithium Alloys for Aircraft Weldments [I. N. Fridlyander, A. G. Bratukhin, et al.; METALLY, No 3, May-Jun 92]	26

Structure and Properties of the Aluminum-Lithium Alloy 1430 [F. M. Yelkin, N. A. Naryshkina, et al.; METALLY, No 3, May-Jun 92]	26
Carbide Phase Stability in Ni-Nb-Cr-C System Alloys [O.M. Barabash, I.V. Burya, et al.; METALLY, No 5, Sep-Oct 92]	26
Fusibility Diagram of Mn-Cu-C System [Yu.A. Kocherzhinskiy, O.G. Kulik; METALLY, No 5, Sep-Oct 92]	27
Effect of Crystal Phase Structure on Y, Sm-Li-Ga Constitution Diagram [Yu.N. Grin, A.A. Fedorchuk; METALLY, No 5, Sep-Oct 92]	27
On Interaction Patterns in $YB_6-Me^{IV-VI}B_2$ Systems [S.S. Ordanyan, Ye.Ye. Nikolayeva, et al.; METALLY, No 5, Sep-Oct 92]	27
Cu- and Fe-Doping of $Cu_{2-x}Se$ Alloys [M.A. Korzhuyev, V.F. Bankina; FIZIKA I KHIKIYA OBRABOTKI MATERIALOV, No 5, Sep-Oct 92]	27
On Relation Between α_1 - and α_2 -Phase Precipitate Morphology and Hysteresis Loop Shape in BCC Fe-Cr-Co-Mo Alloy Singles Crystals [B.Ye. Vintaykin, V.A. Golikov, et al.; FIZIKA METALLOV I METALLOVEDENIYE, No 3, Mar 92]	28
Grain Boundary Current Carrier Scattering in Thin Ti-Group Metal Films [B.L. Melnichuk, Z.V. Stasyuk; FIZIKA METALLOV I METALLOVEDENIYE, No 3, Mar 92]	28
Van Vleck Paramagnetism Anomaly in Ti-Fe Alloy Electron Phase Transition Area [A.S. Shcherbakov, N.I. Kourov, et al.; FIZIKA METALLOV I METALLOVEDENIYE, No 3, Mar 92]	28
Dissipative Acoustic Nonlinearity of Copper [S.V. Zimenkov, V.Ye. Nazarov; FIZIKA METALLOV I METALLOVEDENIYE, No 3, Mar 92]	29
Ti Diffusion in Zr-H and Zr-D Alloys [I.O. Bashkin, Ye.I. Rabkin, et al.; FIZIKA METALLOV I METALLOVEDENIYE, No 3, Mar 92]	29
Interdiffusion in Ti-Nb-Zr System [V.I. Gryzunov, G. Omashova, et al.; FIZIKA METALLOV I METALLOVEDENIYE, No 3, Mar 92]	29
Effect of Small Sc and Mg Additions on Al-Li-Cu-Zr Alloy Structure and Properties Under Natural Aging [L.I. Kaygorodova, A.M. Drits, et al.; FIZIKA METALLOV I METALLOVEDENIYE, No 3, Mar 92]	30
Effect of Small Mg and Sc Additions on Al-Li-Cu-Zr Alloy Structure and Properties Under Artificial Aging [L.I. Kaygorodova, A.M. Drits, et al.; FIZIKA METALLOV I METALLOVEDENIYE, No 3, Mar 92]	30
BCC—FCC and FCC—BCC Transformations in Steel 60N21 Under Pressure [D.I. Tupitsa, A.N. Borychev, et al.; FIZIKA METALLOV I METALLOVEDENIYE, No 3, Mar 92]	30
Acoustic Emission in Ti at Low Temperatures [P.I. Stoyev, I.I. Papirov; FIZIKA METALLOV I METALLOVEDENIYE, No 3, Mar 92]	31
Steel 08G2S Wire Structure and Properties After Electrostimulated Drawing [V.Ye. Gromov, V.I. Danilov, et al.; FIZIKA METALLOV I METALLOVEDENIYE, No 3, Mar 92]	31
Strain Hardening Characteristics of Cast Porous Aluminum Alloys [A.A. Yemelyanov, I.P. Konakova, et al.; FIZIKA METALLOV I METALLOVEDENIYE, No 3, Mar 92]	31

Nonmetallic Materials

Experience in Design of Ceramic Runner for Radial-Axial-Flow Turbocompressor Turbine [A.Ye. Ginzburg, M.I. Gorbatshevich; TYAZHELOYE MASHINOSTROYENIYE, No 7, Jul 92]	33
Load-Bearing Capacity and Rigidity of Efficient Lightweight Prestressed Concrete Roof Slabs for Industrial Buildings [K. I. Vilkov, N. A. Kornev; BETON I ZHELEZOBETON, No 8, Aug 92]	33
Peculiarities of Nonlinear Strain of Concrete at High Compressive Stress Levels in a Complex Stressed State [A. P. Kirillov, A. L. Kukush, et al.; BETON I ZHELEZOBETON, No 8, Aug 92]	33
Internal Corrosion of Concrete [F. M. Ivanov; BETON I ZHELEZOBETON, No 8, Aug 92]	33
Principles for Calculation of the Fire-Resistance Limit of Polymer-Impregnated Reinforced Concrete Structures [V. S. Fedorov; BETON I ZHELEZOBETON, No 8, Aug 92]	34
Cost Effectiveness of Lightweight Concretes [Yu. A. Rogatin, N. A. Aleksandrova, et al.; BETON I ZHELEZOBETON, No 8, Aug 92]	34
Phase Transitions in Al_2O_3 Ceramic, Sintered Under Effect of Microwave Radiation [N.G. Varenova, L.K. Kuznetsov, et al.; FIZIKA I KHIKIYA OBRABOTKI MATERIALOV, No 5, Sep-Oct 92]	34
Theory of the Heat Treatment of Refractories Based on a Resin Binder [P.I. Sham, S.A. Nagornyy, et al.; OGNEUPORY, No 9-10, Sep-Oct 92]	34

Refractory Products for Units To Produce Amorphous Metals and Alloys [I.E. Aleksandrov, T.I. Litovskaya, et al.; OGNEUPORY, No 9-10, Sep-Oct 92]	35
Regulating the Crystallization of a Casting of Baddeleyite-Corundum Products [V.A. Naumenko, N.P. Talakuyev, et al.; OGNEUPORY, No 9-10, Sep-Oct 92]	35
Use of the Method of Induction Melting for Preliminary Synthesis of an Oxide Ceramic in the System ZrO ₂ -Y ₂ O ₃ -Al ₂ O ₃ [V.I. Gutman, A.G. Reznikov, et al.; OGNEUPORY, No 9-10, Sep-Oct 92]	36
The Selection of Refractory Mixtures for Coating the Lining of Ingot Molds' Feedheads [M.Ya. Zavadskiy, A.Yu. Konoplyanik, et al.; OGNEUPORY, No 9-10, Sep-Oct 92]	36

Preparations

Studying the Thermophysical Interaction Between Steel Strip and the Molten Steel in a Continuous Casting Mold [N. I. Revtov, O. B. Isayev, et al.; Moscow IZVESTIYA VYSSHIKH UCHEBNYKH ZAVEDENIY: CHERNAYA METALLURGIYA No 6, Jun 92]	37
The Role of Surface Phenomena in the Removal of Nonmetal Inclusions in the Process of Electroslag Alloying of Metal [V.N. Radchenko; PROBLEMY SPETSIALNOY ELEKTROMETALLURGII, No 1, Jan-Feb-Mar 92]	37
Methods of Producing Nickel Superalloys With Improved Technological Properties [Al.G. Shalimov, Yu.Ya. Reznik, et al.; PROBLEMY SPETSIALNOY ELEKTROMETALLURGII, No 1, Jan-Feb-Mar 92]	38
A Furnace for Pressure Arc-Slag Remelting of Ingots Weighing Up to 5 Tons [B.Ye. Paton, B.I. Medovar, et al.; PROBLEMY SPETSIALNOY ELEKTROMETALLURGII, No 1, Jan-Feb-Mar 92]	38
Magnesium-Phosphate Self-Hardening Sands [S. I. Rivkin, Ye. N. Yurginson, et al.; LITEYNAYE PROIZVODSTVO, No 6, Jun 92]	38
Quality of Sand From Tolmachevo Evaluated [Yu. F. Borovskiy, I. V. Shergin, et al.; LITEYNAYE PROIZVODSTVO, No 6, Jun 92]	39
Making Casting Molds Using Vibration Methods [A. A. Brechko, A. V. Sokolov; LITEYNAYE PROIZVODSTVO, No 6, Jun 92]	39
Casting of Aluminum-Based Composites With Crystallization Under Pressure [N. N. Belousov; LITEYNAYE PROIZVODSTVO, No 6, Jun 92]	39
Making Castings of Metal-Base Composites [V. G. Borisov; LITEYNAYE PROIZVODSTVO, No 6, Jun 92]	40
Ceramic Molds for Relief Surface Castings [F. D. Obolentsev, Yu. A. Kaplunovskiy, et al.; LITEYNAYE PROIZVODSTVO, No 6, Jun 92]	40
Combined Method of Manufacturing Gas Turbine Rings [A. G. Kovalev, A. N. Lemeshko, et al.; LITEYNAYE PROIZVODSTVO, No 6, Jun 92]	40
Synthesis of Multicomponent Casting Alloys [B.B. Gulyayev, Yu. Yu. Zaplatkin; LITEYNAYE PROIZVODSTVO, No 6, Jun 92]	40
Chemical Micrononhomogeneity in Casting Alloys [G.P. Anastasiadi; LITEYNAYE PROIZVODSTVO, No 6, Jun 92]	41
Compound Method of Producing Yokes for Gas Turbines [A.G. Kovalev, A.N. Lemeshko, et al.; LITEYNAYE PROIZVODSTVO, No 6, Jun 92]	41
Applying Catastrophic Failure Theory to Quality Control of Castings [M.A. Yoffe; LITEYNAYE PROIZVODSTVO, No 6, Jun 92]	41
Statistical Models of Production of Low-Porosity Bronze Castings [A.A. Papirovsykiy, G.F. Shemetov; LITEYNAYE PROIZVODSTVO, No 6, Jun 92]	42
Magnetic Properties of Steel 45G17Yu3 Surface Layer After Quenching [V.A. Zavalishin, A.I. Deryagin, et al.; FIZIKA METALLOV I METALLOVEDENIYE, No 2, Feb 92]	42
Effect of Straining on Mechanical Properties of Two-Phase Austenitic-Martensitic Steel [V.G. Serebryakov, E.I. Estrin; FIZIKA METALLOV I METALLOVEDENIYE, No 2, Feb 92]	42
Development of Strength Properties of Ordered Alloys [V.I. Syutkina, A.Yu. Volkov; FIZIKA METALLOV I METALLOVEDENIYE, No 2, Feb 92]	43
Effect of Pressure on Brittle—Ductile Transition and Ductility of Metals With BCC Lattice [R.V. Churbayev, A.V. Dobromyslov, et al.; FIZIKA METALLOV I METALLOVEDENIYE, No 2, Feb 92]	43

Treatments

Effect of Alloying on Phase Transitions in Steels With Pearlite Structure During Laser Heating [D. V. Shtanskiy, I. V. Lyasotskiy; METALLY, No 3, May-Jun 92]	44
--	----

Effect of Temperature on Erosion of Metals Exposed to a Laser Beam <i>[A. Ye. Chmel, A. M. Kondyrev; METALLY, No 3, May-Jun 92]</i>	44
Effect of Heat Treatment on the Structure of Beryllium Foils <i>[V. P. Krivko, Yu. I. Kokovikhin, et al.; METALLY, No 3, May-Jun 92]</i>	44
Mathematical Model of a Multi-Stand Cold-Rolling Mill for Controlling Strip Thickness <i>[B. I. Kuznetsov, R. Koziol, et al.; IZVESTIYA VYSSHIKH UCHEBNYKH ZAVEDENIY: CHERNAYA METALLURGIYA, No 6, Jun 92]</i>	44
Predicting the Effect of Titanium, Aluminum, and Nitrogen on the Hardenability of Medium Carbon Steels Containing Boron <i>[V. V. Popov, A. O. Khomenko, et al.; Moscow IZVESTIYA VYSSHIKH UCHEBNYKH ZAVEDENIY: CHERNAYA METALLURGIYA No 6, Jun 92]</i>	44
Hydrogen Permeability Change in Steel 12Kh18N10T After Nitriding, Oxidation, and H ⁺ and N ⁺ Ion Irradiation <i>[V.V. Fedorov, V.I. Pokhmurskiy, et al.; FIZIKA I KHIMIYA OBRABOTKI MATERIALOV, No 5, Sep-Oct 92]</i>	45
Effect of Pulsed Laser Radiation on V-Ti Alloys <i>[S.A. Maslyayev, V.I. Neverov, et al.; FIZIKA I KHIMIYA OBRABOTKI MATERIALOV, No 5, Sep-Oct 92]</i>	45
Effect of Heating Rate on Thermal Stress Development in Silicon Wafer Under Rapid Annealing <i>[D.A. Sechenov, A.M. Svetlichnyy, et al.; FIZIKA I KHIMIYA OBRABOTKI MATERIALOV, No 5, Sep-Oct 92]</i>	46
Properties and Uses of UF ₆ Plasma: IV. UF ₆ Conversion Mechanism and Kinetics in U-F-O-H Plasma <i>[Yu.N. Tumanov, K.V. Tsirelnikov; FIZIKA I KHIMIYA OBRABOTKI MATERIALOV, No 5, Sep-Oct 92]</i>	46
Properties and Uses of UF ₆ Plasma: V. Uranium Reduction Mechanism and Kinetics During UF ₆ Mixing With Hydrogen Plasma <i>[Yu.N. Tumanov, K.V. Tsirelnikov; FIZIKA I KHIMIYA OBRABOTKI MATERIALOV, No 5, Sep-Oct 92]</i>	46

Welding, Brazing, Soldering

Nitrogen-Niobium Interaction in Molten Steel During Plasma-Arc Welding <i>[B. L. Bozhenko, V. N. Shalimov, et al.; METALLY, No 3, May-Jun 92]</i>	47
Computer Simulation in Determining Weldability and Selecting Welding Parameters for Steels and Alloys <i>[A. N. Khakimov; SVAROCHNOYE PROIZVODSTVO, No 8, Aug 92]</i>	47
Resistance of Gas Mains to Propagation of Extended Continuous Fractures <i>[G. I. Makarov; SVAROCHNOYE PROIZVODSTVO, No 8, Aug 92]</i>	47
Higher Durability for Large Welded Metalwork Subject to Corrosive Environments of the Oil and Gas Industry <i>[A. I. Korolev, A. V. Muradov; SVAROCHNOYE PROIZVODSTVO, No 8, Aug 92]</i>	47
Effect of Laser Treatment on Corrosion Resistance of Steels and Welds <i>[R. D. Radchenko; SVAROCHNOYE PROIZVODSTVO, No 8, Aug 92]</i>	48
Optimization of Composition of Weld Metal in Arc Welding of 10Kh2M1A-A Steel <i>[Zh. A. Lepilina, V. V. Pankov, et al.; SVAROCHNOYE PROIZVODSTVO, No 9, Sep 92]</i>	48
Calculating Penetration Depth in Electroslag Buildup <i>[V. A. Danilov, G. G. Chernyshov; SVAROCHNOYE PROIZVODSTVO, No 9, Sep 92]</i>	48
Hydrogen in Metal of Thick-Walled Weldments. Part I. Hydrogen Cracks in Thick-Walled Weldments <i>[V. I. Panov; SVAROCHNOYE PROIZVODSTVO, No 9, Sep 92]</i>	48
Corrosion Cracking of Welds in Low-Carbon Steels in Phosphate Media <i>[Y. Marcheva, R. Raychev; SVAROCHNOYE PROIZVODSTVO, No 9, Sep 92]</i>	49
Electric Welding Where Work Is Affected by Industrial Magnetic Fields <i>[N. Z. Nevlyutov; SVAROCHNOYE PROIZVODSTVO, No 9, Sep 92]</i>	49
Determining Stress Concentration Factors in a Cracked Weld <i>[N. V. Korikhin, S. N. Egenson, et al.; Kiev PROBLEMY PROCHNOSTI No 9, Sep 1992]</i>	49

Extractive Metallurgy, Mining

Self-Destruction Causes and Heat Treatment Conditions Ensuring Lumpy Nature Preservation of Manganese Carbonate Concentrates <i>[N.P. Lyakishev, M.I. Gasik, et al.; METALLY, No 5, Sep-Oct 92]</i>	50
Effect of Ore Genesis on Roasting Conditions and Quality of Fluxed Pellets <i>[O.A. Dolitskaya, G.V. Chesnokova, et al.; METALLY, No 5, Sep-Oct 92]</i>	50

Phase Transformation During Titanomagnetite Reduction With Hydrogen <i>[G.B. Sadykhov, L.O. Naumova, et al.; METALLY, No 5, Sep-Oct 92]</i>	50
Low-Iron Bauxites of the Vezhayu-Vorykvenskoye Deposit <i>[N.S. Gayenko, S.G. Dolgikh, et al.; OGNEUPORY, No 9-10, Sep-Oct 92]</i>	51

Miscellaneous

Principal Radiation Characteristics of Materials of Dust Emission Particles from Waste-Heat Boilers <i>[M.A. Taymarov; TYAZHELOYE MASHINOSTROYENIYE, No 7, Jul 92]</i>	52
TsKTI (Central Boiler and Turbine Institute) Damper Ensuring High Earthquake and Vibration Resistance of Equipment and Pipelines <i>[V.V. Kostarev, D.Yu. Pavlov; TYAZHELOYE MASHINOSTROYENIYE, No 7, Jul 92]</i>	52
Laser Simulation of Radiation-Induced Single Event Upsets in Integrated Circuits <i>[A.I. Akishin, E.A. Vitoshkin, et al.; FIZIKA I KHIMIYA OBRABOTKI MATERIALOV, No 5, Sep-Oct 92]</i>	52

Physical and Mechanical Properties and Microstructure of Fe-Mo-W Powder Master Alloy

927D0259A Moscow IZVESTIYA VYSSHIKH UCHEBNYKH ZAVEDENIY: CHERNAYA METALLURGIYA in Russian No 6, Jun 1992 pp 7-10

[Article by P. N. Ostrik, M. M. Gasik, and L. N. Gasik, Dnepropetrov Metallurgical Institute; UDC 669.15'28:621.762.242]

[Abstract] The granulometric composition, microstructure, and distribution of iron, molybdenum, and tungsten were studied in powder Fe—60 percent Mo—5 percent W master alloy. The alloy was produced by the hydrogen reduction of a mixture of MoO_3 and WO_3 oxides and water-atomized iron powder. The bulk density was $1.4 \pm 0.1 \text{ g/cm}^3$, which is close to that of reduced Mo powders. The particles were sponge-shaped despite the presence of spherical iron particles in the starting mixture. Granulometric composition was studied conductimetrically using a Coulter TA-II in Isoton-II electrolyte after 30 seconds of ultrasound treatment of an alloy sample suspension with Nonarox additive. There was a close correspondence between particle distribution by size and the Rosen-Rammler formula. The formula was also used to determine the (equivalent) specific surface and volume of an "average" grain ($5.1 \times 10^3 \mu\text{m}^2$ and $51.8 \times 10^3 \mu\text{m}^3$, "average" particle mass $(5.07 \times 10^{-4} \text{ mg}$, and "average" pycnometric density (9.8 g/cm^3) . The alloy powder underwent double-sided compacting at 25 MPa of pressure without a plasticizer. Some of the compacts were sintered at 1473 K for three hours in dry electrolytic hydrogen. X-ray diffraction analysis on a DRON-3.0 revealed the presence of body-centered cubic solid solutions based on molybdenum and iron, as well as the presence of intermetallic compounds. Given the chemical composition and temperature of the phase in question, the iron and tungsten form enriched microzones due to the difference in the partial Gibbs energies for the Fe-Mo and Fe-W interactions in an Mo matrix. When the powder alloy is used, there is greater Mo assimilation than when pure Mo powder is used to make sintered alloy steel articles. Figures 1; references 7: 3 Russian, 4 Western.

Composition and Physical-Mechanical Properties of Silicon Fly Ash From Ferroalloy Production

927D0259B Moscow IZVESTIYA VYSSHIKH UCHEBNYKH ZAVEDENIY: CHERNAYA METALLURGIYA in Russian No 6, Jun 1992 pp 10-12

[Article by G. V. Galevskiy, V. V. Rudneva, and T. V. Kiseleva, Siberian Metallurgical Institute; UDC 669.046:541.123]

[Abstract] Fly ash taken from the flue-gas filters of the ore-smelting furnaces used to produce FS45 and FS65 ferrosilicons at the Kuznets Ferroalloy Plant was analyzed physically and chemically to determine its suitability for utilization in electrothermal processes. X-ray phase analysis, IR spectroscopy, and thermogravimetric

analysis were used to study the phase composition of the ash. Standard methods were used to determine its chemical composition. Specific surface was determined from argon adsorption at the boiling point of liquid nitrogen using specimens "trained" in an inert atmosphere at 383 K to remove sorbed moisture and gasses. A UEMV-100 K electron microscope with an acceleration voltage of 50 kV was used to examine particle morphology. The results showed that the ash consists of predominantly spherical particles of an amorphous silicon of the following composition (wt. percent): 87.45 to 87.98 SiO_2 , 0.18 to 0.20 Si , 1.12 to 1.14 CaO , 0.98 to 1.02 MgO , 1.33 to $1.37 \text{ Al}_2\text{O}_3$, 2.07 to $2.13 \text{ Fe}_2\text{O}_3$, 1.18 to 1.24 C , 0.20 to $0.25 \text{ P}_2\text{O}_5$, and 0.40 to 0.44 MnO . The specific surface of the ash is $20,000$ to $22,000 \text{ sq m/kg}$, and particle size is 1 to $4 \mu\text{m}$. The results of the analysis show that the ash is a potential raw material for a number of electrothermal processes such as the plasma reduction synthesis of silicon carbide, the manufacture of technical enamels, and the production of unpulverized high-dispersity silicon carbide and related products. Figures 3; references 9: Russian.

Crack Resistance of Heat-Treated High-Speed and Tool Steels

927D0259D Moscow IZVESTIYA VYSSHIKH UCHEBNYKH ZAVEDENIY: CHERNAYA METALLURGIYA in Russian No 6, Jun 1992 pp 24-28

[Article by V. I. Petrov, V. A. Kuznetsova, N. A. Chelyshev, and S. L. Semenov, Siberian Metallurgical Institute; UDC 669.14-15:620.1]

[Abstract] The results of a number of recent studies on the effect of various heat-treating procedures on the service properties of different high-speed and tool steels were highlighted. It was concluded that the heat treating temperature must be appropriate for the types of steel used when making tools welded from high-speed and tool steels; that crack resistance parameters can be used as reliability criteria for tools, particularly for determining optimal heat-treating conditions; that the crack resistance of high-speed steels and of the welded joints between high-speed and tool steels depends on grain size, chemical composition, and the nature of heat-treatment; that crack-resistance parameters can be used to evaluate laser heat-treating conditions for U10 steel; that deterioration in hardness occurring after final heat treatment is caused by not heeding the recommended reheating temperatures prior to annealing; and that fractographic examination of crack surfaces can be used to qualitatively determine the effect of a particular heat treatment on the failure process in the fatigue, elongation, and rupture zones. Figures 6; references 6: Russian.

Dynamics of Atoms in Rapidly Quenched $\text{Nb}-^{57}\text{Fe}$ Alloy Formed During Laser Melting

937D0015A Kiev METALLOFIZIKA in Russian Vol 14 No 5, May 92 pp 49-56

[Article by M. M. Nishchenko, Institute of Metal Physics, Ukrainian Academy of Sciences, Kiev; UDC 539.2]

[Abstract] The effect of rapid (10^4 - 10^5 K/s) quenching of Nb- 57 Fe alloy from the molten state after laser melting on the effective Debye temperature and the root-mean-square displacement of atoms in the lattice was investigated. Calculation of these values was accomplished in the Debye approximation according to the temperature (relativistic) shift in the Moessbauer line of the paramagnetic compound NbFe₂. Specimens were obtained by vacuum vapor deposition of a 57 Fe film 0.4 μ thick on the surface of a Nb foil 25 μ thick with subsequent melting of the film and the substrate over the whole surface of the specimen by laser pulses lasting 4 ms. For the compound NbFe₂ formed in a surface layer approximately 1.5 μ thick, the values of the effective Debye temperature and the root-mean-square displacement of atoms were 370 +/- 20 K and 0.13 angstroms, respectively, for rapidly quenched alloy, and 550 +/- 20 K and 0.09 +/- 0.01 angstroms for annealed alloy. The density of s-electrons on the 57 Fe nucleus in the rapidly quenched alloy is lower (line shift 0.05 mm/s) than in the annealed alloy. These changes indicate a weakening of the phonon spectrum in rapid cooling due to a reduction in transfer of 3d-electrons of "paramagnetic" Fe to adjacent atoms and a weakening of the interatomic bond.

Roentgenographic Studies of Surface Relief and Structural Defects of Thin Surface Layers of Single Crystals

937D0015B Kiev METALLOFIZIKA in Russian Vol 14 No 5, May 92 pp 57-61

[Article by I. M. Fodchuk and O. S. Kshevetskiy, Institute of Thermoelectricity, Chernovtsy; UDC 539.21]

[Abstract] Using a Bragg scattering skew-asymmetric diffraction scheme, the surface relief of an InSb/InSb epitaxial structure and a CdTe single crystal after a full cycle of chemical-mechanical and laser treatment was examined. It was determined that at close-to-critical angles of incidence of the X-ray beam, the minimum height of uneven features of the surface profile as determined from topograms is approximately 0.025 μ . The thickness of an amorphous film formed after laser treatment of the surface of CdTe was determined by azimuthal angular scanning around the diffraction vector. The applicability of the given diffraction scheme for examining the structure of thin surface layers of single crystals is demonstrated.

Substructure of Single Crystals of the W-Ta System and Their Microhardness

937D0015C Kiev METALLOFIZIKA in Russian Vol 14 No 5, May 92 pp 77-82

[Article by I. K. Zasimchuk, V. B. Kiselev, L. F. Matviyenko; Institute of Metal Physics, Ukrainian Academy of Sciences, Kiev; UDC 539.53:548.4.55]

[Abstract] The X-ray topography method was used to examine the substructure of single crystals of tungsten and tungsten-tantalum containing 3, 5, 8, and 12 atomic percent tantalum and grown in the <111> direction. The size of subgrains decreased as the tantalum concentration increased to 8 percent at. Ta, and then their size increased somewhat at 11.7-12 percent at. Ta. Angles of disorientation, both integral and among adjacent subgrains, also revealed a minimum at a certain intermediate concentration: 3-5 percent at. Ta for the integral and 8 percent at. Ta for the average among adjacent subgrains. A monotonic increase in microhardness from 3.5 to 4.3 GPa was observed as the Ta concentration increased from 0 to 12 percent at. Mechanisms of the observed changes in structure and properties are discussed.

The Electric Conduction, Heat Resistance, and Temperature Coefficient of Linear Expansion of Dispersion-Strengthened Cu-Y-Mo Materials. Communication 2

937D0016D Kiev PROBLEMY SPETSIALNOY ELEKTROMETALLURGII in Russian No 1, Jan-Feb-Mar 92 (manuscript received 28 Aug 91) pp 57-60

[Article by B.A. Movchan, N.I. Grechanyuk, V.A. Osokin, L.M. Nerodenko, and S.Ye. Litvin, Electric Welding Institute imeni Ye.O. Paton, Ukraine Academy of Sciences, Kiev; UDC 669.187.526.001.5]

[Abstract] A series of comprehensive studies was conducted to determine the structure and properties of dispersion-strengthened Cu-Y-Mo materials. The materials' resistivity (ρ) was determined by the standard four-probe method in a direct current with consideration for the contact difference in potentials. A copper-constantan differential thermocouple was used to record the temperature. The refractory properties of the Cu-Y-Mo materials were determined in creep tests performed in a vacuum at 600°C while a constant stress of 100 MPa was maintained in the specimens. The temperature coefficient of linear expansion (α) was determined on a high-speed dilatometer designed by the Electric Welding Institute imeni Ye.O. Paton. The studies performed established that dispersion-strengthened Cu-Y-Mo materials containing between 0 and 6 percent molybdenum may be classified as materials with a high electric conduction because under normal conditions their resistivity does not exceed $0.1 \times 10^{-6} \Omega\text{-m}$. The heat resistance studies performed demonstrated that dispersion-strengthened Cu-Y-Mo condensates containing 4.2 percent Mo are more durable than both precipitation-hardening alloys and internally oxidized copper-based materials. It was also discovered that, in general, adding precipitation-hardening Mo particles to a Cu-Y matrix alloy results in a decrease in the temperature coefficient of linear expansion of condensed dispersion-strengthened Cu-Y-Mo materials but not in the temperature coefficient of linear expansion of pure copper. Figures 6; references 7: Russian.

Radiation Resistance of Condensed Dispersion-Strengthened Cu-Y-Mo Materials. Communication 3

937D0016E Kiev PROBLEMY SPETSIALNOY ELEKTROMETALLURGII in Russian No 1, Jan-Feb-Mar 92 (manuscript received 28 Aug 91) pp 61-64

[Article by B.A. Movchan, S.A. Fabritsiyev, V.A. Osokin, N.I. Grechanyuk, A.S. Pokrovskiy, and V.R. Barabash, Electric Welding Institute imeni Ye.O. Paton, Prometey TsNIIMKh [not further identified], Saint Petersburg, NIIAR [not further identified], Dimitrovgrad, and NIIIEFA [not further identified], Saint Petersburg; UDC 669.187.526.001.5]

[Abstract] The effect of irradiation in doses of 10^{21} to 10^{22} neutrons/cm² at irradiation temperatures of 350 to 500°C on the strength properties of Cu-Y-Mo dispersion-strengthened materials was compared with that of Cu-Cr-Zr- and MZC-type dispersion-hardening alloys. The study specimens were irradiated in BOR-60 fast reactors and SM-2 reactors with a mixed spectrum. In the BOR-60 reactors, specimens were irradiated in doses up to 0.8×10^{22} , 1.1×10^{22} , and 1.5×10^{22} neutrons/cm² at temperatures of 350, 375, 405, and 420°C. In the mixed-spectrum reactor, specimens were irradiated in doses up to 10^{21} neutrons/cm² at temperatures of 427 and 500°C. After irradiation, the specimens were subjected to tension tests in a vacuum at test temperatures of 20 to 500°C. The swelling of the specimens was estimated based on the change in their density, which was determined by hydrostatic weighing. A Cu-Y-Mo dispersion-strengthened material containing a molybdenum hardening phase in amounts ranging from 4 to 6 percent that was designated DM5 was studied as a representative dispersion-strengthened material. DM5 was found to possess a much higher resistance to radiation-stimulated disordering than did the type MZC alloy tested. After irradiation in the BOR-60 reactor in a dose up to 1.5×10^{22} neutrons/cm² at an irradiation temperature of 420°C, the yield strength of MZC decreased to about 50 MPa while that of DM5 remained at 200 MPa or higher. Metallographic studies established that after irradiation at 420-460°C, the hardening-phase particles in MZC grew much larger (up to tenfold), whereas those in the DM5 remained virtually unchanged. Even under the much harder conditions of irradiation in the SM-2 reactor, which approximated the conditions existing in a thermonuclear reactor, the yield strength of the DM5 remained practically unchanged at irradiation temperatures around 427°C and only decreased by about 100 MPa upon irradiation at a temperature of 500°C. The superior radiation resistance of DM5 was attributed to the fact that its well-developed interface surface is a neutral sink for radiation defects. Figures 4; references 6: 3 Russian, 3 Western.

Diagnosis of Wear and Fracture of Cutting Tool Made of Polycrystalline Superhard Materials

937D0027A Kiev TEKHNICHESKAYA DIAGNOSTIKA I NERAZRUSHAYUSHCHIY KONTROL in Russian No 3, Jul-Aug 92 (manuscript received 12 Mar 91) pp 35-43

[Article by N.V. Novikov, doctor of technical sciences, academician (Ukrainian Academy of Sciences), L.N. Devin, candidate of technical sciences, and O.G. Lysenko, electrical engineer, Institute of Superhard Materials at Ukrainian Academy of Sciences; UDC 620.179:621.9.025]

[Abstract] A new class of superhard materials for cutting tools has been recently developed on the basis of polycrystalline cubic boron nitride (CBN), these material excelling in wear and heat resistance but lacking in adequate stability because of their oversensitivity to changes in the cutting process parameters. In consideration of this problem, the authors have developed an apparatus and a computer program for automatic diagnostic testing of tools during the cutting process by monitoring changes in acoustic emission signals as well as changes in all three x,y,z components of the cutting force components along with changes in the temperature within the cutting zone. All these changes serve as criteria for estimation of tool wear and prediction of tool fracture, the relevant probability indicators such as the Weibull distribution parameters having been established following a dispersion and regression analysis of the readings, analysis of the time series, and digital filtration. This diagnostic testing system was tried out experimentally on cutter plates made of four CBN materials ("kiborit", 051T composite, grade-10 composite, BPC polycrystalline cubic boronitride) cutting Cr15 BB (ball bearing) steel and Cr-W-Mn steel quenched to various degrees of hardness. Special experiments were performed for validating inclusion of the acoustic emission method in the system, acoustic emission signals having, indeed, been recorded during propagation of cracks through a cutter plate held in a vertical impact tester as its cutting edge was struck by a falling weight. The experiments have revealed that most sensitive to imminent fracture is the acoustic emission signal, an increase of its amplitude above some threshold level being the best indicator. The next best indicator of imminent fracture has been found to be the normal component of the cutting force P_z , its magnitude decreasing as fracture becomes imminent. Figures 7; tables 1; references 11

Auxiliary Materials for Diagnostic Testing of Pipelines and Other Welded Structures

937D0027C Kiev TEKHNICHESKAYA DIAGNOSTIKA I NERAZRUSHAYUSHCHIY KONTROL in Russian No 3, Jul-Aug 92 (manuscript received 4 Apr 92) pp 49-53

[Article by A.S. Leshchenko, All-Russian Scientific Petroleum Research Institute, Samara; UDC 534.8.081.7]

[Abstract] A list of 21 special auxiliary materials suitable for diagnostic inspection of welded structures operating under pressure by the acoustic emission method with or without inclusion of the thermoacoustic effect is presented, namely acoustic contact fluids used for loading such structures lightly to far below the nominal operating pressure. They include liquid helium at -268°C, liquid hydrogen at -250°C, liquid nitrogen at -196°C, liquid oxygen at -183°C, liquid argon at -183°C, and liquid methane at -164°C for testing cryogenic devices such as superconductor cables and vessels; liquid pentane at -20°C and liquid carbon tetrachloride at -20°C for testing pipelines and storage tanks in the cold; water (at 4°C), acetone at 20°C, benzene at 20°C, glycerin at 20°C, kerosene at 20°C, and acetic acid at 20°C; methyl, ethyl, and butyl alcohols at 20°C; castor, linseed, olive, and sunflower oils at 15°C. These materials in the solid state, at temperatures ranging from 0°C (water) to -260°C (hydrogen) can be used as mounts for acoustic emission transducers and in either state as sound guides or buffer media for shock waves generated by laser beam so as to enhance both sensitivity and reliability of inspection by the acoustic emission method. Figures 1; references 7.

Inspection of Particles in Hot Gas Jet by Acoustic Emission Method

937D0027E Kiev TEKHNICHESKAYA DIAGNOSTIKA I NERAZRUSHAYUSHCHIY KONTROL in Russian No 3, Jul-Aug 92 (manuscript received 29 Mar 90) pp 64-68

[Article by V.V. Vaynberg, candidate of technical sciences, and M.M. Shpiner, Kishinev Institute of Agriculture imeni M.V. Frunze; UDC 621.791.052.08: 620.170.16]

[Abstract] An experimental study concerning use of acoustic emission for inspection of powder particles of a coating material carried by a hot gas jet was made, the applicability of this inspection method to such a coating process being based on the dependence of the coating characteristics on the solid-gas interactions in the jet as well as on the coating process parameters. While a disk of a to be coated material was struck by the jet, a piezoelectric feeler inserted into the jet perpendicularly generated acoustic emission pulses in response to impact of particles on its surface. A transducer converted these pulses into electric signals, which were passed through a high-frequency channel consisting of a preamplifier, a filter bank, and an attenuator-amplifier to an AF-15 acoustic emission measuring instrument. The first series of tests involved deposition of zinc coatings in an originally designed electric-arc metallizer with an MEZ-500 current source delivering 65 A at 18 V and an air jet nozzle operating at a throat pressure of 0.6 MPa. Zinc wire 2 mm in diameter was fed into it at a rate of 3 mm/min. The feeler, a disk 2 mm in diameter without insulation for "linear" probing, was inserted into the air jet at a 100 mm distance from the electric arc. The acoustic emission measuring AF-15 instrument had been adjusted so that it would not record interference from

both the air jet and the electric arc. The air pressure in the nozzle throat and the wire feed rate as well as the arc current and voltage were held constant, within +/-4 percent maximum deviation limits for each. The readings of both acoustic emission count rate dN/dt and the acoustic emission pulse amplitude A indicated stability of the air jet while the arc was burning. Even then, however, a +/-7 percent wide scatter of dN/dt readings and a +/-17 percent wide scatter of A-readings about their respective averages indicated that both the momentum and the energy of zinc particles passing through a jet cross-section in a unit of time varied even though the process parameters remained constant. This justifies use of both parameters for inspection of particles immediately before their precipitation on the to be coated surface. For the second series of tests a 1 mm thick and 7x18.5 mm² large rectangular copper plate was lap-brazed to the feeler disk at its tip and the distance D from the nozzle throat to the convergence point for the electrodes was varied discretely from 6 mm through 12 mm to 39 mm. These tests were performed with the air jet containing ferroboron powder and with the air jet containing water droplets. The count rate dN/dt was found to decrease linearly with increasing distance D. When the air jet contained solid particles, elastically colliding with the feeler plate, the pulse amplitude A was high and the count rate dN/dt was very low. When the air jet contained liquid particles, inelastically colliding with the feeler plate, the count rate dN/dt was high and the pulse amplitude A was low. Figures 4; references 8.

Amplification of Shock Wave in Condensed Medium Under Explosion Load

937D0044A Kiev PROBLEMY PROCHNOSTI in Russian No 8, Aug 92 pp 3-6

[Article by A.V. Attetkov, V.V. Lazarev, A.Yu. Molyanov, and V.S. Solovyev, Moscow Higher Technical School imeni N.E. Bauman; UDC 539.4]

[Abstract] Configurations of waves in a solid medium loaded by a glancing rather than normally incident detonation wave following an explosion of a charge are analyzed by the method of polar diagrams, with pressure and deflection angle as the independent variables. First is considered direct loading with the explosive charge touching the medium, a shock wave then obliquely propagating through the medium of whatever material and Prandtl-Mayer flow developing in the explosion products. In this case the configuration of explosion decay includes such a shock wave in addition to a Chapman-Jouguet detonation wave and a rarefaction wave, their configuration being influenced by presence of the contact boundary. Next is considered indirect loading through a spacer of a material dynamically softer than the material of the medium. In this "triple-layer" system the configuration of explosion decay also includes an obliquely propagating shock wave in addition to a detonation wave and a rarefaction wave, the contact boundary having been replaced by the point of intersection of the shock polar in the spacer and the

discharge polar in the explosion products. The analysis demonstrates the possibility of shock wave amplification in the affected medium, but only when a spacer is included. This has been confirmed by the response of steel plates to shock waves. Plates of grade-3 carbon steel were tested with 10 mm wide and 8 mm wide rectangular charges of a plastic explosive (density 1.4 g/cm³) and cardboard or plexiglas spacers, detonation waves propagating at a velocity of 7450 m/s. Both plate thickness and spacer thickness were varied, the results revealing a nonmonotonic dependence of the noncracking-threshold plate thickness on the spacer thickness. That threshold thickness was 9.5 mm with either an about 0.28 mm thick cardboard spacer or an about 0.40 mm thick plexiglas spacer, corresponding to maximum shock wave amplification. With spacers thinner than 0.2 mm that threshold was only 8 mm, as in the case of direct-contact loading. With spacers thicker than 0.45 mm that threshold decreased still farther, owing to the damping effect of such spacers. Shock wave amplification thus evidently takes place only upon inclusion of a spacer within a finite range of thickness, in this case 0.20-0.45 mm. Figures 4; references 5.

Low-Temperature Strength of Welded Structural-Steel Joints After Impact Loading
937D0044B Kiev PROBLEMY PROCHNOSTI in Russian No 8, Aug 92 pp 22-26

[Article by G.N. Nadezhdin, S.N. Smirnova, and Yu.I. Fadeenko, Institute of Strength Problems at Ukrainian Academy of Sciences, Kiev; UDC 669.15:539.]

[Abstract] An experimental study of welded 09Mn2Si steel and Cr70 steel joints was made concerning their impact treatment with explosive charge and their strength at temperatures from 373 K down to 77 K after such a dynamic treatment. Tests were performed on Charpy specimens of main-pipe joints with a V-notch only and on such specimens with also a fatigue crack at the tip, after impact treatment with a linearly lumped explosive charge. The purpose object of these tests was to determine the temperature of transition from plane state of strain and ductile fracture to plane state of stress and brittle fracture based on the temperature dependence of the impact values KCV and KCT, of the stress concentration factor as indicator of resistance to dynamic cracking, and of the percentage reduction as indicator of plasticity. The wide spread of data, evidently due to diverse crack propagation patterns revealed by metallographic examination, makes it difficult to precisely evaluate the effect of this treatment on the low-temperature behavior of the joints. They indicate, however, a resulting 10-15°C downward shift of the transition temperature. Figures 6; references 9.

Resistance of Perforated Plates to Cracking Due to Interaction of Holes With Jagged Contours
937D0044C PROBLEMY PROCHNOSTI in Russian No 8, Aug 92 pp 26-30

[Article by Yu.A. Vedernikov and I.D. Suzdalnitskiy, Novosibirsk Institute of Electrical Communication Engineering; UDC 539.3]

[Abstract] The problem of resistance to cracking is tackled for a plate with two identical equilateral curvilinear (cissoid) triangular holes facing each other symmetrically vertex-to-vertex sufficiently close for interaction to occur, this being the simplest special case of a solid body cracking upon its penetration by strikers with polygonal cross-section. The problem is formulated as a two-dimensional axisymmetric one in a Cartesian system of coordinates with the origin O at the center of one hole, the y-axis "parallel" to the curvilinear base of that triangle, and the x-axis passing through the two interacting vertices A,A' to the center O' of the other hole. The boundary conditions along each arm of the contour triangle around the center O are distributed normal stresses and zero tangential stresses, the stress function being the solution to a biharmonic equation appropriate for this configuration. The problem is reduced to a system of four singular integral equations for shearing stress functions $f_{1,2,3,4}(t)$ in the web. The stress distribution in the vicinity of $x = 1$ near the vertex A of the given hole, farthest away from its center O, is described by the expression $\sigma_x = k(x-1)^{1/2}$ and thus with an accuracy down to infinitesimally small terms, the multiplier k being the stress concentration factor proportional to a geometrical factor which is a function of two distances: smallest distance $p = OC$ from the center of the hole to its contour (point C on either of the two arms of the triangular contour) and distance $2H$ between the centers O,O' of the two holes on the x-axis, both normalized to the distance OA from the vertex A to the center O and thus to the largest distance from the center of that hole to its contour. This factor has been evaluated numerically for $p = OC/OA$ ranging from 0.15 to 0.4 and H/OA ranging from 1.2 to 8. It is minimum when $p = 0.35$ with any $2H$, which corresponds to maximum resistance to cracking as a result of stress relief by widening of the hole. This method of calculation and analysis has been extended to an analogous problem of plates with biperiodic arrays of either triangular or hexagonal holes for prediction of their resistance to cracking. Figures 2; tables 1; references 3.

Fracture of Brittle Plate Upon Collision With Plastic Striker
937D0044D Kiev PROBLEMY PROCHNOSTI in Russian No 8, Aug 91 pp 41-45

[Article by A.I. Sadyrin, Nizhnenovgorod State University; UDC 620.178]

[Abstract] Fracture of a brittle plate upon its collision with a cylindroconic elastoplastic striker is analyzed, the problem being formulated as an axisymmetric one in Lagrangian coordinates and solved by numerical simulation according to an explicit scheme of finite differences on triangular grids. As a specific example is considered a 0.8 mm thick disk 3 mm in diameter and a 2.4 cm long striker 0.76 cm in diameter terminating into a conical nose with a 165° vertex angle. The disk is made of a material with a density $\rho = 2.7 \text{ g/cm}^3$, a Young's modulus $E = 210 \text{ GPa}$, and a Poisson's ratio $\nu = 0.32$, a

material which obeys Hooke's law until fracture. The striker is made of a material which behaves in accordance with the differential theory of plasticity with hardening, namely Armco iron with a dynamic yield strength of 0.5 GPa and an ultimate strength varying over the 0.9-2.6 GPa range. Its impact velocity is arbitrarily varied over the 600-800 m/s range. Brittle separation fracture of the plate under tension is regarded as a result of cracking in a plane perpendicular to the direction of maximum tensile stress. Both the stress intensity and the maximum principal stress in the plate, each normalized to a base strength of 2.0 GPa, are calculated in accordance with this model as functions of time: at points on curves extending across the plate from the circular contour of its contact with the striker to its other surface. A strain analysis of such a plate during deformation by impact prior to fracture reveals that first a compression wave forms under the striker and then, as material of the plate moves in the direction of axial striker action, a shear wave forms which produces tensile stresses in the plate. The stress intensity continues to decrease while the maximum principal stress continues to increase during this deformation process until immediately before fracture occurs. An analysis of the stress transients reveals that subsequent fracture appreciably alters the stressed state of the plate, a crack at the contact contour having shielded the points behind it on the affected plate surface and thus influenced the path of further crack propagation. Figures 3; references 3.

Penetration of Thin Plate Into Metal Strip at High Velocity

937D0044E Kiev PROBLEMY PROCHNOSTI
in Russian No 8, Aug 92 pp 45-48

[Article by G.G. Savenkov, St. Petersburg; UDC 539.4]

[Abstract] Penetration of a thin plate into barriers in the form of strips is analyzed concerning the dependence of both penetration depth and notch width on the width of such a strip. The analysis is based on experimental data, a 1 mm thick copper plate having struck a strip of killed grade-28 carbon steel and a strip of OT4 titanium alloy with an impact velocity of 3 km/s. The data, generally without surprises, are interpreted in the approximation of a quasi-static penetration process involving a thin striker plate. In this case $(h+l)^{1/2} = \pi K/2P\sin^{-1}[h/(h+l)]$ (h , plate penetration depth; l , length of crack at equilibrium; K , critical stress concentration factor; P , intensity of tensile stresses) and $P = P_0(z/l)^{-1}$ (P_0 , maximum stress intensity, at plate-barrier contact contour; z , distance from that contour along the crack, normalized to the crack length; $n \approx 2.8$ for the steel and $n \approx 3$ for the titanium alloy). Calculations on the basis of this model reveal that the penetration is deeper in a narrower strip and thus where impact produces a longer crack. The maximum width of the notch, meanwhile, is found to be proportional to the dynamic yield strength of the barrier material and to increase with increasing crack length. Figures 1; references 6.

Pressure Distribution Over Contact Surface After Impact of Deformable Cylinder Against Rigid Barrier

937D0044F Kiev PROBLEMY PROCHNOSTI
in Russian No 8, Aug 92 pp 52-58

[Article by Yu.A. Yemelyanov, A.I. Kozachuk, and A.V. Orlov, Institute of Engineering Physics imeni A.F. Ioffe at Russian Academy of Sciences; UDC 539.4]

[Abstract] Impact of a deformable cylinder against a rigid barrier is analyzed with the aid of experimental data, the measuring rod method having been modified so as to facilitate recording the pressure distribution over the contact surface as a function of time after the impact. The barrier was an about 20 mm thick disk of quenched steel about 80 mm in diameter with a center hole matching the size of the measuring rod to fit into it snugly, both rigidly mounted on a support. Various measuring rods of quenched U10A straight-carbon tool steel capable of transmitting pressures up to about 160 kg/mm² were used, the length of each being different but each being sufficiently long for the pressure pulse returning after reflection at the end of the rod not to interfere with flexural vibrations of the barrier recorded by strain gages mounted on the rod. The striker was a 30 mm long cylinder of ADO aluminum 7.6 mm in diameter terminating into a cone with a 90° vertex angle. The striker was launched by a charge of gunpowder, its velocity being varied over the 200-700 m/s range. It was moving in the axial direction, its axis coinciding with the rod axis so that impact produced an axisymmetric distribution of normal pressure on the barrier and on the rod. When the pressure near the striker axis likely exceeded the dynamic yield strength of the rod material, then the pressure gage recorded at each instant of time the average pressure on the rod. This pressure depended on the relative magnitudes of the rod radius, the barrier radius, and the striker radius. Evaluation of the experimental data, including oscillograms, has yielded the dependence of average contact pressure transients on the impact velocity, and of the maximum average contact pressure on the impact velocity squared, also pressure profiles at several instants of time after impact. Figures 4; references 7.

Review of Monograph "Strength of Cryoengineering Alloys Under Electromagnetic Action" by V.A. Strizhalo, L.S. Novogradskiy, and Ye.V. Vorobyeva

937D0044G Kiev PROBLEMY PROCHNOSTI
in Russian No 8, Aug 92 pp 62-63

[Article by O.A. Troitskiy, doctor of technical sciences, professor, and president of association "Intensive Treatment of Materials Electrotechnology"]

[Abstract] The monograph "Strength of Cryoengineering Alloys Under Electromagnetic Action" by V.A. Strizhalo, L.S. Novogradskiy, and Ye.V. Vorobyeva consists of five chapters following an introduction and

contains a list of 151 bibliographic references. The first chapter deals with electromagnetic fields, electrical and magnetic properties of metals and alloys, electroelasticity and magnetoelasticity, and the effect of electromagnetic action on the mechanical characteristics of materials at cryogenic temperatures. The second chapter deals with methods and means of cooling materials during mechanical tests, peculiarities of deformation and fracture of structural alloys at cryogenic temperatures, the dependence of their deformation and fracture on the loading conditions and the specimen geometry, also their surface condition and intermittent fluidity at 4.2 K. The third chapter deals with methods of studying the effects of electric current pulses on the mechanical characteristics of materials at cryogenic temperatures and on apparatus built for attaining such temperatures, also on the deformation resistance, strength, and plasticity of various structural steels over a wide range of low temperatures. Based on the results of such studies, the authors have found how the resistance of materials to action of a current pulse depends on the degree of their strain hardening. The fourth chapter deals with procedures and apparatus for experimental study of the mechanical characteristics of materials in high-intensity constant and pulsed magnetic fields at temperatures covering the 293-4.2 K range, these characteristics shown to depend on the field penetration depth. The authors consider various possible factors causing a magnetic field to influence the mechanical behavior of metals, the predominance of one or another factor being determined by the field penetration depth in the specimen. The fifth chapter deals with methods developed by the authors for predicting the ultimate state of materials under electromagnetic action. The authors demonstrated the feasibility of utilizing low-temperature hardening as a way to increase the strength of structural components. The main emphasis in this monograph is on experimental studies concerning the mechanical characteristics of potential new cryogenic power engineering materials. The monograph should be helpful to scientists as well as engineers in planning and design of cryogenic power equipment with new materials.

Dynamic Strength and Crack Resistance of Cryogenic Alloys

937D0045C Kiev PROBLEMY PROCHNOSTI
in Russian No 9, Sep 92 pp 48-53

[Article by V. V. Naumenko and A. V. Shiyan; Kiev; UDC 539.4:620.178.7]

[Abstract] The strength and crack resistance of 12Kh18N10T and 03Kh20N16AG6 steels and of AMg6 aluminum-magnesium alloy were studied while the metals were subjected to a strain rate of 0.36 m/s and temperatures of 293 to 77 K. Strength and ductility were studied using smooth cylindrical specimens 4 mm in diameter and 20 mm long in the stressed section. The specimens were cut from sheet in the direction of rolling. Crack resistance was studied using compact specimens 10 and 12 mm thick and notched so that fatigue cracking

would propagate against the direction of rolling. The standardized tests were performed on an Instron testing machine with specialized grips for handling these types of specimens. The AMg6 specimens were tested at 293, 203, 178, 163, and 77 K, and the steel specimens at 293, 178, and 77 K. Load was measured with the Instron's force gage; specimen strain and displacement of the load application point were measured with a resistance strain gage. The pick-up signals were fed to into an oscilloscope that showed the stress-strain diagrams used to calculate tensile strength, ductility, crack resistance, and resistance to crack propagation. The specimens were chilled in a cryostat in which the temperature was regulated by the supply of liquid nitrogen and/or its vapors. Specimen temperature was measured with a chromel-copel thermocouple and recorded by a KSP-4 device. The test results showed that, under the conditions described, the strength, ductility, crack resistance, and crack propagation resistance of the AMg6 alloy all increased. The steels showed increased strength and crack resistance, but lower ductility and crack propagation resistance, especially for the 03Kh20N16AG6 steel. The validity of using the compact specimens to determine the correct critical values for the crack resistance of the 03Kh20N16AG6 steel and the AMg6 alloy was proved, as was the determination of critical crack resistance values at 77 K for the other steel. Figures 3, tables 2; references 12: 11 Russian, 1 Western.

Estimating the Survivability of a Coupling Bolt in a Gas Turbine

937D0045D Kiev PROBLEMY PROCHNOSTI
in Russian No 9, Sep 92 pp 53-57

[Article by V. M. Stepkov and V. T. Krangach; Kherson Industrial Institute, Kiev; UDC 539.4+620.191.33+621.438+621.882.6]

[Abstract] The survivability of a gas turbine coupling bolt was estimated. The bolt in question is made of 26KhNZM2FA steel, is 4500 mm long and 200 mm in diameter, has a thread pitch of 4 mm, and is designed to withstand operating temperatures of 293 to 532 K. Two aspects of bolt survivability were examined: crack propagation time as a result of low-cycle load conditions arising from the thermal expansion of the rotors during startup and the size of non-propagating fatigue cracks resulting from multi-cycle vibrational loads. The estimate was based on these data, which were used in conjunction with tensometric data gathered during operational loading and non-destructive testing data. The crack propagation process was described verbally and mathematically. It was concluded that the critical depth of a ring crack in this type of bolt is 26 mm. From a depth of 10 mm, the crack develops to a critical size after 30,000 operating cycles. When checking for cracks during a major overhaul, resolution of at least 10 to 15 mm in relation to crack size is necessary. A relationship was established between the size of the non-propagating fatigue cracks and the amplitude of variable stresses and the shape of the cracks. When threshold stress is 20 MPa

and b/a is 1, the crack cannot be deeper than 2 mm in the smooth part of the bolt or deeper than 0.9 mm in a bolt made of TsD-M-Sh steel. The limitations are much stricter for crack size in the thread root: 0.035 and 0.013 mm, respectively, for a ring crack. Resolution during the non-destructive testing of a new bolt should be much greater than for a major overhaul. Figures 5; references 4: 3 Russian, 1 Western.

Relationships Between Temperature and the Elastic Properties of Capacitor-Grade Ceramics

937D0045E Kiev PROBLEMY PROCHNOSTI in Russian No 9, Sep 1992 pp 62-64

[Article by V. A. Borisenko and A. I. Troyanskiy; Institute of Strength Problems of the Ukrainian Academy of Sciences; UDC 534.22]

[Abstract] The feasibility of using ultrasound to study the elastic properties of radio engineering ceramics was examined. Two types of titanium-containing ceramic, ε37 and ε40, which were arbitrarily designated as brown and white, respectively, were used in the study. The cylindrical specimens, which were made by reaction sintering, were 8 to 9 mm high and 25 mm in diameter. Of the 20 types of ceramics evaluated by the authors, these two had the greatest thermal stability. The specimens were subjected to an echo-pulse method of ultrasound probing at a frequency of 10 MHz while being heated at a rate of 8 to 10 K/h. Ultrasound wave propagation speed was measured for each one degree change in temperature. Specimen dimensions were considered ideal for these testing conditions. Relative measurement error did not exceed $\pm 1 \times 10^{-5}$. Within a temperature range of 190 to 350 K, the relative change in acoustic wave speed was about 70 m/s for the white ceramic and about 60 m/s for the brown ceramic. These values have ranged from 120 to 930 m/s for other, less thermally stable ceramic materials. By way of comparison, the lowest relative change in longitudinal ultrasound wave propagation speed that has been observed for a solid body within the temperature range indicated is 45 m/s for ArGa and InP semiconductor materials. What is especially notable is the smoothness with which the curves enter and exit the region of local extreme values. This smoothness has only been observed in reaction-sintered ceramic materials. When the values for ultrasound wave propagation speed were plugged into the equations expressing the Poisson coefficient and the moduli of transverse and longitudinal elasticity as a function of temperature, the resulting curves were very similar to those for the transverse and longitudinal ultrasound wave propagation speeds as a function of temperature. Thus, ultrasound studies are a useful way to evaluate the elastic properties of reaction-sintered capacitor-grade ceramics. Figures 2; references 4: Russian.

Domain Structure and Hysteretic Properties of Fine-Grain High-Anisotropy Rare Earth Magnetic Alloys

937D0048A Yekaterinburg FIZIKA METALLOV I METALLOVEDENIYE in Russian No 2, Feb 92 pp 21-26

[Article by N.A. Manakov, G.F. Korzinnikova, V.V. Stolyarov, Institute of Superplasticity Problems of Metals at Russia's Academy of Sciences; UDC 669.27:537.856]

[Abstract] The effect of the domain structure (DS) on the magnetization reversal mechanism and eventually, on the hysteretic properties of R-Co or R-Fe-B alloys where R is a rare earth element (RZE) and the scarcity of domain structure data on fine-grain alloys prompted an investigation into the domain structure studies carried out with the help of Lorentz electron microscopy, especially domain structure observations by methods of defocusing and aperture diaphragm shifting at a 1 MV potential in combination with electron microscope microstructural analyses. Foils and films made by vapor phase deposition and rapid quenching of RCo_5 or $R_2Fe_{14}B$ alloys are studied and the domain structure is defined as amorphous, nanocrystalline, submicrocrystalline, microcrystalline, and fine-crystalline; the hysteretic properties and principal magnetization reversal mechanism are summarized for each category. It is shown that the principal structural factor affecting the domain structure character of these alloys is their dispersivity degree; the classification is based on the ratio of the mean grain size to the domain wall width and critical single-domain dimension. Figures 5; tables 1; references 16: 12 Russian, 4 Western.

Temperature and Electromagnetic Wave Amplitude Relaxation in Tungsten Under Static Skin Effect Conditions

937D0048B Yekaterinburg FIZIKA METALLOV I METALLOVEDENIYE in Russian No 2, Feb 92 pp 27-34

[Article by A.B. Rinkevich, Physics of Metals Institute at the Urals Branch of Russia's Academy of Sciences; UDC 669.27:537.856]

[Abstract] The nonlinear phenomena occurring in metals in electrodynamic systems under the effect of electric current manifested by a change in the electromagnetic wave (EMW) amplitude, harmonic generation, and an amplitude anomaly of the surface electromagnetic wave propagating in a "meander"-like periodic structure are discussed, and an attempt is made to explain the anomalies by assessing the temperature gradient and its life span as well as comparing the electromagnetic wave anomalies to the quantities characterizing thermomagnetic waves. The temperature relaxation after a current pulse and transient phenomena characterizing the electromagnetic wave amplitude and the meander line in a pure W single crystal are measured. The measurements

are taken in a periodic system, making it possible to check the existence of the transient phenomena observed earlier and the instabilities in a compensated metal under static skin effect when the current distribution in the sample cross section has explicit singularities. The static skin effect phenomenon also makes it possible to measure the temperature behavior of the surface metal layer after the effect of a close to 100 μ s current pulse and assess the temperature gradient. The voltage-current curves of the sample, the magnetothermal voltage drop fluctuations, pulsed voltage-current curves of the sample, current and voltage drop oscillograms of the

sample, and temperature relaxation in the meander line are plotted. The method of evaluating the surface layer temperature is suitable for recording the dynamic changes in temperature within a micro- and millisecond range and for measuring the temperature gradients. The transient wave amplitude phenomena are attributed to the traveling thermoelectromagnetic or standing elastic waves, and it is speculated that the latter are more likely than the former. The metastable chaos life span in the wave amplitude exceeds the temperature relaxation time. Figures 6; references 9.

Electron Microscope Studies of Sputtered Niobium Films

927D0258I Moscow METALLY in Russian No 3, May-Jun 92 pp 131-138

[Article by I. D. Voytovich, V. A. Lobodyuk, and S. Ya. Navala; UDC 348.24:620.187.3]

[Abstract] Transmission electron microscopy was used to study the structure, grain size, uniformity by composition and thickness, and state (crystalline or amorphous) of niobium films deposited directly onto oxidized and non-oxidized silicon substrates by electron-beam and magnetron sputtering. Transmission electron microscopy was chosen because it allows inspection of the structural state of separate, extremely thin (60 nm) layers of films. Depending on sputtering conditions, i.e., rate of deposition, temperature and type of substrate, sputtering method (electron beam or magnetron), and film thickness, a wide spectrum of structural features is observed in niobium films. Their structures differ in the size and mutual orientation (uniformity of orientation) of grains. By choosing certain process and substrate conditions, it is possible to select sputtering modes which produce desired structural features in films. In particular, the fine-grain structure with average grain size of 20-40 nm that is necessary for Josephson tunnelling can be produced at a substrate temperature of up to 300°C and a film thickness of 300 nm on both oxidized and non-oxidized substrates of silicon with orientation <100>.

Wear Resistance of Titanium Nitride Coating Deposited by the PVD Method on the Surface of Low-Alloy Steel Subjected to Plasma Nitriding

927D0258K Moscow METALLY in Russian No 3, May-Jun 92 pp 150-158

[Article by T. Bell and Y. Sun, Department of Metallurgy and Materials, Birmingham University, England; UDC 669.295'786.84]

[Abstract] Experiments were performed to evaluate the wear resistance of the low-alloy steel En40B with a TiN coating deposited by the PVD method. Tests were conducted by the slipping and slipping-and-rolling method. Before depositing the coating, one set of quenched and tempered specimens was subjected to plasma nitriding, while the other set was not. The effect of the substrate's durability and the coating's properties was investigated for resistance to wear. It was demonstrated that a TiN coating on steel which has undergone plasma nitriding provides better wear resistance than a TiN coating on steel that has not been pre-treated by this method. Wear resistance tended to decrease as the coating's hardness lessened. Light grinding or sandblasting with dry sand on the surface increased the wear resistance of specimens with coatings. The correlation of properties of the substrate and of the coating was optimized by adjusting the plasma nitriding, surface preparation and coating processes.

The Protective Properties of Co-Cr-Al-Y Coatings

937D0016F Kiev PROBLEMY SPETSIALNOY ELEKTROMETALLURGI in Russian No 1, Jan-Feb-Mar 92 (manuscript received 3 Jul 91) pp 64-68

[Article by Yu.G. Veksler, O.V. Repina, V.P. Lesnikov, and V.P. Kuznetsov, Ural Polytechnic Institute imeni S.M. Kirov, Sverdlovsk; UDC 669.187.526.001.5]

[Abstract] The heat and corrosion resistance of standard gas turbine blade coatings consisting of Co, 23 percent Cr, 12 percent O, and 0.15 percent Y were studied. The study coatings were applied to a substrate of the refractory nickel alloy ChS70VI by electron-beam vaporization. The specimens were aluminized by the circulating gas method at 1,000°C for four hours and then subjected to diffusion annealing in air at the same temperature for two hours. The coated specimens were then subjected to high-temperature oxidation at 1,050°C for 300 hours. For the corrosion tests, the specimens were coated with a layer of a mixture of 75 percent Na₂SO₄ and 25 percent NaCl salts in amounts ranging from 4 to 6 mg/cm² and held at 750 or 900°C for 40 hours. The salt layer was renewed every five hours. A DRON-3 diffractometer was used for phase analysis studies of the specimens, and a Kameka MS-46 was used to analyze the distribution of alloy-forming elements in the coating. The tests performed established that the study Co-Cr-Al-Y coating possesses rather high degrees of both heat and corrosion resistance. During the heat resistance tests, the coating broke down evenly along the entire front. Additional aluminizing proved to even further improve the coating's durability and is recommended for cases where the coatings will be expected to withstand especially high temperatures and corrosive media. Specifically, at 720°C, additional aluminizing stabilized the ε-phase with respect to the γ → ε transformation and facilitated the formation of a thicker Al₂O₃ protective film, and at 900°C, additional aluminizing significantly increased the corrosion resistance of the study coatings. Figures 4; references 6: 5 Russian, 1 Western.

Absorption of Electromagnetic Radiation by a Layer of Adsorbed Molecules

937D0214 Kiev UKRAINSKIY FIZICHESKIY ZHURNAL in Russian Vol 37 No 8, Aug 92 pp 1151-1159

[Article by A. F. Zhuravlev, Institute of Physics of Metals, Ukrainian Academy of Sciences, Kiev, and V. Z. Lozovskiy and B. I. Khudik, Institute of Semiconductors, Ukrainian Academy of Sciences, Kiev; UDC 535.37:539.3]

[Abstract] The effect of interactions among molecules in a layer (lateral interactions) on the polarizability of a submonolayer film of molecules adsorbed on a solid surface was investigated. A self-consistent system of nonlinear equations is formulated to derive the polarizability tensor which correctly describes the properties of such films. It was found that lateral interactions can

cause a considerable widening of electromagnetic radiation absorption lines and even splitting of the lines by the system of adsorbed molecules. For illustration of line splitting, spectra of light absorption by molecules adsorbed on the surface of zinc sulfide were calculated numerically. It was demonstrated that deformation of the absorption line is greatest for molecules that have large static polarizability values.

Vacuum-Plasma Coating Apparatus

937D0022E Moscow TYAZHELOYE
MASHINOSTROYENIYE in Russian No 7, Jul 92 p 37

[Article by A.N. Doroshenko, deputy section manager, "Transmash" (Transport Vehicles) Concern

[Abstract] Replacement of 20-25 µm thick PbSn10Cu wear-in coatings galvanically deposited following a 1-2 µm thick nickel strike on Pb-bronze liners of journal bearings with ion-plasma PbSn10Cu2 coatings vacuum deposited following a nickel strike has been considered for diesel engines, the object being to improve the bearing performance and to make the coating deposition process ecologically clean. Studies made over the 1989-91 period at the Institute of Machine Design and Technology and at the Central Scientific Research Institute of Diesel Engines have revealed that ion-plasma coatings with boundary lubrication excel galvanic ones in terms of a 1.5-2 times stronger adhesion, a 1.5-2 times higher seizure threshold, and a 3 times lower nominal wear rate, also a higher resistance to corrosion in oil and to fretting fatigue. A major other advantage of this new technology is its applicability to other coating materials such as the A020-1 grade. The now commercially built NNV 6.6-II vacuum-plasma apparatus with three electric-arc evaporators is suitable for deposition of refractory nitride and carbide coatings but not of fusible coatings on bearing liners. In order to make such an apparatus available for nickel strike and deposition of multicomponent wear-in coatings in a single operating cycle, it is necessary to equip it with at least six electric-arc evaporators. It is further necessary to isolate the liner from the plasma flux during the initial heating-up stage and to prevent subsequent migration of the cathode material from one group of evaporators to the cathodes of the other group. These problems were discussed at the recent conference held by the Technology of Machine Assembly section at the Science and Engineering Council of the commercial organization "Transmash". It has been recommended that an experimental-industrial prototype of such a special apparatus be developed, built, and tested for subsequent coating of bearing liners at the two Balakovo and Tokmak diesel manufacturing plants, to be followed by field testing of diesel engines with such bearings.

Inspection of Galvanic Nickel Coatings by Magnetomechanical Method of Acoustic Emission

937D0027D Kiev TEKHNICHESKAYA
DIAGNOSTIKA I NERAZRUSHAYUSHCHIY KONTROL in Russian No 3, Jul-Aug 92 (manuscript received 5 Dec 90) pp 59-64

[Article by S.A. Novikov, candidate of technical sciences, and G.I. Khilko, mechanical engineer, Institute of

Applied Physics at Byelorussian Academy of Sciences, Minsk; UDC 621.791.052.08:620.179.16]

[Abstract] An experimental study was made concerning use of magnetomechanically induced acoustic emission for inspection of galvanic nickel coatings on nonmagnetic materials, specifically on copper alloys. Such coatings were deposited on disks of 08 Cr chromium bronze, 2-200 µm thick coatings on one face of 4 mm thick disks 30 mm in diameter. That face had been ground, chemically degreased, etched, and activated according to standard procedure prior to being coated. The coatings were magnetized in a 50 Hz alternating magnetic field of an electromagnet, before and after they had been annealed at various temperatures from 150°C to 900°C under a vacuum of 5-6 mPa. A piezoelectric transducer covering the 0.02-0.2 MHz frequency range picked up acoustic vibrations and transmitted them to an AF-15 acoustic emission recording instrument. The transducer had been pressed against a disk by a spring, through either a thin layer of transformer oil for measurements by the contact method or through a 3-4 mm thick layer of water inside a polyethylene beaker for measurements by the immersion method. The coatings were inspected for thickness, quality of heat treatment, and loss of adhesion bond in the form of peeling or swelling. Relevant information was drawn from the total acoustic emission count and the maximum acoustic emission pulse amplitude recorded within 10 s periods. Structural and metallographic examination of the coatings included microhardness measurement, x-ray spectrum microanalysis for a determination of both copper and nickel distributions at the coating-substrate interface, and measurement of the thickness of the diffusion layer with a Microscan-5 instrument. The tests have revealed how both the total count and the maximum pulse amplitude depend on the coating thickness and on the annealing temperature. An analysis of the results indicates that the total magnetomechanically induced acoustic emission count is the more sensitive parameter and can serve as the basis for inspection of such coatings by immersion, inspection by contact being unreliable because of contact variability and instability. Figures 3; tables 1; references 11.

Optimizing the Composition of Deposited Metal and Parameters of Wear-Resistant Buildup Techniques

937D0034C Moscow SVAROCHNOYE
PROIZVODSTVO in Russian No 8, Aug 92 p 19

[Article by L. S. Livshits, Doctor of Technical Sciences, and O. Yu. Yelagina, engineer, State Academy of Oil and Gas im. I. M. Gubkin; UDC 621.791.927.93]

[Abstract] A computer program was developed for calculating conditions of build-up of worn parts by the manual arc method and the structure of the deposited metal for the purpose of optimizing the conditions according to wear-resistance criteria. Controllable input parameters of build-up conditions included the current and voltage of the arc, rate of build-up, and heating of

the part; uncontrollable parameters included ambient temperature, thickness of the part, and chemical composition and thermophysical properties of the primary and electrode metals. For the calculated values a set of factors was established which affect the stability of the process and the quality of the deposited layer: critical length of the arc, incomplete fusion of the primary metal, maximum permissible pressure of the arc on fused metal, and maximum permissible heating of the electrode by the passing current.

It was found that analysis of values of build-up process parameters permits selection of conditions for obtaining the required dimensions of the bead and the fusion zone. Changing build-up conditions results in a substantial change in the structural-phase state of the deposited metal, and consequently its wear resistance. Given the availability of a variety of materials for building-up, it is possible to select not only build-up conditions but also a chemical composition of deposit metal which ensures the highest hardness.

Laser Technology for Imparting Tribotechnical Characteristics to Friction Surfaces

*937D0034E Moscow SVAROCHNOYE
PROIZVODSTVO in Russian No 8, Aug 92 pp 22-25*

[Article by V. S. Avanesov, Candidate of Technical Sciences, State Academy of Oil and Gas im. I. M. Gubkin; UDC 621.791.947.72:621.375.826]

[Abstract] Causes of parasitic perturbations in laser forming of the microrelief of friction surfaces using melting and some ways of suppressing them to reduce allowances were investigated. Phenomenological models of the formation of periodic surface structures (pronounced periodicity in a wavy relief) make it possible to discern some approaches to suppressing parasitic perturbations.

A model experiment was used to investigate the kinetics of fusion of micro-unevennesses on surfaces. Conical specimens with different tip angles were melted with a CO₂ laser with 0.9 kW power and a focal spot diameter of 4 mm. The possibility of using a laser to improve surface microrelief (laser "polishing") was demonstrated.

The possibility of laser etching of friction surfaces to create a system of depressions that form a regular relief for lubricants was also demonstrated. These "oil channels" increase the stability of the lubricant film that forms and facilitate the removal of products of wear from the friction zone.

Modification of the Surface Layer of Parts by Micro-Arc Oxidation

*937D0034G Moscow SVAROCHNOYE
PROIZVODSTVO in Russian No 8, Aug 92 pp 29-30*

[Article by V. A. Fedorov, Candidate of Technical Sciences, State Academy of Oil and Gas im. I. M. Gubkin; UDC 621.794.61:621.357.8:669.715]

[Abstract] Results of investigation of surface layers of aluminum alloys hardened by the micro-arc oxidation process are presented. The alloys were categorized into four groups according to mechanical properties, chemical composition, and other parameters, and specimens of specific brands of alloys from each group were treated using three different modes of micro-arc oxidation. The composition and structure of the resulting hardened layers were examined by X-ray diffraction. It was found that in most of the alloys the hardened layer has a crystalline structure, unlike anode oxide films formed by conventional anodizing. The phase composition of the hardened layer depends on the micro-arc oxidation mode, the layer thickness, and the chemical composition of the oxidized material. Oxide phases were not found to have a pronounced grain orientation, indicating a random orientation of crystals in the hardened layer. Results of studies of micromechanical properties, crack formation, and tribotechnical characteristics of hardened layers are also presented.

Wear Resistance of Coatings Based on Metalide Alloys

*937D0034H Moscow SVAROCHNOYE
PROIZVODSTVO in Russian No 8, Aug 92 pp 33-34*

[Article by V. A. Neumyin, S. A. Shelukha, G. A. Leontyeva, and Ye. N. Tarasenko, Norilsk Mining and Metallurgical Combine; UDC 621.791.052:539.538]

[Abstract] Results of investigation of the main characteristics of different metalide coatings under conditions of abrasive wear and how these characteristics differ depending on spray-coating conditions are presented. Coatings were applied using the plasma spraying unit WSP 1500/500. Materials for spray coating were the metalide alloys PN85Yu15 (Ni-Al system) with a 160-micrometer fraction, and PN55T45 (Ni-Ti) with 10-45 and 40-100 micrometer fractions. Test results showed that relative wear of metalide coatings of the Ni-Ti system (PN55T45) is on average 3.2 times lower than that of coatings of the Ni-Al system (PN85Yu15). The best characteristics in conditions of abrasive wear belong to the coating PN55T45 using a powder fraction of 10-45 micrometers and a sublayer of the Ni-Cr alloy Kh20N80. It was also found that in spraying coatings of the Ni-Ti system, additions of hydrogen in the plasma jet can lead to increased pore formation and cracking of the coating, which is due to increased enthalpy of the plasma flow.

Effect of Annealing and Ion Bombardment on Hydrogen Content and Properties of Adamantine Films

937D0043B Moscow FIZIKA I KHIMIYA OBRABOTKI MATERIALOV in Russian No 5, Sep-Oct 92 pp 16-20

[Article by S.M. Klotsman, S.A. Plotnikov, A.P. Rubinshteyn, I.Sh. Trakhtenberg, V.B. Vykhodets, Yekaterinburg; UDC 546.26.-162.02]

[Abstract] The unique range of performance and physical properties of diamondlike films and methods of making them, e.g., by hydrocarbon breakdown, are discussed; the difficulty of interpreting the phenomena observed during the diamondlike film (APP) irradiation with ion beams is noted. As a result, an attempt is made to investigate the change in the hydrogen content in films produced in high-frequency direct current plasma under the effect of a 900 keV deuteron beam. The study is carried out using both the original films and films annealed at various temperatures. The nuclear reaction method is used to measure the hydrogen concentration and its variation under irradiation and annealing. The films are deposited on single crystal Ge from DC methane plasma in a cold cathode source. An electrostatic Van de Graaf accelerator is used as the beam source. The films are annealed in a vacuum. The dependence of the hydrogen content in films on the annealing temperature and subsequent ion irradiation dose, the dependence of the carbon content in films on the annealing temperature, the dependence of the oxygen and nitrogen content in the film on the annealing temperature, and the effect of the radiation yield of hydrogen on the preannealing temperature are plotted. An analysis shows that a decrease in the hydrogen content in the film is the primary outcome of thermal and radiation exposure whereby the film structure plays a dominant role: polymer-like formations in C-H films cause thermal C removal from the free hydrocarbon radicals; in diamondlike film there is no such effect. The hydrogen's radiation-induced yield decreases with an increase in the dose and annealing temperature while the effect of temperature on the radiative effect starts only at the temperatures at which a change in composition is observed. Figures 4; references 13: 2 Russian, 11 Western.

Effect of Ion-Plasma Rhenium Coating on Mechanical Properties of Molybdenum Wire

937D0043C Moscow FIZIKA I KHIMIYA OBRABOTKI MATERIALOV in Russian No 5, Sep-Oct 92 pp 21-27

[Article by A.G. Kolmakov, V.F. Terentyev, V.T. Zabolotnyy, Ye.Ye. Starostin, Moscow; UDC 621.793:669.849]

[Abstract] The nonuniformity of the dislocation structure evolution in the sample cross section under static tension, fatigue, and creep in metallic materials and its

relevance to vacuum sprayed coats produced with simultaneous ion bombardment which makes it possible to deposit coats with a good adhesion without diffusion annealing are discussed, and the effect of the thickness of Re coats produced by vacuum deposition with simultaneous argon ion bombardment on the mechanical properties of Mo wire is investigated. To this end, 1 mm dia. MCh-grade drawn Mo wire is used. The mechanical tensile tests are conducted at a $3.3 \times 10^{-3} \text{ s}^{-1}$ rate in an Instron TT-DM tester; the Re coat thickness is measured by a Neophot 2 optical microscope and fractographic studies are carried out in a Joel JSM-U3 scanning electron microscope. The behavior of the mechanical characteristics of wire samples is plotted. The chemical composition of the wires and the mechanical properties of the wires under tests without the coat and with a coat of a varying thickness are summarized. The study shows that as the coat thickness increases from 0.4 to 4.1 μm , the static tensile strength and elongation increase by 28 and 12 percent vs. uncoated wires while ultimate strength changes little; ductility remains unchanged. The surface layer fracture patterns also change as a function of thickness. The findings confirm that for polycrystal BCC metals, the effective ordered layer thickness formed during the microflow stage is within several micrometers, i.e., on the order of the grain size; the study also demonstrates good adhesion of vacuum deposited Re films produced under irradiation. Figures 7; tables 2; references 16: 11 Russian, 5 Western.

Plasma Chemical Deposition of Colored Coats on Polymer and Inorganic Materials

937D0043J Moscow FIZIKA I KHIMIYA OBRABOTKI MATERIALOV in Russian No 5, Sep-Oct 92 pp 74-81

[Article by V.F. Sokolov, Yu.A. Sokolova, G.V. Trofimova, Ivanovo; UDC 537.525.1:541.64]

[Abstract] Interest in plasma chemical deposition of thin colored coats on the surface of various materials is noted, and the conditions and mechanism of the colored anthraquinone and copper acetylacetone on polymer and silicon bases in a low-temperature oxygen plasma are investigated. The selection of these compounds is due to an attempt to combine the staining process with the dye synthesis process under the effect of glow discharge. The design of the experimental reactor is described and its schematic diagram is cited. The anthraquinone and copper acetylacetone electron absorption spectra and the potential distribution between the reactor cathode and anode are plotted. The resulting coats' hues are summarized: depending on the experiment conditions, pink, yellow, and brown colors are produced on the basis of anthraquinone and blue, navy, green, and brown on the basis of copper acetylacetone. The initial substance modification under the effect of the glow discharge is studied by infrared and ultraviolet spectroscopy. The change in coloration in the anthraquinone case occurs due to the OH-group and Al atom implantation and in the copper acetylacetone case—due to its partial decay into copper oxides. The

material is colored in the discharge's cathode areas. Figures 4; tables 1; references 32: 26 Russian, 6 Western.

Ni-Based Alloy Powders With Laves Phases for Gas Thermal Spraying

937D0043K Moscow FIZIKA I KHIMIYA
OBRABOTKI MATERIALOV in Russian No 5,
Sep-Oct 92 pp 86-89

[Article by I.N. Gorbatov, L.K. Shvedova, A.Ye. Terentyev, Karpenko, S.V. Nagornyy, Kiev; UDC 539.231:621.793:621.762:669.24]

[Abstract] The use of Laves phase materials—intermetallic compounds whose stoichiometric composition is described as AB_2 —for wear and corrosion resistant coats is discussed, and the crystal structure of Laves phases is classified. Laves phase materials whose principal components are Ni, Co, Mo, Cr, and Si, which maintain their good corrosion and wear resistance properties at up to 500–800°C, are considered. The chemical composition of triballoy, the tensile strength, bending strength, compressive strength, and HRC hardness of the T-400 alloy, and Laves phases and their melting points are summarized. In particular, alloys produced by DuPont, Union Carbide, Cabot, and SCM Inc. in the United States and Elmer Walles Ltd. in Great Britain, and Heganes AV in Sweden are examined. The study confirms that alloys reinforced with Laves phases have a combination of resistance and strength properties which make them suitable for numerous applications. The need to continue efforts aimed at expanding their applications for gas thermal spraying and at developing new spraying compositions is stressed. Tables 3; references 17: 3 Russian, 14 Western.

Composite Structure and Properties Under Laser Modification of Plasma-Sprayed Coats on Powder Materials

937D0043L Moscow FIZIKA I KHIMIYA
OBRABOTKI MATERIALOV in Russian No 5,
Sep-Oct 92 pp 90-100

[Article by A.M. Shmakov, N.N. Ivshina, Perm; UDC 621.793.7:621.375.862:621.762]

[Abstract] The shortcomings of gas thermal coat deposition (GTN) on cast and powder materials prompted the development of laser thermal modification (LTM) as a means of improving the physical and mechanical properties and performance of deposited coats. The characteristic features of the phase and structure formation during the laser thermal modification of three coat compositions on powder steel and titanium are investigated in order to optimize the range of physical and mechanical properties and tribological characteristics of hybrid materials. To this end, commercial grade PGN12N-02 and PN55T45 materials (TU 48-4206-156-82 and 14-1-3282-81, respectively) and the KNT-65k composite powder as well as powder steel and

titanium are used in the experiments. The powder coats are deposited by an Ar-N plasma-forming mixture, and laser treatment is performed using an LT1-2M CO₂ laser with a power meter. The phase and chemical composition is studied using DRON, MAP-2M, Jamp-10, Culumatic-C, and MS diffractometers, the microstructure is examined under a Neophot-21 optical and Jeol electron microscopes, and the wear surface morphology is examined under a scanning electron microscope REM-200; the microhardness analysis is performed in a PMT-3 tester under a 0.5 N load while the porosity is measured by Glagolev's method. Regression and statistical analyses of the findings are made on PC/XT microcomputers by special routines. The chemical composition of the sprayed materials is summarized, and Auger spectra of the KNT-65k coat are plotted. The structure, hardening parameters, fracture toughness, and wear resistance of self-fluxing intermetallic and composite coats are examined as a function of the LTM laser treatment. The composite coat thickness is an important structure-sensitive treatment factor which ensures Ti microstructure fluctuations of the hardening phase; the regression equations make it possible to find sound optimum LTM conditions. An up to threefold wear resistance increase is noted. The authors are grateful to Academician V.N. Antsiferov for guidance and fruitful discussions. Figures 5; tables 1; references 9: 5 Russian, 4 Western.

Damage Probability Assessment for Enamel-Coated Chemical Reactors

937D0045B Kiev PROBLEMY PROCHNOSTI
in Russian No 9, Sep 1992 pp 24-29

[Article by V. M. Plastinin; Scientific Research Institute of Enamel Coatings for Chemical Equipment, Poltava; UDC 539.2+539.4+519.24]

[Abstract] An empirically based statistical model of brittle failure was used to assess the probability of damage to the enamel coatings of chemical reactors. The model describes the inverse relationship between damage probability, on the one hand, and, on the other, the average surface concentration of random defects such as microcracks, pores, nicks, and so forth in the total surface area of a hypothetical reactor. In this model, the average number of surface defects must decrease as surface area increases in order to keep the probability of coating damage the same for all representative reactors. This approach was used to assess coating damage probability in two typical chemical process situations involving internal temperatures and pressures: one in which the coatings have perforation-type defects caused by using screws to fasten various types of equipment to the reactors, and one in which the coatings have no such defects. During a review of some of the relevant technical documentation from Japan (Kobi Steel's specifications), the USSR, and Switzerland (national standards), it was found that only the Swiss document satisfied the model's basic requirement, namely that the average number of surface defects must decrease as surface area increases. The Swiss standard calls for reinforcing the

glass matrix of the coatings with single crystal fibers of refractory chromium, zirconium, and aluminum oxides, which have the effect of localizing coating damage and increasing fracture toughness. These findings are applicable to both types of situations, but the reinforcement is most effective when $pS \leq 3$ (p = average concentration of surface defects, S = total reactor surface area. Figures 4; references 9: 8 Russian, 1 Western.

Structure and Electric Properties of Ag-W Films in Metastable States

937D0048C Yekaterinburg FIZIKA METALLOV I METALLOVEDENIYE in Russian No 2, Feb 92 pp 66-73

[Article by B.F. Bashev, F.F. Dotsenko, I.S. Miroshnichenko, V.M. Pasalskiy, Dnepropetrovsk State University; UDC (669.22+669.27):539.216.2:620.181]

[Abstract] Scientific and practical interest in producing metastable states in alloys whose elements are not fully miscible even in the liquid state and which have abnormally high positive formation heat values prompted an attempt to establish a correlation between the alloys' formation heat and their tendency to pass to metastable states (including amorphous) in the course of vapor

deposition. To this end, the ion plasma vacuum sputtering method is used with Ag-W ganged targets made as statistically uniformly placed W and Ag squares. The Ar, Ag and W atoms knocked out from the ganged target acquired an additional kinetic energy due to acceleration when they collided with the substrate. The vapor deposition process is conducted in a special unit at a 20 mA target current and -2 kV target potential with a 360 and 720 s spraying time. An schematic diagram of the accelerating unit is cited; the dependence of the surface resistance and temperature coefficient of resistance (TKS) on the sputtering duration, an X-ray pattern of the W and Ag+84 percent W alloy at a 360 s deposition time, resistance polytherms of the Ag-W alloy, and the Ag-W film stability after heat treatment at 85°C for 1,000 h are plotted. The use of the additional acceleration unit makes it possible to increase the kinetic energy of the Ar ions colliding with the Ag-W target by four- to fivefold and thus attain an amorphous state and supersaturated solid solutions in the films within a broad composition range; in alloys with a close-to-equiatomic composition, the formation and decay of the metastable AuCu intermediate phase is observed within a 440-720°C range. The curve inflections on the temperature coefficient of resistance and resistance at a ≥ 85 percent W concentration are attributed to shifts in the amorphous short-range order film in the direction typical of BCC coordination. Figures 6; tables 1; references 5: 3 Russian, 2 Western.

High-Temperature Metal-Matrix Composite

92D9258J Moscow METALLY in Russian No 3, May-Jun 92 pp 145-149

[Article by O. A. Bannykh, K. B. Povarova, V. A. Kutyenkov, A. G. Fridman, T. Ye. Golovkina, and Ye. K. Zavarzina; UDC 669.018.9]

[Abstract] On the basis of the thermally stable Cr-W system, a high-strength composite is proposed which can operate at temperatures of 1600-1900 K in oxidizing media. Compositions and production processes have been developed for components of the composite material—chromium alloy VKh2U and tungsten alloy VMRK—and technology has been developed for manufacturing sheet bars and roll-formed parts as well as articles with complex shapes from the Cr-W composite. They include models of a nozzle vane for a gas-turbine engine with a bend radius on the leading edge equal to 0.8 mm at an angle of 46°. The material has good high-temperature strength at 1473-1773 K; articles made from it have been tested successfully at 1900 K, which is higher than the melting point of contemporary nickel-base superalloys.

Changes in the Structure of Polyphosphazene Film Under Biaxial Tension

93D0018A Riga MEKHANIKA KOMPOZITNYKH MATERIALOV in Russian No 4, Jul-Aug 92 (manuscript received 7 Jan 92) pp 453-456

[Article by A.Kh. Kurzennieks, V.M. Parfeyev, D.R. Tur, and E.V. Smurova, Polymer Mechanics Institute, Latvian Academy of Sciences, Riga, Elementoorganic Compounds Institute imeni A.N. Nesmeyanov, USSR Academy of Sciences, Moscow, and Cardiovascular Surgery Institute imeni A.N. Bakulev, Moscow; UDC 541.64:547.241]

[Abstract] A study was conducted to determine the structural changes occurring in poly-bis-trifluoroethoxyphosphazene films subjected to unidirectional and biaxial tension. Polyphosphazene films 0.25 +/- 0.03 mm thick were produced by the technique of pouring from a solution. A DRON-2 diffractometer was used to perform wide-angle x-ray diffraction studies of the films. Measurements were taken in both reflected and through beams with different degrees of stretching. Strips of the study films 12 mm wide were subjected to uniaxial stretching by using a special removable attachment on the diffractometer. Biaxial tension was created by the blowing method or by stretching the strips over a punch. The X-ray diffraction studies established that the restructuring of the study polyphosphazene films resulting from even biaxial stretching is very different from the changes induced by uniaxial stretching. Unidirectional tension produces rather strong fibers. The structure of the polyphosphazene film specimens subjected to biaxial stretching, on the other hand, becomes somewhat similar to that of a monocrystal. Biaxial

stretching results in a very distinct and complete reorientation of the crystallites that in turn causes the crystallographic axis of all of the crystallites to become uniformly oriented relative to the plane of the film. Figures 4; references 9: 8 Russian, 1 Western.

The Rational Design of Curved Cross-Ply Fiberglass-Reinforced Plastic Pipes

93D0018B Riga MEKHANIKA KOMPOZITNYKH MATERIALOV in Russian No 4, Jul-Aug 92 (manuscript received 7 Apr 89; after revision 3 Dec 91) pp 470-475

[Article by G.P. Zaytsev and V.N. Tyshkevich, Moscow Aviation Technology Institute imeni K.E. Tsiolkovskiy and Komsomolskiy-na-Amur Polytechnic Institute; UDC 539.3]

[Abstract] Curved cross-ply fiberglass-reinforced plastic pipes made of T-10 fabric and UPE 22-27 binder (32 to 33 percent) were studied to determine the optimum design of pipes made of the said materials. The pipes' stress-strain state was determined based on the Karman effect. A modified Mises-Hill criterion was developed to estimate the ultimate strength of cross-ply fiberglass-reinforced plastic pipes such as those studied. The optimal angles of reinforcing the study pipes were determined on a Unified System [YeS] computer by parametric analysis. Curves of the values of the critical strength function (i.e., the modified Mises-Hill criterion) at the most stressed point as a function of the reinforcement angle (varied from 0 to 90°) were plotted for different combinations of loads. The critical values of the shear stresses and axial tensile and compressive forces with respect to the bending moment of fiberglass-reinforced pipes with varying degrees of curvature were also plotted. The studies, which were performed for pipe with a curvature parameter of $\mu \leq 35$, established that annular or nearly annular ($\phi = 90^\circ$) is best for curved cross-ply fiberglass-reinforced pipes subjected to plane bending or the combined effect of flexural moment and internal pressure. Figures 5, table 1; references 7: Russian.

Laser Interferometry Investigation of the Size Stability of Graphite-Epoxy Resin Composite

93D0018C Riga MEKHANIKA KOMPOZITNYKH MATERIALOV in Russian No 4, Jul-Aug 92 (manuscript received 2 Apr 91; after revision 9 Dec 91) pp 508-515

[Article by Zh. Zhelkobayev, S.S. Sobolev, and G.A. Yurlova, All-Union Scientific Research Center for the Study of the Properties of a Surface and Vacuum, Moscow, and Moscow State University imeni M.V. Lomonosov; UDC 624.074:678.067:531.714.2]

[Abstract] The technique of laser interferometry was used to study the size stability of domestically produced

type KMU-4I graphite-epoxy resin composite. A stabilized He-Ne laser operating at a wavelength of 0.63299 μm was used for the studies. An IMTs 100 x 50 optical microscope was used to establish the starting linear dimensions of the study specimens. A total of 13 specimens were measured to determine their dimensional stability after various time intervals from 2.5 minutes to 6 hours. The studies performed established that laser interferometry is a most sensitive, precise, and reliable method of measuring microchanges in the geometric dimensions of materials such as KMU-4I graphite-epoxy resin composite specimens inasmuch as the changes that do occur in this material are on the order of fractions of the wavelength of laser radiation. The geometric dimensions of "dry" and "moist" specimens under natural conditions were found to drift during the first several hours of the measurement process. Different specimens had drifts with different signs: The "dry" specimens became saturated with moisture, and their linear dimensions increased. The "moist" specimens, on the other hand, underwent a swelling process, which is to say that their linear dimensions decreased. Preliminary treatment by thermal cycles stabilized the geometric dimensions of KMU-4I graphite-epoxy resin composite and increased its size stability. Wetting-drying cycles did not, however, increase the graphite-epoxy resin composite's size stability. The addition of reinforcing fibers in the surface layers of the graphite-epoxy resin composite only affected the size stability of dried specimens. Specimens in which the reinforcing fibers were arranged lengthwise underwent less drift. Specimens stored for an extended period and then chemically dried to a constant mass were found to possess the same size stability as freshly manufactured specimens subjected to treatment by thermal cycles. Figures 4, tables 4; references 7: 3 Russian, 4 Western.

Forecasting the Life of Hot-Pressed Ceramic Nozzles of Closed-Drift Thrusters by Comprehensive Nondestructive Tests

937D0018D Riga MEKHANIKA KOMPOZITNYKH MATERIALOV in Russian No 4, Jul-Aug 92
(manuscript received 20 Sep 91) pp 521-527

[Article by Ya.I. Bulbik, Krasnoyarsk Space Technology Institute; UDC 620.179.14:629.78.036.7]

[Abstract] From a design standpoint, the nozzle of a closed-drift thruster has the configuration of a body of revolution with an annular discharge channel that is intended to 1) generate a plasma flow from some active medium injected into the anode region of the activity medium and 2) accelerate the plasma flow formed and focused by the magnetic field in an axial electric field. The performance characteristics of the ceramic nozzle of a closed-drift thruster are determined by a set of electro-physical properties such as resistivity of its subsurface layers and resistance to thermal shock, ablation, and erosion. Local changes in the resistivity of a nozzle's surface layer due to high-temperature ablation and erosion processes in turn cause variations in the near-wall

conduction and variations in the thrust vector of the closed-drift thruster. All other conditions in the operation of a closed-drift thruster being equal, local discontinuities in the density of the hot-pressed ceramic composite used to manufacture its nozzle and other discontinuities in the regularity of its microstructure also accelerate the processes of the ablation and erosion of the nozzle's surface. Each of these hard-to-forecast factors plays an essential role in estimates of the life of a closed-drift thruster and, ultimately, the useful life of the spacecraft of which the closed-drift thruster and its nozzle are a part. The author of this article has proposed a procedure for predicting the life of hot-pressed ceramic nozzles of closed-drift thrusters by complex nondestructive evaluation methods that give consideration to each of the above factors. The method requires the combined application of the effects of thermal and strong pulse-excited electric fields to specimens of the ceramic used to manufacture the given nozzle. A simple model representing the mechanism of migration polarization is used for parametrization of the specimen's transient dielectric response. The theoretical analysis presented establishes that the effect of transient injection currents on the nondestructive testing data may be reduced by restricting the duration of the pulse-excited electric field. The analysis also confirms the presence of regions of decreased electric resistance, and lower energies of activation of the process of abrupt transfer of the electric charge carriers may be detected and monitored on the basis of a characteristic function of the redistribution of a test electric field on the surface of sensitive electrodes of an electric charge transducer. The proposed nondestructive testing method is said to also be suitable for use in similar situations, such as quality control of the advanced radar absorbing material (ADRAM)-class composite materials that are now used in aerospace technology and elsewhere. Figures 3; references 18: 10 Russian, 8 Western.

Flash Nondestructive Testing of Materials' Thermophysical Characteristics

937D0018E Riga MEKHANIKA KOMPOZITNYKH MATERIALOV in Russian No 4, Jul-Aug 92
(manuscript received 20 Aug 91; after revision
21 Nov 91) pp 534-538

[Article by O.Yu. Troitskiy, Tomsk Polytechnic Institute imeni S.M. Kirov; UDC 536.2+536.7.081]

[Abstract] Existing methods of determining materials' thermophysical characteristics may be subdivided into stationary and nonstationary methods. Nonstationary methods may in turn be further subdivided into purely nondestructive methods using only the initial stage of heating or cooling and methods based on a regular mode. The flash method is a purely nonstationary method of making a nondestructive determination of a material's thermophysical characteristics. It is based on solving the problem of the δ -pulse heating of the end surface of a plate with a specified thickness (L), a specified heat capacity (c_p), and a specified thermometric conductivity

(a). The addition of two new techniques, namely shift differentiation and step-by-step integration, to the flash method offers significant advantages over the conventional Parker method. Specifically, shift differentiation and step-by-step integration make it possible to determine a material's thermophysical characteristics by using just a portion of the temperature response function. They also eliminate errors due to heat losses and a finite pulse-time effect. The accuracy of shift differentiation and step-by-step integration was compared with that of the Parker method by comparing the results obtained by each method with the results of actual experiments involving tungsten disks (diameter, 20-32 mm; thickness, 1-2 mm) intended for use in rectifying elements. The measurements were made by using an infrared pyrometer based on an FSG-22-3A2 photoresistor. The proposed measurement methods, i.e., shift differentiation and step-by-step integration, produced the most reliable results. The error resulting from the use of the shift differentiation method did not exceed 2.4 percent, while that resulting from step-by-step integration did not exceed 1.75 percent, regardless of the thickness of the specimen. Figures 3, table 1; references 12: 6 Russian, 6 Western.

Casting of Aluminum Composites With Crystallization Under Pressure

937D0025D Moscow LITEYNAYE PROIZVODSTVO in Russian No 6, Jun 92 pp 14-16

[Article by N.N. Belousov, Institute of Mechanics; UDC 621.74.043.2: 669.715]

[Abstract] Formation of aluminum composites by the plasma-jet method has been improved by combining three operations: 1) injection of powder or fibers of a refractory metal such as titanium into the aluminum alloy melt by means of an argon (or other inert gas) plasma jet, the aluminum alloy having been formed by such injection of the alloying element to the aluminum melt; 2) mixing the components by means of an MHD device; 3) deeply penetrating ultrasonic treatment of the thus formed composite so as to ensure a microscopically as well as macroscopically uniform distribution of components. Sedimentation and subsequent local agglomeration of the reinforcing phase are avoided by casting with crystallization under pressure. The process has been adapted for combining aluminum alloys with thermodynamically stable compounds such as intermetallic ones covering a wide range of stoichiometry, particles of these compounds being injected into the melt after they had been purified by ion blast. Aluminum composites of the "Altik" type without and with 4 percent, 6 percent, 8 percent Ti respectively were produced by this method and also by vortex mixing of powder or fibers in the melt. Cylindrical and "cup" specimens of these composites cast by this method in a vertical hydraulic machine were, after plastic deformation by cold or half-hot working, tested for mechanical characteristics. Increasing the Ti content or the amount of intermetallic compounds was found to slightly improve their strength

characteristics at temperatures up to 350°C. Experimental batches of "Altik" pistons for internal combustion engines produced by this process in the experimental-industrial laboratory of the Perm Polytechnic Institute (T.N. Lipchin) were found to have a low-porosity fine-grain microstructure and excellent mechanical characteristics. Figures 2; tables 2; references 6.

Producing Cast Composites With Metal Base

937D0025E Moscow LITEYNAYE PROIZVODSTVO in Russian No 6, Jun 92 pp 16-17

[Article by V.G. Borisov, Scientific-Industrial Association: All-Russian Scientific Research and Planning Institute of Aluminum, Magnesium, and Electrode-Manufacturing Industry; UDC 621.74.011:669.715]

[Abstract] A new method of producing aluminum casting alloys is proposed, namely injection into the aluminum melt an intermetallic compound of the alloying element with aluminum and slowing down the diffusion processes in the liquid-solid state as well as in the solid state. Injection of a thus chemically bound alloying element prevents oversaturation in the solid state and thus allows adding more of this element, which facilitates development of new alloys. The technologically most important distinguishing feature of this method is that injection of solid additives at temperatures within the liquidus-to-solidus range results in an alloy which at this stage appears in the form of a suspension. In the solid state such an alloy has a wear resistance as well as a tensile strength and a modulus of elasticity by far exceeding those of conventionally produced aluminum alloys. The effectiveness of this method is demonstrated on the Al + 4 percent Fe casting alloy, iron having been added to liquid aluminum in the form of Al₃Fe particles and this intermetallic compound having been produced by self-propagating high-temperature synthesis. Another example is the Al + 5 percent Ni casting alloy, nickel having been added to liquid aluminum in the form of AlNi particles. The method is also applicable to Al-Si alloys used in composites with an up to 20 percent SiC fraction, a high wear resistance and a high modulus of elasticity being attainable without any loss of strength and plasticity. Figures 2.

Predicting Ultimate Strength of Unidirectionally Oriented Composite Material by Acoustic Emission

937D0027B Kiev TEKHNICHESKAYA DIAGNOSTIKA I NERAZRUSHAYUSHCHIY KONTROL in Russian No 3, Jul-Aug 92 (manuscript received 10 Apr 91) pp 43-46

[Article by Ye.S. Pereverzev, doctor of technical sciences, D.G. Borshchevskaya, candidate of physical and mathematical sciences, T.S. Tremba, T.Ya. Evina, and T.N. Bogomaz, Institute of Engineering Mechanics at Ukrainian Academy of Sciences, Dnepropetrovsk; UDC 620.179: 678.067]

[Abstract] An experimental study involving a unidirectionally oriented composite material was made, its object being to use acoustic emission for predicting the ultimate strength of such a material under uniaxial tension. The material consisted of EDT-10 epoxy and ZhSVM-5 synthetic high-modulus high-polymer reinforcing fibers. Flat specimens of this material were tested in UM-10, UM-104, and Instron machines at several different constant deformation rates covering the 5-10 mm/min range, the load being stepwise increased for successive tests. Acoustic emission signals were recorded with an NEZ-220 defectoscope and measured with an AF-15 instrument. Information was extracted from the number of acoustic emission pulses, total acoustic emission count N, rate of acoustic emission count, amplitude distribution of acoustic emission pulses, and acoustic noise. The specimens were also examined by metallographic methods under MIM-8M and Neophot-2 optical microscopes. The results of tests performed on nine specimens reveal that a wider peak of acoustic noise intensity indicates a lower tensile strength. A relation has been found to exist between the ultimate strength σ of this material and two parameters characterizing the acoustic noise generated in it under load: maximum intensity N of that noise and area S under the acoustic noise curve. A regression analysis has yielded the following general relation $\sigma = b_0 + b_1(\log N) + b_2S$ and specifically, for prediction of the breaking load $\sigma = 2758.5 - 219.48(\log N) - 18.91S$ with an average 2.45 percent error based on a 0.962 correlation coefficient. Figures 1; tables 1; references 4.

High-Temperature Kinetic Properties of the Contact Zones in Explosive-Welded Titanium-Based Bimetals

937D00404 Moscow TEPLOFIZIKA VYSOKIH TEMPERATUR in Russian, Vol 30 No 5, Sep-Oct 1992 pp 935-939

[Article by I. G. Korshunov; UDC 531]

[Abstract] Transition contact zone thermal conductivity and electrical resistivity were studied in explosive-welded titanium-zirconium, titanium-hafnium, zirconium-hafnium, titanium-tantalum, titanium-molybdenum, and titanium-tungsten bimetal specimens made from elements with a purity of 99.9 wt. percent. The specimen contact zones ranged in thickness from 21 to 122 μm . The two properties were studied at temperatures ranging from 800 to 1800 K. To measure contact zone thermal conductivity, the plane temperature wave method was used to generate experimental data on the effective temperature conductivity of thin (less than 0.7 mm) explosive-welded bimetal specimens and specimens made of the component metals only. These data were used in conjunction with the contact zone thickness values and available data on the heat capacity, density, and the coefficients of linear expansion of the component metals to construct polytherms of thermal conductivity for the bimetal specimens. All specimens were pre-annealed in an atmosphere of highly pure helium for

2 h at 1300 to 1500 K. Electrical resistivity was measured by using the Wiedemann-Franz law as a basis for constructing polytherms from the thermal conductivity data. It was found that the contact zones had low thermal and electrical conductivities (roughly 7 to 15 W/m K and resistivity of $220-900 \times 10^{-8} \Omega \text{ m}$, respectively) and activation-type conductance. The mean free path length of the electrons in the contact zones reached its maximum, meaning that it was equivalent to the average atomic spacing, and, in a number of instances, localization of the electron states was possible, indicating that the structure of the contact zone is highly disordered. This conclusion was corroborated by X-ray diffraction analysis performed with a DRON-3M, which showed that amorphization occurs in the contact zones during explosive welding. Figures 2, tables 1; references 15: 14 Russian, 1 Western.

Physical Properties of Zirconium-Barium Titanate-Lead/Nickel Ferrite Composite Ceramic

937D0041A St. Petersburg PISMA V ZHURNAL TEKHNICHESKOY FIZIKI in Russian Vol 18, No 15, Aug 1992 pp 27-30

[Article by V. M. Laletin, Viteb Division of the Institute of Solid-State Physics and Semiconductors and the Belarus Academy of Sciences; UDC 05.2; 12]

[Abstract] The physical properties of composite ceramics made from zirconium-barium titanate-lead (Z-BT-L) and nickel ferrite were studied. Specimens were made by sintering compacts pressed from mixtures of pre-synthesized ferrite and piezoelectric powders at 1200°C for two hours. The piezoelectric material was based on industrial-grade Z-BT-L-3. The specimens were polarized for one hour at room temperature in a 4 kV/mm electric field. E7-8 and E6-13A instruments were used to measure dielectric characteristics and resistivity. The magnetoelectric effect was determined by measuring induced electromotive force while a variable and a constant magnetic field were applied simultaneously to the ferromagnetic specimens. The results showed that, in sharp contrast to similar ceramics made with cobalt ferrite, this type of ceramic has very high resistivity throughout the range of component proportions tested. This property, which is attributed to the appearance of a high-ohm layer between the ferrite and piezoelectric grains, allows high magnetoelectric values to be obtained through high-voltage polarization and enables the ceramic to have a long charge-relaxation period (2-10 s), thus making it possible to construct devices that can operate within a wide frequency range. Permittivity and loss angle tangent behaved typically for composite materials of this type. This combination of properties and characteristics is superior to that of analogous ceramic materials. Figures 2; references 5: 3 Russian, 2 Western.

Effects of Radiation on the Physical Properties of Ferrite-Piezoelectric Composite Ceramics

937D0041B St. Petersburg PISMA V ZHURNAL TEKHNICHESKOY FIZIKI in Russian Vol 18, No 15, Aug 1992 pp 31-34

[Article by N. F. Kurilovich, V. M. Laletin, and V. V. Mikhnevich, Viteb Division of the Institute of Solid-State Physics and Semiconductors and the Belorus Academy of Sciences; UDC 05.2; 12]

[Abstract] A study was performed to determine how electron and gamma radiation affect the permittivity, loss-angle tangent, induced e.m.f., and the magnitude of the electromagnetic effect in ferrite-piezoelectric composite ceramic materials. Conventional ceramics technology was used to prepare the specimens, which consisted of 60 wt. percent zirconium-barium titanate-lead and 40 percent wt. percent nickel ferrite. The specimens were exposed to gamma-quantum irradiation on a Cobalt-60. The dose was 450 R/s, and specimen temperature did not exceed 60°C. Electron irradiation was performed on an ELU-4 electron-beam unit utilizing 4 MV of energy and a current density of 2×10^{12} el/sq cm. Three specimens were subjected to each type of radiation. The properties were measured before and after irradiation, and the results averaged and presented in the form of a relative change in values. The specimens proved to be resistant to the effects of radiation. The relative change in the value of the magnetoelectric effect did not exceed 10 percent, as the defects formed during irradiation had a negligible effect on polarization. Increases in permittivity and the loss-angle tangent and a reduction in induced e.m.f. were observed only at high gamma-radiation doses. In these cases, the appearance of defects in the interphase layer increases its conductivity and changes the role played by the piezoelectric-interlayer-ferrite chain from that of an electrical insulator to that of an electrical conductor. This increases the loss angle tangent and permittivity, and, if polarization remains unchanged, reduces induced e.m.f. It is reasonable to conclude that all ceramics of this type exhibit the same behavior. Figures 1, tables 1; references 4: 2 Russian, 2 Western.

Thermoelectric Materials for Temperatures Below 150 K

937D0041C St. Petersburg PISMA V ZHURNAL TEKHNICHESKOY FIZIKI in Russian Vol 18, No 15, Aug 1992 pp 79-82

[Article by V. A. Kutasov, M. V. Vedernikov, P. P. Konstantinov, Yu. I. Ageyev, G. T. Alekseyev, L. N. Lukyanova, Yu. I. Ravich, and M. I. Fedorov; UDC 05.2; 12]

[Abstract] Researchers investigated the possibility of using specially developed thermoelectric materials based on solid solutions of bismuth and arsenic chalcogenides to make coolers for high-temperature semiconductor applications at temperatures between 80 and 150 K. The

relationships between temperature and electrical conductivity, thermoelectromotive force, and thermal conductivity were used as a basis for analyzing the relationship between temperature and the thermoelectric merit value (z), while taking the effective charge carrier scattering parameter into account. This analysis revealed that, in the n- $\text{Bi}_2\text{Te}_{2.7}\text{Se}_{0.3}$, a decrease in temperature can lead to an increase in z . The concentration of charge carriers was optimized by adding stoichiometrically surplus Te to the melt. This had the effect of shifting the maximum z value to the 240-250 K region and the average z value to $2.75 \times 10^{-3} \text{ K}^{-1}$ at temperatures between 140 and 220 K. A similar result was achieved with the directionally crystallized p- $\text{Bi}_{2-x}\text{Sb}_x\text{Te}_3$ by substituting not more than 3 at. percent Se atoms for Te atoms, provided $x < 1.5$. Both materials were used to make the two cold cascade junctions in a four-junction thermoelectric cooler, in which a coolant mixture of ethanol and carbon dioxide was used to keep the temperature of the hot cascade junction at 225, thereby obviating the construction of powerful pre-cooling cascade junctions. Thermal stresses were also minimized by making the hot cascade junction from four separate components. Element distribution among the four junctions was 2:10:74:388, required power was 45 W, and power supply current was 16 A. A temperature of 142 K was obtained on the cold junction of the upper cascade junction. Lower temperatures can be achieved by refining the thermoelectric materials and optimizing cooler design. Figures 2; references 9: 6 Russian, 3 Western.

The Physicochemical Basis of Creating Composite Ceramic Materials Based on Refractor Compounds

937D0051D Moscow OGNEUPORY in Russian No 9-10, Sep-Oct 92 pp 10-14

[Article by S.S. Ordanyan, Saint Petersburg Technological Institute; UDC 666.798.2.001.4]

[Abstract] Information regarding the compatibility of refractory metals with different refractory compounds may be obtained by analyzing the structure of the phase diagrams or phase relationships in the Me'-X-Me'' (X = B, C, N, O) systems on which sintered composite ceramic materials (cermets) are based. These systems may be tentatively divided into four groups: 1) systems involving metal analogues in which both metals and metal compounds form unsaturated solid solutions; 2) systems involving metals from adjacent groups in which three-phase equilibrium fields appear; 3) systems in which an Me'-X-Me'' section triangulates the system (which is to say when the condition of the compatibility of an Me'-based refractory compound with an Me'' refractory metal is met); and 4) systems in which ternary compounds are realized. Only the third of these four types of compounds can serve as the basis for selecting quasi-binary Me'-X-Me'' systems that can in turn be used as a basis for creating sintered cermets with improved strength and fracture toughness, as well as for dispersion

strengthening of metal alloys with solid refractory phases. The author of this article has presented a classification system that encompasses all possible and thermodynamically permissible (from the standpoint of the principle of phase compatibility) combinations of refractory compounds into quasi-binary systems. The classification system is recommended for use in performing such materials science-related tasks as selecting hardening phases in metal alloys, creating diffusion barrier layers and protective coatings, and creating composite

materials themselves. The proposed classification of quasi-binary systems may also be used to establish the most important quasi-ternary and quasi-quaternary systems involving refractories. The author concludes by noting that the vast majority of possible systems are eutectics that may in turn serve as the basis for producing a large group of oriented-crystallization eutectics with a unique combination of physicomechanical properties. Figures 3, table 1; references 15: Russian

Failure of Carbon Tool Steel During Heat Treatment

927D0259G Moscow *IZVESTIYA VYSSHIKH UCHEBNYKH ZAVEDENIY: CHERNAYA METALLURGIYA* in Russian No 6, Jun 1992 pp 58-60

[Article by V. S. Starikov, Siberian Metallurgical Institute; UDC 669.046:621.78.019]

[Abstract] Failures caused by unfavorable heat-treating conditions were studied in three carbon tool steels. Cylindrical and square billets of U7, U8, and U12 steels 65 to 160 mm in width and 200 to 680 mm in length underwent intensive symmetrical heat treatment in a cylindrical kerosine-fired chamber furnace or in an electric Tamman furnace. The specimens were heated to a temperature lower than that which would induce structural transformations, and some were cooled in a tank with running water. The specimens were annealed to remove residual thermal stresses and were then examined to determine the effects of the heating and cooling conditions. The specimens were ultrasonically inspected for ruptures both before and after heat treatment. Platinum-rhodium/platinum thermocouples and a high-speed multi-point electronic potentiometer were used to measure and record temperatures every three seconds. The study showed that change in the cross-section temperature differential is extreme in nature and that the failure-inducing temperature difference is the maximum difference that occurs in the region of temperatures associated with elastic and elasto-ductile deformation in the steel. Visual inspection of the cracks found in some of the specimens showed that they formed as a result of tearing. The cracks were deep and, for the most part, ran along the length of the specimens. The fracture surfaces had a crystalline structure. These types of cracks constitute a first-order failure and, in terms of size, are several orders of magnitude larger than the structural elements and cause the specimens in question to break completely apart. The thermographic data obtained in the experiment was used to construct graphs and formulas that can be applied to calculate core and surface temperature differences that will not result in product failure. Figures 4; references 3: Russian.

Formation of and Adsorbed Impurity Film at Its Boundary With a Fine Solid Solution Layer

937D0007A Kiev *METALLOFIZIKA* in Russian Vol 14 No 4, Apr 92 pp 28-34

[Article by E. L. Feldman, T. N. Fursov, and V. M. Yurchenko, Institute of Applied Physics, Donetsk; UDC 620.191.8:620.192]

[Abstract] Mathematical analysis was used to investigate the segregation process that occurs on a free surface due to the diffusive mass transfer of impurities from the finite bulk of a material to its surface. The equations adduced describe the relationships between time and, respectively, surface segregation, rate of segregation, and the concentration of impurity in the specimen. The

analysis showed that, initially, there occurs an almost complete elimination of impurities in that part of the solid solution that is contiguous with the adsorbed film. The concentration profile then behaves differently depending on whether the film is thick or thin. In a thick film, due to the inflow of impurities from remote regions, the concentration in the near-film zone begins to increase. In a thin film, this growth does not take place because of an insufficient quantity of impurity. Therefore, pronounced depletion gradually reaches parts of the layer that are further and further away from the adsorbed film until the specimen is virtually free of impurities. Graphs of concentration profiles at different points in time can be easily constructed from one of the equations (18). References 6: 5 Russian, 1 Western.

Characteristics of Martensitic Transformation and the Shape Memory Effect on TiNi Alloys Microalloyed With Cr and Cu

937D0007B Kiev *METALLOFIZIKA* in Russian Vol 14 No 4, Apr 1992 pp 39-45

[Article by V. A. Lobodyuk and M. M. Medykh, Institute of Physical Metallurgy of the Ukrainian Academy of Sciences, Kiev; UDC 536.42:539.37]

[Abstract] Microalloying with 0.43-1.20 at. percent Cr or 0.36-0.80 at. percent Cu and thermal cycling (1-100 cycles) were studied to determine their effect on the characteristics of martensitic transformation and shape memory in equiatomic TiNi alloys. Twenty-gram ingots were made in an electric-arc furnace in a purified argon atmosphere by remelting electrolytic Ni and iodide-process Ti five times. The ingots were annealed in sealed vacuum quartz ampules at 1273 K for 5 h and quenched in a 10 percent aqueous NaCl solution. Alloy composition was determined using X-ray fluorescence analysis. Specimens 20 x 3 x 0.7 mm were cut from the specimens and chemically reduced to a thickness of 0.30 mm. Current and potential leads made of copper wire and two copper-Constantan thermocouples were spot-welded near the ends of the specimens to measure the characteristic transformation temperatures from deviations in the linear temperature coefficient of resistance. Shape memory was tested by bending the specimens around a mandrel 4 mm in diameter and measuring reversible deformation in a special optical cryostat. It was learned that negligible quantities of alloying elements (0.4 at. percent Cr or Cu) are sufficient to induce change in the martensitic transformation characteristics. TiNi alloys containing up to 1 at. percent Cu exhibit a B2 to R to M phase transformation sequence. The rhombohedral R-phase does not form when the concentration of Cu exceeds 5 at. percent. Five thermal cycles are sufficient to cause fundamental changes such as a drop in the characteristic martensitic transformation temperature and an increase in hysteresis and direct and inverse martensitic transformation intervals. Full shape recovery of the original phase in the martensitic state occurs only in those alloys with 0.83 or 1.20 at. percent Cr; in those alloys with other Cr or Cu concentrations,

shape recovery varies from 50 to 90 percent. Figures 2; tables 2; references 9: 5 Russian, 4 Western.

Studying the Effect of the Cooling Rate on the Structure of Chromium Alloys With Zirconium Carbide

937D0007C Kiev METALLOFIZIKA in Russian
Vol 14, No 4, Apr 1992 pp 46-52

[Article by V. G. Ivanchenko and V. V. Pogorelaya, Institute of Physical Metallurgy of the Ukrainian Academy of Sciences, Kiev, and O. N. Samgina and A. G. Fridman, VILS [All-Union Light Alloy Institute] Scientific Production Association, Moscow; UDC 669.26:548.5]

[Abstract] An effort was made to establish cooling conditions that would ensure the uniform distribution of zirconium carbide particles throughout a chromium matrix, with the dispersity being higher than that obtainable by mechanically working and heat-treating the ingots. Specimens weighing 50 g were made in a laboratory electric-arc furnace from electrolytic chromium, iodide-process zirconium, and spectrally pure graphite remelted five times by a non-consumable tungsten electrode in a copper water-cooled crucible in a purified argon atmosphere at an overpressure of 30 kPa. The melt was poured into permanent copper molds 8, 12, and 16 mm in diameter. The effect of the cooling rate on the structure of pre-eutectic alloys with a low eutectic degree was studied by suspension casting into graduated permanent copper molds with sections 16, 8, 4, and 2 mm in diameter and by solidifying strip 30 to 150 μm thick on a copper disk rotating at 2,000 to 5,000 min^{-1} . (For the latter specimens, the melt was made in a helium atmosphere at an overpressure of 50 kPa.) Specimen structure was studied on compacts extruded from the strip at 1200°C in steel capsules and compared with heat-treated specimens. It was found that the eutectic in Cr-ZrC alloys belongs to the polyhedral-dendritic class; ZrC is the phase that starts and promotes eutectic crystallization. Increasing the cooling rate to 10^3 K/s and higher yields a fine-grained chromium structure with ZrC particles dispersed both inside the grains and along the grain boundaries in specimens with a thickness of 4 mm or less. A cooling rate of about 10^5 K/s combined with hot extrusion yields a material with a uniform distribution of dispersed ZrC that is preserved even after high-temperature soaking. Figures 4; references 16: 12 Russian, 4 Western.

Effect of the Composition of Amorphous Iron and Cobalt-Based Metal Alloys on Their Electron Structure

937D0007D Kiev METALLOFIZIKA in Russian
Vol 14, No 4, Apr 1992 pp 66-69

[Article by V. L. Karbovskiy, A. P. Shpak, and A. N. Yaresko, Institute of Physical Metallurgy of the Ukrainian Academy of Sciences, Kiev; UDC 535.33/.34]

[Abstract] Two methods, one experimental and one theoretical, were used to study $\text{Co}_{80}\text{B}_{20}$, $\text{Co}_{80-x}\text{Fe}_x\text{B}_{20}$ ($x = 6, 10, 20$), and $\text{Co}_{85-x}\text{Fe}_x\text{B}_{15}$ ($x = 60, 73$) amorphous metal alloys in order to learn how their composition affects their electron structure. The experimental method, X-ray emission spectroscopy, was performed using fluorescence excitation to obtain Fe and Co X-ray $\text{K}\alpha_{1,2}$ and $\text{K}\beta_1$ -emission spectra on a DRS-2M spectrophotograph. For the theoretical analysis, $\text{K}\alpha$ -bands were recorded by an RSM-500 spectrometer in order to calculate clusters for modelling the effect of the nearest atomic orbit on electron structure. The spectroscopic data and the model cluster calculations led to the following conclusions: When the number of cobalt atoms in the nearest iron atom orbit is increased, spinning electron density is transferred downward from the iron to the cobalt, leading to an increase in the local magnetic moment on the iron atom and to a decrease in this property on the cobalt atoms; in amorphous metal FeCoB alloys, there is an effective charge transfer from the boron atoms to the metal atoms that is substantially greater for the cobalt than for the iron; the local magnetic moment on the iron increases as the concentration of cobalt in the alloy increases, reaches a maximum in alloys with equal concentrations of iron and cobalt, and then begins to decrease; the inverse is true for the magnetic moment on the cobalt. Figures 4, references 6: 4 Russian, 2 Western.

Effect of Annealed VT16 Titanium Alloy Structure on Its Resistance to Brittle Failure and Toughness Reserve

937D0007E Kiev METALLOFIZIKA in Russian
Vol 14, No 4, Apr 1992 pp 70-74

[Article by O. M. Iavashin, P. Ye. Markovskiy, Yu. Ya. Meshkov, G. A. Pakharenko, and A. V. Shevchenko, Institute of Physical Metallurgy of the Ukrainian Academy of Sciences, Kiev; UDC 669.14:539.89]

[Abstract] The influence of structural parameters on the mechanical properties of VT16 titanium ($\alpha + \beta$)-alloy was studied. The metal was heat-treated in various ways to effect wide variations in β -grain size, the size of the α -phase columns, the thickness of the α -plates in the columns, and the thickness of the grain boundary α -phase. All heat-treating procedures were carried out in a vacuum furnace with a negative pressure of at least 10^{-3} Pa . Metallographic analysis was performed on a NEO-PHOT-32 microscope. Fracture surfaces were examined on a JEM-35CF electron microscope. The aforementioned structural parameters were measured and statistically analyzed on a Morphomet automated statistical processor. The mechanical properties (strength σ , yield stress $\sigma_{0.2}$, ultimate stress S_u , and necking ψ) of standard cylindrical specimens were tested on an Instron-1251 equipped with a low-temperature chamber in which the temperature could be varied from +20°C to -196°C. When necessary, brittle failure tests were performed with the aid of a helium cryostat. The experimental data showed that the brittle failure resistance of the plate

structures of annealed VT16 alloy does not depend on the size of the β -grains or the α -plate packets; rather, it is determined by the thickness of the grain boundary α -phase. This structural parameter is also the key to the alloy's toughness reserve and reaches its greatest value when the thickness of the outline of the α -phase β -grain is minimal. Figures 4, tables 1; references 2: 1 Russian, 1 Western.

Properties of and Possible Applications for Superferritic Steel EP882

937D0022D Moscow TYAZHELOYE MASHINOSTROYENIYE in Russian No 7, Jul 92 pp 33-35, 37

[Article by S.P. Tomina, candidate of technical sciences, V.I. Gerasimov, candidate of technical sciences, and A.V. Ryabchenkov, doctor of chemical sciences, Scientific-Industrial Association Central Scientific Research Institute of Heavy Machinery; UDC 669.14.018.8+669:620:197]

[Abstract] A superferritic Cr-Mo economy steel with a higher than 25 percent Cr content but no nickel content has been developed which, like all superferritic steels, is resistant to intergranular corrosion and has a much lower cold-shortness threshold than open-hearth ferritic ones. It can therefore be cold rolled and be welded without preheating. The steel was tested for resistance to stress corrosion and crevice corrosion as well as for general corrosion resistance in water with a high Cl-ion ($MgCl_2$, $NaCl$) and/or oxygen content. It was tested for heat resistance at temperatures up to 350°C under pressures up to 16.5 MPa. Each test revealed its superiority over the conventional E1448 18Co-2Mo (10Cr17Ni13Mo2Ti) steel. The results of these tests along with the thermophysical and mechanical properties of this steel recommend it for heat exchangers and auxiliary equipment in nuclear and thermal electric power plants, typically for condensers and steam generators in nuclear power plants operating with RK-50 MW and RBMK-1000 MW channel reactors. The steel is also suitable for apparatus used in the cellulose-paper and other chemical industries. Figures 3; tables 6; references 12.

Effect of Spheroidizing Modification on Mechanical Properties of Cast Irons With Spheroidal Graphite

937DF0025C Moscow LITEYNAYE PROIZVODSTVO in Russian No 6, Jun 92 p 8

[Article by G.A. Kosnikov, E.N. Korniyenko, and L.M. Morozova, St.Peterburg State Technical University and Industrial Association "Yelgava Automobile Manufacturing Plant"; UDC 621.74:669.131.7]

[Abstract] Spheroidizing was selected as method of producing ingots of austenitic-bainitic high-strength nodular cast irons: 600 MPa minimum compressive strength

and 380 MPa minimum 0.2 percent yield strength without heat treatment, 900 MPa and 520 MPa respectively after isothermal heat treatment. Cast irons containing 3.45-3.65 percent C, 0.2-0.25 percent Mn, up to 0.08 percent P, up to 0.02 percent S were selected for this process. Converter iron was melted in an MGP-2 high-frequency induction furnace-crucible with a basic lining, with carbon-steel and ferro-alloy tailings added to the charge and with modifiers added in the ladle. As spheroidizers were used ZhKMK-4R ferrosilicon (49.6 percent Si, 9.5 percent Ca, 8.6 percent Mg, 4.7 percent rare earth metals), 91.4 Cu - 8.6 Mg alloy, and 90 Ni - 9 Mg - 1 Ce alloy. As graphitizer was used FS75 ferro-alloy and as flux was used K2 cryolite. Four different combinations of modifiers were tried: 1) 2.5 percent ZhKMK-4R for the cast irons containing also 2.9-3.1 percent Si; 2) 0.6 percent Ni-Mg-Ce alloy + 0.6 percent Cu-Mg alloy + 0.6 percent FS75 for the cast irons containing also 2.4-2.6 percent Si, 0.49-0.52 percent Cu, 0.48-0.52 percent Mg; 3) 1.1 percent Ni-Mg-Ce alloy + 0.6 percent FS75 for the cast irons containing also 2.4-2.6 percent Si, 0.85-0.93 percent Ni; 4) 1.2 percent Cu-Mg alloy + 0.6 percent FS75 for the cast irons containing also 0.78-0.81 percent Cu. An austenitic-bainite structure was obtained by heat treatment in two stages: austenitization at 900°C in a salt bath for 30 min (hardenability test specimens for one hour) - isothermal heat treatment in a niter bath for two hours successively at 1) 300°C, 2) 350°C, 3) 380°C, followed by air cooling. In a separate experiment FS-Mn5 alloy was used as modifier, but added in the mold. Tables 1; references 1.

On Steel-Hydrogen Interaction Mechanisms at High Temperatures and Pressures

937D0038D Moscow METALLY in Russian No 5, Sep-Oct 92 pp 38-44

[Article by M.I. Kaplan, St. Petersburg; UDC 669.14:669.788:639.4]

[Abstract] Two phenomena accompanying the failure of steel under a high-temperature hydrogen attack—methane formation in the microcavities and voids and steel interaction with hydrogen which leads to decarburization—are outlined, and the priority ranking of these two processes and their relative effect on the growth of microvoids under extended steel contact with hydrogen at high temperatures and pressures are discussed. The concept of the methane pressure rise's effect on an increase in internal stresses and structural changes is debated, and the carbide decay mechanism and carbon impoverishment of the ferrite matrix are addressed. The carbide dissolution process is examined; the carbide mobility distribution in the sample and the theoretical and experimental incubation period of St20 as a function of pressure are plotted. The incubation period is inversely proportionate to the equilibrium concentration of mobile carbon which, in turn, is inversely proportionate to the carbide component stability. The conclusion is drawn that the microvoid growth under the effect of tensile stresses forming due to the decay of the carbide

component rather than the methane pressure is the dominant factor in steel failure. Figures 3; references 13: 8 Russian, 5 Western.

On Cerium's Gaseous Hydrogen Removal Ability in Liquid Fe-C Melts

937D0038E Moscow METALLY in Russian No 5,
Sep-Oct 92 pp 45-49

[Article by L.P. Vladimirov, T.G. Sabirzyanov, N.V. Bosyy, Kirovograd; UDC 669.536.7]

[Abstract] The increasing use of rare earth metals (RZM) in metallurgy and the scarcity of data on whether cerium, which accounts for half of rare earth metals in the earth crust, promotes the removal of gaseous hydrogen from pig iron and steel prompted an investigation into cerium's hydrogen removal ability in liquid Fe-C melts. To this end, a thermodynamic analysis of four cerium

hydride formation reactions are conducted for a 0.1 percent Ce and 0.01 percent hydrogen concentration within a 1,400-2,000K temperature range. To compare the spread of the results, the equilibrium characteristics of each reaction are determined by approximate single-step method, almost precise single-step method, and precise Vladimirov-Vagner method. The dependence of the Gibbs energy on temperature for Ce and H₂ dissolved in the melt vs. Gibbs interaction energies of pure substances is plotted. An analysis of the data shows that cerium which is a highly efficient deoxidizing agent and pig iron and steel inoculant does not promote hydrogen gas removal due to the thermodynamic impossibility of its hydride formation under the conditions where liquid Fe-C melts exist. The real values of the isobaric reaction potential produced allowing for the elevated hydrogen bubble pressure also point toward the impossibility of cerium interaction with hydrogen. Figures 3; tables 3; references 6.

Phase Transitions in Reduction of Magnesioferrous Ilmenites

927D0258A Moscow METALLY in Russian No 3,
May-Jun 92 pp 12-15

[Article by N. I. Talmud, M. S. Model and T. V. Olyunina; UDC 669.094.1:553.31'494]

[Abstract] With the location of potential deposits of ilmenites containing from 6 to 18 percent MgO, it was of interest to investigate the effect that the amount of magnesium has on the character of phase transitions in the mineral. Roentgenography, mineralogy, and analytical chemistry techniques were used to study phase transitions in the reduction of monomineralic magnesioferrous ilmenites (1.46-15.58 percent MgO) at 1250° C. It was found that as iron and titanium are reduced simultaneously, two solid solutions of variable composition are formed which contain titanium of lower valences: anosovite and tagirovite. Lattice constants were determined for them, and it was demonstrated that these constants depend on the degree of reduction of iron from the starting material. The presence of magnesium in lattices of tagirovite and anosovite promotes two main reactions simultaneously: formation of anosovite from tagirovite and of tagirovite from anosovite, which leads to prolonged conservation of iron in both phases.

Mechanism of Formation of Titanium Carbide in the Process of Carbothermic Reduction of Titanium Dioxide

927D0258B Moscow METALLY in Russian No 3,
May-Jun 92 pp 16-21

[Article by V. D. Lyubimov, T. A. Timoshchuk and M. V. Kalacheva; UDC 669.295.34]

[Abstract] Intermediate products of titanium dioxide's interaction with carbon at 1300 and 1700° C in a vacuum were investigated using chemical, X-ray phase, and electron microscope methods of analysis. It was found that titanium dioxide's reduction by solid carbon proceeds sequentially through all oxide phases that exist in the stable constitution diagram and ends with disproportionation of titanium monoxide with subsequent interaction of the metallic phase. As the temperature increases, the amount of oxygen in the end product decreases, and the equilibrium moves toward formation of titanium carbide, which in the conditions of the experiments formed at 1700° C. In the process there is a change in the granulometric composition of the reaction products due to recrystallization. By varying the time and temperature, it is possible to produce a large effect on the chemical as well as granulometric compositions of the end product.

Aluminum-Lithium Alloys for Aircraft Weldments

927D0258F Moscow METALLY in Russian No 3,
May-Jun 92 pp 117-119

[Article by I. N. Fridlyander, A. G. Bratukhin and V. G. Davydov; UDC 669.715'884-122:620.17]

[Abstract] Characteristic properties of sheets made of the aluminum-lithium alloy 1420 are presented: ultimate strength, yield strength, elongation, resistance to low-cyclic fatigue, growth rates of fatigue cracks, and characteristics of welds. Technological parameters of melting, casting, and deformation of blanks made of alloy 1420 are reviewed. The effectiveness of alloy 1420 used in aircraft weldments is discussed. The welded fuselage made of the alloy on the MIG-29 airplane made it possible to reduce the weight by 24 percent in comparison with a riveted fuselage made of duralumin, including by 12 percent thanks to lower density of the alloy and 12 percent thanks to elimination of sealants and riveted and bolted connections. In addition, the amount of labor employed in fabricating the fuselage was reduced, and the health hazard posed by riveting was eliminated.

Structure and Properties of the Aluminum-Lithium Alloy 1430

927D0258G Moscow METALLY in Russian No 3,
May-Jun 92 pp 120-125

[Article by F. M. Yelkin, N. A. Naryshkina, V. N. Ananyev, A. V. Rudoy; UDC 669.715'884:669.017.3]

[Abstract] The effect of extrusion temperature and degree of deformation during post-quenching cold straightening on the structure and properties of extruded strips of the aluminum-lithium alloy 1430 was investigated. Data on the chemical composition, mechanical properties after extrusion, and effect of different time periods of natural ageing on mechanical properties of strips of alloy 1430 are presented. Optimum ageing conditions were determined for the alloy (125-150° C, 16-64 hr), and diagrams of levels of mechanical properties and phase transitions were constructed. The alloy is not susceptible to notching. Heat treatment conditions which result in practically total absence of anisotropy of properties in a strip with section 15X220 mm are adduced.

Carbide Phase Stability in Ni-Nb-Cr-C System Alloys

937D0038F Moscow METALLY in Russian No 5,
Sep-Oct 92 pp 92-95

[Article by O.M. Barabash, I.V. Burya, S.P. Oshkaderov, Kiev; UDC 661.8:621]

[Abstract] Violations of the γ -NbC interface and the fiber itself in eutectic composites due to the carbide formation in γ -NbC alloys which are widely used for

making high-temperature materials prompted a thermodynamic analysis of the phase stability on the Ni-Nb-Cr-C system in the areas rich in nickel within a 400-1,400°C temperature range at discrete Cr concentration steps within a 0-20 percent range. The interstitial element concentration in the four-component A-B-Q-C system in the case of a γ -solid solution-interstitial phase equilibrium is analyzed for solid solutions with an FCC lattice. The thermodynamic parameters used in computing the interstitial element solubility are summarized and the isothermal cross sections of the Ni corner of the Ni-Nb-Cr-C constitution diagram at various Cr concentrations are plotted. The findings show that at a Cr concentration under 10 percent, the phase composition remain unchanged and as the Cr content rises to 20 percent, the chromium carbide formation in the alloy becomes likely; of the various carbides forming in the system, Cr_3C_2 is more stable at low temperatures of 400-600°C and Cr_7C_3 —at high temperatures of 1,200 to 1,400°C. The free carbon domain (for Cr content) is the widest at medium temperatures of 800-1,200°C. Figures 1; tables 1; references 11.

Fusibility Diagram of Mn-Cu-C System

937D0038G Moscow METALLY in Russian No 5.
Sep-Oct 92 pp 158-163

[Article by Yu.A. Kocherzhinskiy, O.G. Kulik, Kiev;
UDC 669.3'74'784.017.13]

[Abstract] The lack of data on the behavior and properties of Mn-Cu-C systems and their constitution diagrams and the uncertainty about the carbide development in the system prompted differential thermal, metallographic, and radiographic analyses of the Mn-Cu-C alloys in the cast state. The samples for the study are prepared from OSCh-grade GMZ graphite, electrolytic Mn, and oxygen-free Cu. The samples are made mostly by fusing the initial components in MgO crucibles in an Ar atmosphere. A number of ternary alloys is made from alloying compositions. A portion of the Mn-Cu-C constitution diagram liquidus projection on the concentration triangle at an up to 40 percent oxygen content and polythermal $\text{C}-\text{Cu}_{60}\text{Mn}_{40}$ and $\text{C}-\text{Cu}_{20}\text{Mn}_{80}$ cross sections of the Mn-Cu-C constitution diagram are plotted. Nonvariant and monovariant equilibria in the fusibility domain of the Mn-Cu, Mn-C, Cu-C, and Mn-Cu-C systems are summarized. Limited solubility of components in the Mn-Cu-C liquid system and the existence of five nonvariant equilibria three of which participate in the immiscible liquid are established. Figures 3; tables 3; references 4: 2 Russian, 2 Western.

Effect of Crystal Phase Structure on Y, Sm-Li-Ga Constitution Diagram

937D0038H Moscow METALLY in Russian No 5.
Sep-Oct 92 pp 206-209

[Article by Yu.N. Grin, A.A. Fedorchuk, Lvov; UDC 548.736.4]

[Abstract] X-ray phase analyses (RFA) of a number of Y, Sm-Ga and Y, Sm-Li alloys annealed at a 470K temperature are conducted in order to check published data and obtain standard powder patterns of double gallides; the alloys for the X-ray phase analyses in ternary systems are made by fusing a charge with varying compositions. These X-ray phase analyses of 20 alloys confirm the existence of $\text{LiGa}_{3.42}$, Li_5Ga_4 , Li_3Ga_2 , Li_2Ga , and Li_3Ga compounds. The atomic coordinates and anisotropic temperature corrections in the $\text{Sm}_{1-x}\text{Ga}_2$ system and the crystallographic features of Y, Sm-Li-Ga compounds are summarized and the projections of the $\text{Sm}_{1-x}\text{Ga}_2$ system on the yz plane and the coordination polyhedrons of Sm and Ga atoms as well as the isothermal cross section of the Y-Li-Ga and Sm-Li-Ga system phase equilibria are plotted. The dual crystal chemistry role of lithium in the systems under study is noted. New ternary gallides are discovered in some Y-Li-Ga and Sm-Li-Ga systems and immiscibility is observed in binary Y, Sm-Li systems. Attempts to establish the crystal structure of some compounds were unsuccessful as were attempts to confirm multiple Sm substitution with Ga atom pairs. Figures 2; tables 2; references: 3 Western.

On Interaction Patterns in $\text{YB}_6-\text{Me}^{\text{IV-VI}}\text{B}_2$ Systems

937D0038I Moscow METALLY in Russian No 5.
Sep-Oct 92 pp 213-214

[Article by S.S. Ordanyan, Ye.Ye. Nikolayeva, I.K. Khoroshilova, St. Petersburg; UDC 621.462]

[Abstract] The constitution diagrams of pseudobinary $\text{YB}_6-\text{Me}^{\text{IV-VI}}\text{B}_2$ systems which are described by eutectic constitutions diagrams in which the components are characterized by a virtually total lack of reciprocal solubility in the subsolidus area are examined using traditional methods of physical and chemical analyses. The melting point, eutectic temperature, stability loss factor, formation heat, and other properties of the system under study and its components are summarized; the constitution diagram of the TB_6TiB_2 and YB_6CrB_2 systems and the dependence of the MeB_2 formation heat on its concentration in the eutectics are plotted. The donor-acceptor properties of transition metals which determine the strength and chemical bond character in refractory compounds are discussed. Figures 2; tables 1; references 7.

Cu- and Fe-Doping of Cu_{2-x}Se Alloys

937D0043N Moscow FIZIKA I KHIMIYA
OBRABOTKI MATERIALOV in Russian No 5.
Sep-Oct 92 pp 150-156

[Article by M.A. Korzhuyev, V.F. Bankina, Moscow;
UDC 546.56'231;546.682]

[Abstract] The possibility of doping thermoelectric semiconductor materials with a loose crystal lattice with fast diffusing dopants by the method of autoelectrochemical

injection (AEKhL)—a version of electrochemical injection of the dopant spontaneously in shorted electrochemical cells—is considered, and an elevated diffusive mobility of Fe in Cu_{2-x}Se is reported. Joint Fe- and Cu-doping by injecting the dopant into the material by two methods is studied: from the melt and by autoelectrochemical injection at room temperature. The experimental procedure is outlined in detail, and a section of the Cu-Fe-Se system constitution diagram is shown. The dependence of electric conductivity, thermoelectromotive force, and EMF of galvanic cells in alloys under study on the Fe concentration in various cross sections, the dependence of the hole mobility, Fermi energy, and effective mass of the state density on the Fe content in various cross sections, the dependence of the galvanic cell EMF on the Se content in the alloy, and the dependence of the thermo-EMF on the sample exposure to a shorted galvanic cell are plotted. The findings point toward the donor action of Fe and make it possible to establish its limit of solubility in the solid solution (about 5 percent). The interaction of fast diffusing dopants added from the melt and by electrochemical injection with each other is examined, and it is shown that the properties of doped alloys do not depend on the doping method. Figures 5; tables 1; references 10: 9 Russian, 1 Western.

On Relation Between α_1 - and α_2 -Phase Precipitate Morphology and Hysteresis Loop Shape in BCC Fe-Cr-Co-Mo Alloy Singles Crystals

937D0049A Yekaterinburg FIZIKA METALLOV I METALLOVEDENIYE in Russian No 3, Mar 92 pp 46-52

[Article by B.Ye. Vintaykin, V.A. Golikov, V.V. Dudarev, Institute of Physics of Metals and Metal Science at the Central Scientific Research Institute of Ferrous Metallurgy imeni I.P. Bardin; UDC 669.15'26'25'28:548.73]

[Abstract] The study of BCC Fe-Cr-Co-Mo alloy single crystals which began in *FMM* No. 6, 1990 is continued. The single-phase α -solid solution stratification into a highly magnetic Fe- and Co-enriched phase (α_1) and a weakly magnetic Cr-rich phase (α_2) is discussed, and the correlation between the magnetic properties and morphology of α_1 - and α_2 -phase precipitates in Fe-Cr-C-Mo alloy's Bridgeman-grown single crystals is studied in detail. All samples are α -solution hardened and heat treated by gradual tempering (SO) and diffusion annealing (GO). The magnetic properties are measured in a closed magnetic flux in a slowly varying field in the [001] direction and in a number of special cases—in the [100] direction; both minor and major hysteresis loops are recorded. The most representative conditions of the initial stage of alloys with and without heat treatment (TO) and the volume fraction of the α_1 -phase after heat treatment is summarized, and the hysteresis loops of alloys after various heat treatment conditions as well as the magnetic hardness spectrum of the hysteresis loops are plotted. The structural features of the alloys are

studied, and such magnetic properties as independent coercive force and hysteresis loop squareness control, hysteresis loop shape control in various sections, and partial magnetization reversal cycles are examined. By forming the corresponding structure, one can develop magnetic materials with a specified range of properties. One can also attain structural states with special α_1 - and α_2 -phase distributions in the magnetization reversal field strength domain which are characterized by a quasiconstant relative squareness and coercive force of minor hysteresis loops. Figures 5; tables 1; references 7: 4 Russian, 3 Western.

Grain Boundary Current Carrier Scattering in Thin Ti-Group Metal Films

937D0049B Yekaterinburg FIZIKA METALLOV I METALLOVEDENIYE in Russian No 3, Mar 92 pp 53-57

[Article by B.L. Melnichuk, Z.V. Stasyuk, Lvov State University imeni I.Ya. Franko; UDC 539.2.537]

[Abstract] The properties of thin Ti, Zr, and Hf films, particularly the grain boundary scattering contribution to the total carrier relaxation time, are examined in the frameworks of the findings obtained earlier by Mayadas and Shatzkes, Tosser *et al*, Bedda *et al*, and Tijani *et al*. To this end, the electric conductivity of thin films deposited onto substrates cooled to 78K and annealed at 373K is investigated in a deep vacuum whereby special attention is focused on the substrate and other vacuum device degassing procedures. Electron microscope and electron diffraction studies of the film structures is conducted; they show that solid metal layers thicker than 10 nm have a crystal lattice similar to that of a massive metal piece and the average grain size does not depend on the layer thickness. The dependence of the Ti and Hf film resistivity on thickness, the dimensional dependence of resistivity and temperature coefficient of resistance of Zr films, and the dependence of the Hf film resistivity and the Zr film temperature coefficient of resistance on the reciprocal thickness are plotted. The resistivity of infinitely thin films and the mean carrier path length in them and the charge transfer parameters in metal films are summarized. The authors' findings are interpreted with the help of models which take into account the current carrier scattering by the external film surfaces or grain boundaries. The consistency of the results with earlier published data is noted. Figures 3; tables 2; references 14: 3 Russian, 11 Western.

Van Vleck Paramagnetism Anomaly in Ti-Fe Alloy Electron Phase Transition Area

937D0049C Yekaterinburg FIZIKA METALLOV I METALLOVEDENIYE in Russian No 3, Mar 92 pp 58-61

[Article by A.S. Shcherbakov, N.I. Kourov, E.G. Valiulin, Physics of Metals Institute at the Urals Branch of Russia's Academy of Sciences; UDC 669.15'295:537.621/622]

[Abstract] The issue of the degree to which the Mott-Hubbard transition (MKh) in the electron subsystem in the *d*-state of metals extends to other systems where the impurity atoms do not have localized magnetic moments (LMM) is addressed and an experimental verification confirming the hypothesis about the impurity *d*-band formation is cited using the example of a $Ti_{1-x}Fe_x$ system where Fe impurities do not possess the localized magnetic moments. In addition, attention is focused on the fact that a study of Van Vleck's paramagnetic susceptibility component can serve as a powerful tool in examining the electron structure in systems experiencing an electron phase transition (EPT). The concentration dependence of the critical temperature, paramagnetic susceptibility, electron heat capacity coefficient, and Debye temperature in Ti-Fe alloys, the concentration behavior of the "seed" electron state density at the Fermi level and Pauli component of susceptibility, the concentration dependence of the measured and Pauli's susceptibility difference, and the concentration dependence of Van Vleck's susceptibility per Fe atom and the presumed *d* band formation pattern with an increase in the impurity concentration are plotted. The findings are the first direct experimental confirmation of the autonomy of the *d*-electron impurity subsystem from the conduction band of the matrix in Ti-Fe alloys and the concentration evolution of the electron structure of Ti-based transition metal alloys. Figures 3; references 10: 9 Russian, 1 Western.

Dissipative Acoustic Nonlinearity of Copper

937D0049D Yekaterinburg FIZIKA METALLOV I
METALLOVEDENIYE in Russian No 3, Mar 92
pp 62-65

[Article by S.V. Zimenkov, V.Ye. Nazarov, Applied Physics Institute at Russia's Academy of Sciences; UDC (669.3-669.17):539.67]

[Abstract] The use of acoustic diagnostics methods based on the internal friction (VT) phenomenon which leads to nonlinear attenuation and a change in the acoustic wave propagation velocity is discussed, and the effect of sound attenuation discovered in annealed Cu due to its abnormal dissipative acoustic nonlinearity is investigated experimentally. This dissipative nonlinearity does not lead to a change in the medium's modulus of elasticity but changes only the damping factor. Oxygen-free Mo copper rods containing 99.97 percent Cu are tested after annealing in a vacuum furnace. A block diagram of the experiment whereby acoustic vibrations are excited by a piezoelectric ceramic resonator is cited, and the dependence of the damping factor on the pump wave deformation amplitude is plotted. The findings show that in contrast to other metals, annealed Cu has an abnormally high dissipative acoustic nonlinearity; the need for comprehensive acoustic, metallographic, and thermodynamic studies in order to establish a correlation between the copper state and the above behavior is stressed. The authors are grateful to L.A. Ostrovskiy and

A.M. Sutin for interest in the effort and constructive remarks. Figures 2; tables 1; references 8.

Ti Diffusion in Zr-H and Zr-D Alloys

937D0049E Yekaterinburg FIZIKA METALLOV I
METALLOVEDENIYE in Russian No 3, Mar 92
pp 73-80

[Article by I.O. Bashkin, Ye.I. Rabkin, B.B. Straumal, Solid State Physics Institute, Chernogolovka; UDC 669.296.539.219.3]

[Abstract] The effect of hydrogen saturation of titanium alloys on their deformability under certain conditions is outlined, and the issue of hydrogen's effect on self- and heterodiffusion of substitutional impurities in the matrix is addressed. Titanium heterodiffusion in zirconium saturated with hydrogen or deuterium is investigated, and the Ti-Zr constitution diagram characterized by total reciprocal solubility in the solid state, both below and above the allotropic HCP α -phase-BCC β -phase transformation, is studied. In order to simplify the task, diffusion is examined at a temperature above this phase transition. An X-ray diffraction microanalysis is carried out. The titanium concentration in the diffusion zone of the Ti-Zr pair after annealing at a 983°C temperature, the dependence of the Ti-Zr interdiffusion coefficient on the Ti concentration at 1,063°C, the temperature dependence of the interdiffusion of various Ti-Zr-H and Ti-Zr-D combinations, the dependence of the interdiffusion activation energy on the hydrogen and deuterium content, and the dependence of the interdiffusion coefficient on the hydrogen and deuterium concentration at various temperatures are plotted. It is noted that compared to published data, the Ti and Zr interdiffusivity without hydrogen or deuterium differs by three- to fivefold at comparable temperatures. Hydrogen or deuterium doping increases the activation energy and the preexponential factor of titanium's chemical diffusivity, attesting to the fact that an addition of hydrogen or deuterium brings zirconium's diffusion properties closer to those of ordinary rather than abnormal materials. Of the two, deuterium increases the matrix diffusion activation energy more than hydrogen does, and both lower the ordering tendency in a β -Ti- β -Zr solid solution. The authors are grateful to Ye.G. Pomyatovskiy and L.S. Shvindlerman for fruitful discussions and V.G. Glebov and N.F. Vershinin for help with preparing the samples. Figures 5; tables 2; references 18: 9 Russian, 9 Western.

Interdiffusion in Ti-Nb-Zr System

937D0049F Yekaterinburg FIZIKA METALLOV I
METALLOVEDENIYE in Russian No 3, Mar 92
pp 89-93

[Article by V.I. Gryzunov, G. Omasheva, B.K. Aytbayev, G.V. Shcherbedinskii, Kazakh Chemical Engineering Institute, Chimkent; UDC 539.219.3]

[Abstract] The lack of data on the interdiffusion in the Ti-Nb-Zr system which behaves as a continuous series of solid solutions crystallizing as BCC lattices at high temperatures prompted a study of the interdiffusion in the Ti-Nb-Zr system at a 1,000°C temperature using 99.97 percent titanium and zirconium iodides and 99.9 percent electron beam smelted niobium as the initial materials. The samples are smelted in an electric arc furnace in a purified argon atmosphere and annealed for 24 hours to relax the stresses developed under machining. The diffusion pairs are annealed for 400 hours in double quartz vials which were evacuated and filled with Ar. The diffusion layer are studied in metallographic sections under an MS-46 Kameka X-ray microanalyzer at a 20 kV voltage by TiK and ZrK and NbK lines. Formulae are derived for calculating the weight factors. The diffusion paths in the Ti-Nb-Zr system at 1,273K are plotted and the interdiffusion coefficients are calculated at various Ti and Zr concentrations. The TiTi, TiZr, ZrZr, and ZrTi correlations are computed at 26 points. The study reveals that both diagonal and nondiagonal diffusion coefficients are interrelated, and a close correlation exists between the interdiffusion coefficients and the fusibility curves. Figures 1; tables 2; references 8: 4 Russian, 4 Western.

Effect of Small Sc and Mg Additions on Al-Li-Cu-Zr Alloy Structure and Properties Under Natural Aging

937D0049G Yekaterinburg FIZIKA METALLOV I METALLOVEDENIYE in Russian No 3, Mar 92 pp 94-99

[Article by L.I. Kaygorodova, A.M. Drits, Ya.V. Zhingel, T.V. Krymova, V.A. Rassokhin, Physics of Metals Institute at the Urals Branch of Russia's Academy of Sciences; UDC 669.71'3'296'884:666.046.516:621.785.78]

[Abstract] Interest in Sc-doping of aluminum alloys due to its effect on increasing the recrystallization temperature of strained semifinished products and good modifying properties and the resulting need to improve existing Al alloys prompted a study of the effect of Sc alone and Sc together with Mg on the structure and properties of the Al-Li-Cu-Zr alloy under natural aging, since exposure to room temperature is an unavoidable stage in various process operations. The study is carried out by electron microscope and radiographic analyses and by measuring the electric resistance and mechanical properties. The behavior of electric resistance at the initial stages of natural aging is plotted. An analysis of research data shows that Sc- and Sc+Mg-doping of the Al-Li-Cu-Zr alloy affects the supersaturated solid solution decay kinetics and the nucleation mechanism of the precipitates. Scandium doping retards the δ'-, θ'', and θ'-phase precipitation while combined doping activates it. Single doping increases the density of two-layer δ'/dispersoid particles and combined doping facilitates the δ'/[dv] double-layer particle formation. An increase in the strength properties after one month is attributed to the fining of the cast structure, the development of a

subgranular structure, and an increase in the dispersoid density. Figures 4; references 10: 7 Russian, 3 Western.

Effect of Small Mg and Sc Additions on Al-Li-Cu-Zr Alloy Structure and Properties Under Artificial Aging

937D0049H Yekaterinburg FIZIKA METALLOV I METALLOVEDENIYE in Russian No 3, Mar 92 pp 100-106

[Article by L.I. Kaygorodova, A.M. Drits, Ya.V. Zhingel, T.V. Krymova, I.N. Fridlyander, Physics of Metals Institute at the Urals Branch of Russia's Academy of Sciences; UDC 669.71'3'296'884:666.046.516:621.785.78]

[Abstract] The possibility of ensuring a combination of optimum strength and ductility properties of Al-Li-Cu-Zr alloys after high-temperature aging prompted an examination of the effect of Cs- and Mg-doping on the structure and properties of this alloy after aging at elevated temperatures. To this end, strained semifinished product samples with and without Sc and Sc+Mg additions are water hardened at 530°C for 15 min with subsequent aging at 140°C for 24 hours and 180°C for 24 hours. An electron microscope analysis of the structure is carried out by the thin foil method using a JEM-200 CX unit while an X-ray diffraction analysis is performed in a DRON-3 diffractometer in CuK radiation. The studies show that after aging for 24 h at 120°C, δ', θ'', and T_1 phases precipitate in all alloys. Doping in general, and Sc+Mg-doping in particular, affects the precipitate phase nucleation, growth, and volume fraction while aging increases the θ'-phase density; additional Mg-doping greatly activates the homogeneous disperse T_1 particle precipitation due to a decrease in the Cu solubility in Al. Two-layer δ'/dispersoid particles begin to form in both alloys. The additions help to increase strength while maintaining ductility an acceptable level due to the grain structure fining, an increase in the dispersoid density, and nucleation and growth features of various phases. Figures 4; references 9: 4 Russian, 5 Western.

BCC—FCC and FCC—BCC Transformations in Steel 60N21 Under Pressure

937D0049I Yekaterinburg FIZIKA METALLOV I METALLOVEDENIYE in Russian No 3, Mar 92 pp 150-151

[Article by D.I. Tupitsa, A.N. Borychev, Ye.G. Chernyshov, Physics of Metals Institute at the Urals Branch of Russia's Academy of Sciences; UDC 669.15'24-196:536.42:539.89:539.172.3]

[Abstract] BCC—FCC and FCC—BCC transformations in steel 60N21 under pressure are conducted *in situ* using nuclear gamma resonance (YaGR) transmission spectroscopy with a $^{57}\text{Co}(\text{Cr})$ source and using X-ray diffraction in MoK radiation in a lab diffractometer with a transmission geometry. Nuclear gamma resonance spectra of the alloy are recorded at room temperature

after water quenching at a 1,420K temperature and subsequent cooling to 77K. The study shows that a 5 GPa pressure causes a reversible $\alpha \rightarrow \gamma/\gamma \rightarrow \alpha$ phase transition (baroelastic transformation) with a martensitic mechanism; this effect is preserved under at least five compression treatment cycles. Figures 1; references 5: 2 Russian, 3 Western.

Acoustic Emission in Ti at Low Temperatures

937D0049J Yekaterinburg FIZIKA METALLOV I METALLOVEDENIYE in Russian No 3, Mar 92 pp 117-122

[Article by P.I. Stoyev, I.I. Papiro, Kharkov Engineering Physics Institute at the Ukrainian Academy of Sciences; UDC 539:620.179.17]

[Abstract] The difficulties of acoustic-emission nondestructive testing at low temperatures due to the low operating temperature range of the TsTS-19 piezoelectric ceramics used for this purpose ($\approx 290^\circ\text{C}$ Curie temperature) and the problem of nitrogen boiling near the vessel walls in experiments in liquid nitrogen prompted an investigation of the acoustic characteristics of Ti deformed at a low temperature. To this end, samples for mechanical tests are cut from 2 mm-thick VT1-0 titanium sheets and the samples are examined in the original state and after heat treatment in a vacuum at 903 and 1,123K; tensile tests are conducted in a 1958 U10-1 machine at a 0.77 mm/min rate and an M400 complex which makes it possible to record pulses of varying amplitudes is used to record acoustic emission (AE) signals. The straining curve is recorded simultaneously with the acoustic emission parameters. The mechanical and acoustic characteristics of original samples and annealed samples at room and low temperatures and the amplitude distribution of the acoustic emission signals during tests are plotted. The study shows that cooling leads to an increase in the acoustic emission activity in nonannealed samples and that annealing lowers the acoustic emission activity; the latter is attributed to the grain growth and a change in the deformation character of the resulting more equilibrium material. The contribution of high-amplitude pulses to the acoustic emission activity increases sharply at low temperatures, probably due to the twinning processes which are enhanced by a decrease in temperature. Figures 3; references 10: 9 Russian, 1 Western.

Steel 08G2S Wire Structure and Properties After Electrostimulated Drawing

937D0049K Yekaterinburg FIZIKA METALLOV I METALLOVEDENIYE in Russian No 3, Mar 92 pp 129-135

[Article by V.Ye. Gromov, V.I. Danilov, V.Ya. Tsellemayer, O.V. Sizova, L.B. Zuyev, Strength Physics and Materials Science Institute at the Siberian Department of Russia's Academy of Sciences, Tomsk; UDC 669.046:621.317.3:621.778.1.06]

[Abstract] The outlook for the method of plastic deformation by applying powerful electric current pulses to the strained metal and the lack of data on the properties of steels and alloys after electrostimulated deformation vs. conventional plastic working prompted a systematic study of the structure, mechanical properties, and fracture character of steel 08G2S alloy after conventional (OV) and electrostimulated cold drawing (ESV). The process is electrically stimulated by unipolar current pulses at a 1.3 GAm² density and 245 Hz frequency whereby the surface temperature measured by an infrared sensor did not exceed 180°C. The diffraction patterns of cold drawn steel in the initial material and wire drawn by both methods and the temperature dependence of the normalized impact fracture work of the initial material and wire drawn by both methods are plotted. Failure and fractography analyses are conducted during impact bending tests of samples with a stress concentrator. The outcome of a comparative study demonstrates that electric stimulation leads to an increase in the ready wire ductility while maintaining the ultimate rupture strength at the same level with a small decrease in the yield strength; the latter is attributed to a partial relief of the cold work due to the additional energy contributed by the pulses. The differences in the metal structure are attributed to the enhancement of the recrystallization and structural stabilization processes under electric stimulation. An X-ray diffraction analysis confirms the energy contribution theory; the impact resistance of ESV wire remains at the same level as that of conventionally drawn wire. Figures 5; references 12: 10 Russian, 2 Western.

Strain Hardening Characteristics of Cast Porous Aluminum Alloys

937D0049L Yekaterinburg FIZIKA METALLOV I METALLOVEDENIYE in Russian No 3, Mar 92 pp 136-140

[Article by A.A. Yemelyanov, I.P. Konakova, Ye.L. Furman, Urals Polytechnic Institute imeni S.M. Kirov; UDC [621.7.011:539.389.2]:669.715]

[Abstract] The constantly rising demand for porous cast aluminum with through porosity which can be used as a mechanical filtering element for various media, sound absorbers, and mechanical dampers and the scarcity of data on the behavior patterns of this material's structure and properties under straining prompted an investigation into the characteristics of strain hardening and the structure and properties of A97 aluminum and the AL2 alloy in the initial state and after various types of straining. Strain hardening tests are carried out by compressive tests and a metallographic analysis is carried out under a computer-aided Epikvant structure analyzer. The microstructure of porous cast aluminum and AL2 alloy is examined. The dependence of stress on the straining degree in porous cast aluminum and AL2 alloy and the dependence of stress and density of the AL2 porous alloy on the straining degree are plotted. An analysis of the strain hardening curves plotted within a

range from room temperature to 500°C shows that the process has a two-stage character due to a slight change in the porous material structure and density at the first stage and a significant change in the second. The findings demonstrate the possibility of using the resulting data for

analyzing the strength properties of porous materials under tests with other types of stressed state. The behavior of the pore shape, size, and volume fraction under varying straining conditions is established. Figures 3; tables 1; references 4: 3 Russian, 1 Western.

Experience in Design of Ceramic Runner for Radial-Axial-Flow Turbocompressor Turbine

937D0022A Moscow TYAZHELOYE
MASHINOSTROYENIYE in Russian No 7, Jul 92

[Article by A. Ye. Ginzburg, candidate of technical sciences, M.I. Gorbatsevich, candidate of technical sciences, and V.M. Podskrebko, Scientific Research and Technological Institute of Power Machinery; UDC 621.438:539.4]

[Abstract] Redesign of radial-axial-flow turbine runners with ceramic materials for turbocompressors now built with cermet turbine runner disks is considered, a key problem being to ensure adequate mechanical strength at high operating temperatures. As the design model has been selected a 5 kg/s air compressor driven by a gas turbine with the following parameters: gas temperature and pressure at turbine inlet 1300°C and 3.0 MPa, expansion ratio 1.56, runner speed 52,000 rpm, air temperature and pressure at compressor inlet 203°C and 1.27 MPa, compression ratio 2.44, service life 12,000 hours. The two ceramic materials most suitable for such turbine runners are hot pressed Si_3N_4 and SiC, based on a composite mechanical strength and thermal expansion criterion (Al_2O_3 , $\text{Al}_2\text{O}_3 + \text{ZrO}_2$, and $\text{Al}_2\text{O}_3 + \text{Y}_2\text{O}_3$ not being suitable). The aerodynamic design of such a runner with these materials must necessarily be optimized by minimizing the probability of fracture under given severe conditions, the peripheries of the free disk surfaces being most vulnerable. For a most reliable design optimization, the method of approximate representations has been combined with the method of finite elements and the Weibull distribution method of statistical analysis. Figures 4; references 8.

Load-Bearing Capacity and Rigidity of Efficient Lightweight Prestressed Concrete Roof Slabs for Industrial Buildings

937D0023A Moscow BETON I ZHELEZOBETON
in Russian No 8, Aug 92 pp 2-4

[Article by K. I. Vilkov, Nizhegorod Institute of Architecture and Construction, and N. A. Kornev, Scientific Research Institute of Concrete and Reinforced Concrete; UDC 624.012.45:666.973]

[Abstract] Results of testing of lightweight, hollow prestressed concrete roof slabs for their load-bearing capacity, rigidity, and resistance to cracking are presented. The slabs were designed at the Nizhegorod Institute of Architecture and Construction for construction of one-story industrial buildings in various regions with a mean winter day temperature as low as minus 35°C; their rated load capacity is 1.5 kN/m². The slabs come in sizes of 1.5X6 and 3X6 m with thicknesses of 240, 260, 280 and 300 mm. Their weight and cost are 11-15 percent lower as compared with ordinary ribbed slabs. Tests of the lightweight, hollow prestressed concrete slabs showed they possess sufficient strength, rigidity, and resistance to cracking. The first normal cracks

appeared in them only after their rated load capacity was exceeded. Slabs broke only when the yield stress was reached followed by marked flexure and a sharp increase in the width of normal cracks (0.8-1 mm). All the slabs meet strength and rigidity requirements of construction standards.

Peculiarities of Nonlinear Strain of Concrete at High Compressive Stress Levels in a Complex Stressed State

937D0023B Moscow BETON I ZHELEZOBETON
in Russian No 8, Aug 92 pp 4-6

[Article by A. P. Kirillov, VNIINTPI, A. L. Kukush, E. Ya. Bagriy, and V. N. Zavyalov, Makeyevka Civil Engineering Institute; UDC 691.327:539.376]

[Abstract] Results of experimental-theoretical studies of the creep flow of heavyweight concrete under biaxial compression are presented. Previous studies had demonstrated that even at relatively low levels of loading, when biaxial compression was involved theoretical curves constructed on the basis of creep theory did not always satisfactorily correspond to creep flows measured in tests. Analytical relationships for a plane stressed state are proposed which introduce directionally different functions of loading regimes for linear and nonlinear components of creep flow. Using the proposed relationships, comparison of experimental and theoretical data produced good results in describing relative creep flows in the direction of each of the acting stresses.

Internal Corrosion of Concrete

937D0023C Moscow BETON I ZHELEZOBETON
in Russian No 8, Aug 92 pp 8-10

[Article by F. M. Ivanov, Scientific Research Institute of Concrete and Reinforced Concrete; UDC 691.327:620.193]

[Abstract] General information from decades of studies of internal corrosion of concrete caused by alkali-aggregate reaction is reviewed. Rocks containing minerals that are reactive with cement alkalis are categorized by type and by their geographical distribution in Russia. The use of additives containing salts of alkali metals has contributed lately to the problem, and data are given showing the influence of the type of salt on the alkali-aggregate reaction. A testing scheme is presented for determining the potential reactivity of various aggregates. The aggregate is tested chemically to determine the presence of active (soluble) silica. If necessary, potential reactivity in a specific composition of cement and aggregate can be determined by measuring the expansion strain of specimens of concrete in humid conditions at high temperature. The method takes six months, but a way of reducing this time is being sought.

Principles for Calculation of the Fire-Resistance Limit of Polymer-Impregnated Reinforced Concrete Structures

937D0023D Moscow BETON I ZHELEZOBETON in Russian No 8, Aug 92 pp 26-29

[Article by V. S. Fedorov, Moscow Institute of Railroad Transportation Engineers; UDC 624.012.45:536.468]

[Abstract] A general method for calculating the fire-resistance limit of polymer-impregnated reinforced concrete structures which are statically indeterminate is presented. It is explained that at present the fire-resistance limit is determined primarily for statically determinate elements under compression and bending, although the fire-resistance of such elements in structures of buildings is entirely different in a real fire. In a fire, each element of a statically indeterminate structure is heated differently, depending on its location and geometrical and thermophysical characteristics.

On the basis of full diagrams of deformation of polymer-impregnated concrete and reinforcements with heating temperatures taken into account, a computerized strength analysis is developed for normal cross-sections under applied external forces in general, and for random cross-section shapes. A discrete calculation model for normal cross-sections is presented; equilibrium equations are given and a method of calculating elements of the matrix of rigidity of cross-sections is described. A general diagram of the thermomechanical state of polymer-impregnated concrete under short-term compression is constructed, taking into account heating temperature and physical nonlinearity.

Cost Effectiveness of Lightweight Concretes

937D0023E Moscow BETON I ZHELEZOBETON in Russian No 8, Aug 92 pp 29-31

[Article by Yu. A. Rogatin, N. A. Aleksandrova, and V. I. Glukhov, Scientific Research Institute of Concrete and Reinforced Concrete; UDC 691.327:666.973.2.003.13]

[Abstract] Results of a study of the cost effectiveness of using outer wall panels made of lightweight concretes with varying densities for industrial, residential, and office buildings in various parts of the CIS are presented. In evaluating the technical-economic effectiveness of lightweight concretes as compared with that of other concretes, two criteria were applied: the economic preference factor (necessity of application), and the performance preference factor (adequacy of application). Results for different concretes with varying densities and numbers of panel layers in 12 different geographical regions are given.

Phase Transitions in Al_2O_3 Ceramic, Sintered Under Effect of Microwave Radiation

937D0043M Moscow FIZIKA I KHIMIYA OBRABOTKI MATERIALOV in Russian No 5, Sep-Oct 92 pp 131-135

[Article by N.G. Varenova, L.K. Kuznetsov, N.D. Malygin, V.N. Perevezentsev, M.Yu. Shcherban, Nizhniy Novgorod; UDC 539.91:539.12.04]

[Abstract] The excessively high sintering temperature and long duration which make aluminum oxide ceramic products too expensive despite their unique heat resistance, mechanical strength, wear, corrosion resistance, hardness, insulating properties, etc., prompted an investigation into the behavior of Al_2O_3 ceramic phase composition during sintering under the effect of microwave (millimeter band) irradiation. The phase states of Al_2O_3 ceramics are discussed, and the principal data on the structural characteristics and phase transition temperatures of the three main Al_2O_3 phases are summarized, and the diffraction patterns of samples sintered under the effect of microwave radiation at 1,400 and 1,600°C at a 50°C/min rate as well as the dependence of the amount of β - and γ -phases forming under irradiation on the sintering temperature and heating rate are plotted. The study demonstrates that ceramic sintering under irradiation is accompanied by nonequilibrium phase transitions which are not usually observed under thermal sintering: the equilibrium α -phase turns into nonequilibrium β - and γ -phases whose amount increases with the sintering temperature and duration. The chemical composition of the phases is established. The development of an X-ray amorphous phase under microwave heating to above 1,400°C is noted. Figures 4; tables 1; references 8: 4 Russian, 4 Western.

Theory of the Heat Treatment of Refractories Based on a Resin Binder

937D0051A Moscow OGNEUPORY in Russian No 9-10, Sep-Oct 92 pp 2-4

[Article by P.I. Sham, S.A. Nagornyy, and Ye.A. Kirsanova, Mariupolsk Metallurgy Institute, and A.P. Nagornyy, Azovstal Combine; UDC 666.762.38.017:621.785.01]

[Abstract] The sublimation of volatile resins subjected to heat and the effect of this heat on the quality characteristics of refractories based on a resin binder were studied under laboratory conditions. A nonpressed periclase-limestone compound was mixed with resin and studied along with refractory specimens made of the very same mixture that had been pressed under a pressure of 100 N/mm² in the form of cubes measuring 100 mm on a side. The composition of the study specimens was as follows (wt.—percent): magnesite powder, 35; dolomite, 60; pitch tar, 5; and resin, 6. Coal tar from the Donetsk By-Product Coke Plant was used in manufacturing the specimens. At 20°C, the coal tar had a density of 1.246 g/cm³, a coking value of 50 percent, and a viscosity of

$C_{80}^{10} = 81$ s. Two series of tests were conducted to determine the amount and composition of volatile resins released under the effect of temperatures ranging from 150 to 350°C and the effect of this process on the mechanical strength of the study refractories, their residual carbon content, and impregnation of the dolomite grains with resin. The studies established that the volatiles released from the nonpressed compound in the temperature interval studied consisted primarily of resin components with a boiling point within the very same temperature interval or else close to it. The refractories were found to release far less heat than the nonpressed compound: At 150°C, the amount of volatiles released from the refractories was a factor of 2.7 less than that released from the starting compound, and at 350°C the amount of volatiles released from the refractories was less than that released from the starting substances by a factor of 11.8. At the sublimation temperatures studied (300 and 350°C), an increase in the release of volatiles to 5-6 percent of the resin's mass was found to result in an increase in the specimen's compression strength. When a greater amount of volatiles was sublimated, the refractories' mechanical strength and residual carbon content decreased. The rate of heating and temperatures of the refractories, as well as impregnation of the dolomite grains with resin also proved to be important. A series of experiments established that refractories will not develop cracks or other flaws if they are heated to 300°C in a furnace while subjected to the combined effects of thermal radiation with an intensity of 5.6 to 8.4 kJ/(m² x s) and an oxidizing gas medium consisting of fuel combustion products with an excess-oxygen coefficient of 1.2 and sublimation of the resin at temperatures of 380 to 400°C at a pressure not exceeding atmospheric pressure. The refractories should be held at a temperature of about 300°C for 2 to 3 hours. Further studies established that when the resin-based refractories have a surface temperature of 300°C or below, they will not develop cracks provided that they are cooled slowly enough so that the drop in their surface temperature does not exceed 3.7°C/min. This is said to correspond to a process of open-air cooling at a temperature of at least 20 to 23°C. More rapid cooling was found to result in crack formation. Figures 4.

Refractory Products for Units To Produce Amorphous Metals and Alloys

937D0051B Moscow OGNEUPORY in Russian
No 9-10, Sep-Oct 92 pp

[Article by I.E. Aleksandrov, T.I. Litovskaya, S.P. Aleksandrova, and Yu.Ye. Pivinskiy, All-Union Refractories Institute; UDC 666.762.14.001.4]

[Abstract] Centrifugal casting units are generally used in the process of manufacturing amorphous metals and alloys. Until recently, the bowls of these units were generally made of graphite or copper and were cooled with water. These bowls often corrode after a single use and contaminate the metals and alloys produced in them. A study was conducted to find a new material for

casting unit bowls that would not cause these problems. A series of studies was conducted to develop an optimum compound and process for use in manufacturing amorphous metal and alloy products characterized by long-lasting mechanical strength and heat and corrosion resistance. Six different test compounds were produced from synthetic mullite (TU 14-8-450-83), artificial corundum (TU 14-196-39-84), GK alumina, and special additives. The compounds were molded into cubes (measuring 30 mm on a side) in metal molds by the vibroforming technique. After being allowed to dry naturally in the molds, the specimens were removed from the molds and further dried at temperatures of 80 to 100°C. They were then annealed at 1,200 and 1,400°C and held for 2 hours. The ultimate strength of each of the specimens was determined by placing the specimens into a furnace at 1,250°C and heating them for 10 minutes. The specimen's compression strength was measured after 8 and 40 heat treatment cycles. One of the compounds (which was found to have a residual strength of 99/89 percent after 8 cycles and 98/73 percent after 40 cycles) was used to manufacture a test batch of bowls that were then tested under actual operating conditions. Another of the test compounds (determined to have a residual strength of 95/95 percent after 8 cycles and 85/75 percent after 40 cycles) was used to manufacture crucibles for melting borates of alkaline earth metals under laboratory conditions. Tests of the bowls established a build-up of metal on the bowl surface and individual small particles measuring 0.02 to 0.11 penetrating the surface to a depth of no more than 1.5 mm. Although this adsorption of particles by the surface layer caused the bowls to discolor, both X-ray spectral microanalysis and petrographic analysis confirmed that the contact layer did not undergo any changes in structure or phase composition. Tests of the crucibles established that they too performed in a satisfactory manner and that they lost no more than 0.05 percent of their mass after holding a borate melt for 1 hour. Figures 4, tables 3; references 10: 8 Russian, 2 Western.

Regulating the Crystallization of a Casting of Baddeleyite-Corundum Products

937D0051C Moscow OGNEUPORY in Russian
No 9-10, Sep-Oct 92 pp 8-10

[Article by V.A. Naumenko, N.P. Talakuyev, PZOI [not further identified], and B.F. Norkin, Bemes Enterprise; UDC 666.762.5.065.5]

[Abstract] A series of experiments was conducted to regulate the crystallization of the baddeleyite-corundum products BKCh-34 (TU 14-8-219-86) and BKVK-34 (TU 196-04-14-89). Castings of these materials measuring 600 x 400 x 250 mm were subjected to a controlled crystallization process that entailed the following operations. The melt was poured from an OKB-2126AM electric furnace into the casting mold. After only its surface had crystallized, the casting was freed from the mold and placed on a water-cooled metal tray. Compressed air was fed onto the side walls of the casting from

four sides to intensify its cooling. In accordance with the proposed controlled crystallization process, crystallization parameters are monitored and controlled at 10 points (at 5-minute intervals from 5 to 50 minutes after the beginning of the process). It is known that a casting made of bakor-33 and originally measuring 600 x 400 x 250 mm has a shrink size of $11 \times 10^{-3} \text{ m}^3$ and a shrink weight of 35 kg. When the technique of cooling in a hot box is used, compensation for shrinkage from the head culminates in 3 hours. The shrinkage compensation time is reduced to 1 hour when the technique of thermal regulation is used, however. After heat treatment in accordance with the 10-point process described, products did not require any further annealing in a hot box. The BKVK products produced by the proposed method had a microstructure and macrostructure far superior to those of products produced by the conventional process from BKCh. The baddeleyite-corundum refractory castings produced by the new controlled crystallization technique were free of shrink holes, and the fine-grained structure of their intergrown baddeleyite and corundum crystals made them highly corrosion resistant, which in turn made it possible to extend the service life of the glassmaking furnaces in which they were used by 20 to 25 percent. BKVK refractories containing between 33 and 41 percent ZrO_2 were found to have an integral structure and a density of 3.65 to 3.9 g/cm^3 , which is on a par with the best foreign analogues. The proposed controlled crystallization method made it possible to increase the live zone of products 250 mm thick to 200 mm, reduce top losses of melt by as much as 70 percent, free up the production areas occupied by hot boxes, and improve labor conditions and productivity. Figures 2, tables 2; references 6: 5 Russian, 1 Western.

Use of the Method of Induction Melting for Preliminary Synthesis of an Oxide Ceramic in the System $\text{ZrO}_2\text{-Y}_2\text{O}_3\text{-Al}_2\text{O}_3$

*937D0051E Moscow OGNEUPORY in Russian
No 9-10, Sep-Oct 92 pp 14-19*

[Article by V.I. Gutman, A.G. Reznikov, M.D. Lyubalin, V.A. Pismennyy, L.G. Bochkareva, A.V. Mishin, Ye.M. Chernomorskaya, All-Union Scientific Research and Technology Institute of Power Machinery Building, Yu.B. Petrov, A.M. Lyubomirov, and A.Yu. Pechenkov, Leningrad Electrical Engineering Institute imeni V.I. Ulyanov; UDC 666.762:621.365.5]

[Abstract] The process of liquid-phase synthesis of materials in the system $\text{ZrO}_2\text{-Y}_2\text{O}_3\text{-Al}_2\text{O}_3$ by the method of induction melting in a cold crucible was studied. Type TsrO-1 zirconium dioxide, TsI-15.5 zirconium dioxide stabilized in accordance with specification TU 48-0502-63/0-86, and type GEB commercial-grade alumina were used as primary materials to test the new induction melting unit that was especially designed for use in a process involving a cold crucible. Preliminary studies of the new induction melting unit established that the new equipment was quite promising but that smaller ingots (diameter, 48 mm; weight, 1 kg) had a more uniform

chemical composition than did their larger counterparts (diameter, 90 mm; weight, 10 kg) and had a more uniform chemical composition throughout their cross sections. Ultrapure zirconium dioxide, chemically pure aluminum oxide, and type ITO-V yttrium oxide were used as reagents in the subsequent oriented crystallization process. A differential thermal analysis was performed on ingots produced from six different starting compounds produced from the system $\text{ZrO}_2\text{-Y}_2\text{O}_3\text{-Al}_2\text{O}_3$. The analysis established that processes of eutectic melting are most characteristic of compounds containing from 4.4 to 6.8 percent Y_2O_3 . The studies confirmed that the method of induction melting with a cold crucible and the new equipment designed for that purpose are suitable for use in synthesizing materials to be used as the starting material in oriented crystallization processes. Figures 7, tables 6; references 5: Russian

The Selection of Refractory Mixtures for Coating the Lining of Ingot Molds' Feedheads

*937D0051G Moscow OGNEUPORY in Russian
No 9-10, Sep-Oct 92 pp 33-37*

[Article by M.Ya. Zavadskiy (deceased), A.Yu. Konoplyanik, Dnepropetrovsk Construction Engineering Institute, and A.I. Belkin, Metallurgy Combine imeni Illich; UDC 666.974.2:666.762.3]:[621.746.464:66.043.1]

[Abstract] A study was conducted to determine the best refractories for coating the lining of ingot mold feedheads. Nine different mixtures were tested. Eight of the mixtures were based on magnesite powder; the ninth consisted of an aqueous solution of magnesium sulfate and commercial-grade lignosulfonate. Coatings produced from each of the study mixtures were subjected to tests in which steel was actually poured into ingot molds whose feedheads had been lined with the coatings. Chemical, petrographic, and X-ray phase analyses were also performed on the zones where the study refractories interacted with the slag. On the basis of the studies performed, the authors recommended four of the nine refractory mixtures studied for use as protective coatings for the ingot mold feedheads. The first mixture recommended contained the following (percent): magnesite powder, 61.0; dust wastes from the production of silicon-containing ferro alloys, 11.3; and commercial-grade lignosulfonate, 27.7. The second mixture recommended contained 60.0 percent magnesite powder, 10.6 percent dust wastes from the production of the aforesaid ferro alloys, and 29.4 percent aqueous magnesium sulfate solution. The third mixture recommended contained 51.3 percent magnesite powder, 17.2 percent refractory alumina, and 31.5 percent commercial-grade lignosulfonate. The fourth mixture recommended contained 53.1 percent magnesite powder, 18.1 percent refractory alumina, and 28.8 percent aqueous magnesium sulfate solution. Figures 3, tables 3; reference 1: Russian.

Studying the Thermophysical Interaction Between Steel Strip and the Molten Steel in a Continuous Casting Mold

927D0259F Moscow *IZVESTIYA VYSSHIKH UCHEBNYKH ZAVEDENIY: CHERNAYA METALLURGIYA* in Russian No 6, Jun 1992 pp 48-52

[Article by N. I. Revtov, O. B. Isayev, O. V. Nosochenko, V. G. Lenskiy, and I. G. Nikolayeva, Mariupol Metallurgical Institute; UDC 621.746.27]

[Abstract] The macrostructure of continuously cast steel slabs was studied to determine how it is affected by the temperature of the steel in the tundish, casting speed, and mold size. The effect of these parameters was studied during the course of more than 200 heats of St3sp, 09G2S, and 09G2FB steels cast on curved machines into 250 x 1650 and 300 x 1850 mm slabs. Computer-aided statistical analysis of the results showed that the temperature of the metal in the tundish has the greatest effect on macrostructure. Increasing the casting speed from 0.6 to 0.8 m/min leads to a slight increase in the percentage of columnar dendrites. The effect of mold size is insignificant. Overheating the metal to a point 10°C or more above the liquidus promotes the persistent growth of directional crystallization zones while simultaneously reducing the size of the chill and equiaxed zones and increasing the number of defects in the axial zone. A number of tests were performed to determine whether inserting steel strip into the molten steel in the upper part of the mold could prevent excessive overheating and its deleterious effects. The tests showed that, depending on the type of steel strip used (08kp, St3ps, and St5sp steels were tested), strip geometry and melting point, and the rate and location at which the strip is introduced into the melt, excessive overheating and its accompanying side effects can be avoided. The test data were used to construct quantitative methods that can be used to determine optimum strip geometries and melting points and the rate at which strip should be introduced into a melt depending on casting conditions and mold geometries. The proper use of steel strip to prevent overheating dramatically improves the quality and workability of both cast and rolled steel. Figures 4, tables 2; references 4: Russian.

The Role of Surface Phenomena in the Removal of Nonmetal Inclusions in the Process of Electroslag Alloying of Metal

937D0016A Kiev *PROBLEMY SPETSIALNOY ELEKTROMETALLURGI* in Russian No 1, Jan-Feb-Mar 92 (manuscript received 11 Jan 91) pp 19-22

[Article by V.N. Radchenko, Donetsk Polytechnic Institute; UDC 669.187.56.001.5]

[Abstract] A study was conducted to examine the role of surface phenomena in the removal of nonmetal inclusions in electroslag alloying. The steel 12CrNi3Mo was smelted in an electroslag remelting furnace from the

intermediate product 10sp. Satellite-electrodes made of an iron-chromium-nickel-molybdenum foundry alloy were used to alloy the steel. The resultant metal was compared with metal produced after electroslag remelting of a consumable electrode with the final chemical composition. The metal produced by the new technique (i.e., the experimental metal) proved superior to the conventionally produced (i.e., control) metal from the standpoint of its plastic properties. Both metals were nearly identical from the standpoint of the amounts of gases and toxic impurities contained in them. The experimental metal contained far fewer nonmetal inclusions than did the conventionally produced metal. Specifically, the experimental metal was given an oxide rating of no higher than 2 points, whereas the control steel was given a rating of 4 points. The volume fraction of oxides in the experimental and control steels, as counted on the basis of 300 fields viewed by an optical microscope with a magnification of 400x, amounted to 0.0153 and 0.0202 percent, respectively, and their oxide contents with respect to mass in the sediment amounted to 0.005 percent and 0.008 percent, respectively. The experimental metal did, however, contain a lower percentage of aluminum oxide (20 to 40 percent) than the control metal did (40 to 60 percent). These differences in composition led the researchers to conclude that surface phenomena play a decisive role in the behavior of nonmetal inclusions. Specifically, they hypothesized that molten metal of the final chemical composition (in the case at hand, 12CrNi3Mo steel) reacts with the refining slag during the remelting process. To test this hypothesis, the researchers examined the reaction of the flux ANF-6 with the steels 10sp and 12CrNi3Mo produced by converter smelting with an iron-chromium-nickel-molybdenum foundry alloy produced in an induction furnace. They also examined the possibility of refining the said steels to remove aluminum oxide inclusions. The reaction of the study metals with solid aluminum oxide inclusions was examined at 1.873 K. The interface stress between the metal and slag was found to be closely tied to the nature of the interaction of the two phases, which in turn was found to depend on the chemical composition of the phases, their structure, and the orientation of the molecules and the ions. Specifically, the closer the properties of the two contacting phases, the lower the interface stress and, consequently, the lesser the interaction of the phases and transfer of components from one phase to the other. This same pattern was also found to apply to the transfer of nonmetal inclusions through the interface. The studies further established that, all else being equal, the following facilitate the assimilation of nonmetal inclusions by slag: poor wetting of the inclusions by the metal; good wetting of the inclusions by the slag; and optimal wetting of the metal by the slag. The interface stress at the metal-inclusion interface of the steel with the final composition turned out to equal 1,290 MJ/m², while those of the intermediate product and foundry alloy turned out to equal 1,660 and 1,520 MJ/m², respectively. The surface stress at the slag-inclusion interface was found to equal 620 MJ/m². The changes in free energy during assimilation

of the aluminum oxide by the slag were thus found to equal -1,040 MJ for the intermediate product, -900 MJ for the foundry alloy, and -670 MJ for the steel with the final chemical composition. Tables 2; references 8: 7 Russian, 1 Western.

Methods of Producing Nickel Superalloys With Improved Technological Properties

937D0016B Kiev PROBLEMY SPETSIALNOY ELEKTROMETALLURGI in Russian No 1, Jan-Feb-Mar 92 (manuscript received 22 May 91) pp 22-28

[Article by Al.G. Shalimov, Yu.Ya. Reznik, Yu.E. Vasil'yev, L.P. Sopov, O.N. Vlasova, V.I. Yeremenko, and G.M. Rakovshchik, Central Scientific Research Institute of Ferrous Metallurgy, Moscow; UDC 669.187.56.001.5]

[Abstract] If the technical and economic indicators of the production of billets from high-alloy refractory nickel alloys, i.e., superalloys, are to be improved significantly, existing methods of smelting, heat-treating, and straining ingots must be modified. Vacuum arc remelting, which is currently used to produce nickel alloys, results in nickel superalloys with inadequate low-cycle fatigue strength. Ingots produced by the conventional methods of smelting in a water-cooled continuous casting mold (vacuum arc remelting and electroslag remelting) have a coarse dendrite structure with an elevated liquation level that adversely affects plasticity. A new method, referred to as vacuum two-electrode remelting, has been proposed for producing ingots. It entails remelting two horizontal consumable electrodes by an electric arc burning between their faces in a vacuum and forming an ingot in a noncooled rotating ingot mold. The new method results in a fine-grained nondirected structure. The superheating of the metal in the remelting during the new process is not sufficient for refining of the metal to occur, however. In an effort to remedy this situation, researchers studied the feasibility of combining vacuum two-electrode remelting with electroslag remelting. The quality of nickel-based superalloys produced by a combination of the two remelting methods was compared with that of superalloys produced by vacuum arc remelting and by electroslag remelting. The studies were conducted at temperatures of 650 to 750°C. Regardless of the method by which they were produced, all of the specimens were found to be characterized by micro-porosity linked to the formation of excess phases of eutectic origin, carbides, and borides. The specimens produced by electroslag remelting exhibited less micro-porosity than did specimens produced by vacuum arc remelting but contained more excess eutectic phases and a greater dispersion of carbides with regular faceting. The specimens produced by a combination of vacuum two-electrode remelting and electroslag remelting manifested elevated microporosity of a shrinkage nature, a uniform fine-grained structure with a grain size of about 50 µm, a small number of excess phases, a high dispersion of carbides with regular faceting, and a low degree of microchemical inhomogeneity. In the metal produced by

the combined technique the ordering γ'-phase was virtually evenly distributed in the form of disperse segregated deposits, whereas in the metal produced by vacuum arc remelting about 10 percent of the total amount of γ'-phase was in the form of excess eutectic segregated deposits. The nickel superalloys produced by a combination of vacuum two-electrode remelting and electroslag remelting possessed especially good plasticity that was attributed to the favorable combination of 1) the high purity of the metal thanks to the use of intermediate refining electroslag remelting and 2) the fine-grained homogeneous ingot structure resulting from vacuum two-electrode remelting. Figures 7, tables 2; references 3: 2 Russian, 1 Western.

A Furnace for Pressure Arc-Slag Remelting of Ingots Weighing Up to 5 Tons

937D0016C Kiev PROBLEMY SPETSIALNOY ELEKTROMETALLURGI in Russian No 1, Jan-Feb-Mar 92 (manuscript received 23 Jul 91) pp 28-31

[Article by B.Ye. Paton, B.I. Medovar, A.G. Bogachenko, V.Ya. Sayenko, V.A. Tikhonov, V.V. Slavutskiy, V.Ya. Maydannik, R.S. Dubinskiy, G.B. Shchupak, and I.A. Lantsman, Electric Welding Institute imeni Ye.O. Paton, Ukraine Academy of Sciences, Kiev; UDC 669.187.56.002.2]

[Abstract] The USh-180 furnace, which is intended for producing ingots weighing up to 5 tons by the method of arc-slag remelting in nitrogen under pressures up to 4 MPa, was developed at the Electric Welding Institute imeni Ye.O. Paton. The new furnace was based on the technological and design decisions underlying the USh-178 arc-slag remelting furnace. The new furnace's basic bearing structure and mechanisms for moving the carriages of the electrode holder and autoclave were taken from the EShP-5 electroslag furnace, which is in operation at the Experimental Special Electrometallurgy Plant of the Electric Welding Institute imeni Ye.O. Paton. The design of the USh-180 and the operations that may be performed on it are proof that it is possible to redesign conventional electroslag units with a cantilever electrode suspension so that they may be used for smelting ingots under pressure in a nitrogen atmosphere. Figures 2.

Magnesium-Phosphate Self-Hardening Sands

937D0024A Moscow LITEYNAYE PROIZVODSTVO in Russian No 6, Jun 92 pp 10-11

[Article by S. I. Rivkin and Ye. N. Yurginson, Izhora Plant Production Association, and L. G. Sudakas and L. I. Turkina, State Scientific Research and Planning Institute of the Cement Industry; UDC 621.742.48]

[Abstract] The experience with use of magnesium-phosphate self-hardening foundry sands for large and medium-size steel castings at the Izhora Plant Production Association is described. Cores are made of silica

and zircon-based magnesium-phosphate sands weighing from 4 kilograms and 4 tons, with a total annual production of 3,000 tons in the association's foundry. Magnesium-phosphate sands can be combined with sands with water-glass and synthetic-resin binders for use as facing and filler sands. The magnesium-phosphate self-hardening sands contain three primary groups of substances: an active component (binder) consisting of a magnesium powder component and a phosphate liquid component; a filler (sand) which provides certain thermal, gas-dynamic and contact properties; and modifier additives which provide necessary hardening conditions. Thanks to high binding capacity of the magnesium-phosphate mixture, the total amount of magnesium-containing powder and liquid component is only 3-5 percent. The low content of the active component in these sands makes core knock-out easy to perform with conventional methods such as knock-out grids and by hand.

Quality of Sand From Tolmachevo Evaluated

937D0024B Moscow LITEYNAYE PROIZVODSTVO
in Russian No 6, Jun 92 pp 11-12

[Article by Yu. F. Borovskiy, I. V. Shergin, and Yu. N. Zinin, Northwest Correspondence Polytechnical Institute; UDC 621.742.85]

[Abstract] Sand from the Tolmachevo quarry was evaluated for its potential as a substitute for Lyubertsy sand, which is the core sand of choice at the "Zvezda" Plant in St. Petersburg for casting aluminum diesel blocks and manifold parts. The mineral content of the sands was determined by the X-ray diffraction method. Strength tests of cores made of the two different sands and using three different binders showed that Tolmachevo sand cannot qualify as a full-fledged substitute for Lyubertsy sand. Used core sand from Tolmachevo and a shop mixture of the two sands were reclaimed on a dry mechanical unit, and the reclaimed products were also treated in a "pseudo-fluidized bed" unit. Tests of the reclaimed products showed that they can be used as a partial substitute for Lyubertsy sand.

Making Casting Molds Using Vibration Methods

937D0024C Moscow LITEYNAYE PROIZVODSTVO
in Russian No 6, Jun 92 pp 12-14

[Article by A. A. Brechko and A. V. Sokolov, Foundry Machinery Institute; UDC 621.742.4]

[Abstract] A promising way of improving the process of making large molds and cores of sodium silicate and resin sands is to reduce the surface energy and viscosity of the binder with the aim of efficiently distributing filler among the grains and to reduce internal stresses in the binder. Molding sands with a minimum binder content are characterized by high mobility, which allows vibration methods of compaction to be used for making molds and cores with low energy costs. Sodium silicate sands

with a plasticizing additive were tested for three conventional hardening methods: the CO₂ process, fast drying with heat, and cold hardening with solid and liquid hardeners. In all three methods the use of a plasticizer was effective in allowing less binder to be used while maintaining desirable strength and friability properties. In sands with furan resins, binder content was reduced by lowering the binder's viscosity and surface energy. The best result was achieved by using a monomer plasticized with a polymer as the base.

Molds made of the sands with reduced binder content were compacted by vibration in the vertical and horizontal directions on test benches to study the effect of vibration on disperse systems (quartz sand + binder). It was found that a mold structure obtained by horizontal vibration compaction is the most efficient, providing maximum structural strength. This method allows for minimum energy expenditure for compaction per unit weight of sand, and allows molds to be made in a wide range of weights.

Casting of Aluminum-Based Composites With Crystallization Under Pressure

937D0024D Moscow LITEYNAYE PROIZVODSTVO
in Russian No 6, Jun 92 pp 14-16

[Article by N. N. Belousov, Institute of Mechanics; UDC 621.74.043.2:669.715]

[Abstract] In conventional gravity casting of composite material parts, there can occur sedimentation of hardeners, which leads to local coarsening and the development of liquation processes. One way of preventing this is the method of casting with crystallization under pressure (forging of molten metal), which was developed in St. Petersburg under the direction of V. M. Plyatskoy. Aluminum alloy-based composites made by one of two established methods (vortex process, in which powders or fibers of refractory metals, carbides, nitrides, etc. are mixed intensively in the molten metal; or plasma injection, in which the hardeners are introduced with a plasma jet of an inert gas) are cast into steel molds mounted on hydraulic presses.

This process was used to produce test lots of internal-combustion engine pistons made from the composite "Altik". Metallographic studies of the pistons showed a high density and fine-grain structure of the composite, with hardeners distributed uniformly. Study of mechanical properties showed decreased ductility as the content of titanium or intermetallic compounds increased, as well as increased strength at temperatures up to 300-350° C. The process was also used to make mold inserts for injection-molding machines. Studies showed that the wear resistance of inserts made of composites is much higher than that of inserts made of steel when used in injection molding of glass-fiber-reinforced plastics.

Making Castings of Metal-Base Composites

937D0024E Moscow LITEYNAYE PROIZVODSTVO in Russian No 6, Jun 92 pp 16-17

[Article by V. G. Borisov, Scientific and Production Association "All-Union Institute of Aluminum and Magnesium"; UDC 621.74.011:669.715]

[Abstract] A method of making cast aluminum-base composites is described in which structure formation is controlled by adding particles of an intermetallic compound to the molten base metal when its temperature is in the range between the liquidus and solidus curves. For example, if iron is added to molten aluminum in the form of particles of the intermetallic Al_3Fe , within the liquidus-solidus range the degree to which the particles dissolve will be determined by the temperature of the melt, the size of the particles, and the time that they are in the melt. Also, intermetallic compounds having a different stoichiometry (e.g., Al_5Fe_2) can affect the thermodynamics of the process because of their different properties. In the system Al-Ti, there are nine types of Al and Ti compounds with differing stoichiometry, crystal lattice types and parameters, and physicochemical properties. Use of these compounds makes it possible to obtain alloys of the same general chemical composition but with widely varying structures and mechanical properties.

To implement the method, the intermetallic compound is added in the form of a powder to the melt in a reactor equipped with a device for batching, heating, and ionic pickling of the surface of added particles, and a crucible with a device for mixing the melt as the compound is added. This equipment and technology for forming the produced composites were developed at the Scientific and Production Association "All-Union Institute of Aluminum and Magnesium". Materials have been produced which are tens of times more wear-resistant than known alloys and which possess a higher modulus of elasticity, strength, and other properties. Composites based on Al-Si alloy have been produced with a SiC content of up to 20 percent. In them, strength and ductility properties are retained while increasing the modulus of elasticity (to 85 MPa), with wear resistance increased by dozens of times.

Ceramic Molds for Relief Surface Castings

937D0024F Moscow LITEYNAYE PROIZVODSTVO in Russian No 6, Jun 92 pp 18-20

[Article by F. D. Obolentsev, Yu. A. Kaplunovskiy, and L. M. Mirson, All-Union Planning and Technological Institute of Casting Machinery Manufacture; UDC 621.74.045]

[Abstract] Processes for making ceramic molds for castings with relief surfaces are described. Molds made by these processes include cores made of a sand and sodium silicate mixture which are ceramic-coated using a gelled suspension poured around the cores inside engraved

plaster boxes; shells made of a quartz-water slip poured around a plaster core inside an engraved plaster box; and shells made of hot suspensions such as molten quartz which are pressed into plaster boxes, and after setting the shells are removed and sprinkled with aluminum oxide and fired up to 1000° C for solid-phase sintering of the refractory material. Also described is a process for making molds with coordinated engraving on a core.

Combined Method of Manufacturing Gas Turbine Rings

937D0024G Moscow LITEYNAYE PROIZVODSTVO in Russian No 6, Jun 92 pp 20-21

[Article by A. G. Kovalev, A. N. Lemeshko, and N. V. Levnikov, "Neva Plant" Production Association; UDC 621.74.002.6:669.14]

[Abstract] Results of casting gas turbine rings by two different methods are reported. One method involves investment casting of separate sections of a ring in ceramic molds heated to 900° C, and the other involves casting of the whole ring in a metal mold. The weight of each cast ring section was 60 kg, and the weight of the wholly cast ring was 1500 kg with a wall thickness of 82-108 mm. Heat treatment of the castings consisted of cooling from 1200° C for 3 hours, quenching in water, followed by ageing at 800° C for 10 hours.

Tests of mechanical properties of the castings showed that the metal cast in ceramic molds had lower ductility and impact strength, whereas the metal cast in a metal mold had mechanical properties on a par with those of gas turbine rings manufactured by the traditional forging method. Tests of the castings for long-term strength showed that the long-term ductility of the metal cast in a metal mold was twice that of the metal cast in ceramic molds. As a result, a process has been developed and introduced for manufacturing castings for gas turbine rings from TsZh-13L steel to replace forgings, which increases the yield of fit metal by 30 percent and saves labor costs.

Synthesis of Multicomponent Casting Alloys

937D0025A Moscow LITEYNAYE PROIZVODSTVO in Russian No 6, Jun 92 pp 4-7

[Article by B.B. Gulyayev and Yu.Yu. Zaplatkin, St.Peterburg State Technical University; UDC 621.74:669.5]

[Abstract] Synthesis of ternary solid-solution casting alloys is considered, three criteria being proposed which relate to the polythermal constitution diagram and a quasi-equilibrium crystallization model which neither requires uniform distribution of all phases nor thus needs to conform to thermodynamics of reversible processes. Two of these criteria, both dimensionless, are analogs of criteria α and β for binary alloys. The first criterion A refers to the combined solubility limit for the two alloying elements in the solvent and is the maximum which the sum of their concentrations can reach when

the ratio of their concentrations remains constant. The second criterion B is the sum of their concentrations at a binary eutectic or peritectic point for a given ratio of their concentrations. The third criterion Ω , applicable specifically to ternary alloys, is the ratio of the concentrations of the two alloying elements in the solid phase and in the liquid phase respectively. This criterial approach was first tested for validation on the Zn-Al-Cu system of casting alloys, a well known system characterized by relatively wide solubility ranges and absence of allotropic transformations. Experimental data on the mechanical properties and chemical composition of these alloys processed in accordance with the numerical "Aladin" program (A.I. Kruchenko) of regression-correlation analysis and the graphical "Serfer" program of three-dimensional diagrams analysis as well as by the A-B- Ω criterial analysis. Following its validation, this criterial analysis was applied to Al-Mg-X ($X = Si, Mn, Fe, Cu$) systems of casting alloys. The results of this analysis explain why such ternary casting alloys now produced and used (except Al-Mg-Fe alloys) have much better characteristics than alloys without the third (X) component. Figures 4; references 4.

Chemical Micrononhomogeneity in Casting Alloys
*937D0025B Moscow LITEYNOYE PROIZVODSTVO
in Russian No 6, Jun 92 pp 7-8*

[Article by G.P. Anastasiadi, Institute of Machine Design; UDC 621.745.55]

[Abstract] Microscopic nonhomogeneity in macroscopically homogeneous cast ferrous materials is analyzed from the standpoint of phase transformations, the kinetics of attendant restructurization depending on the quantitative relation between dissipation of heat and diffusion of atoms. This relation is expressed as the ratio of respective Fourier numbers $N_{Fo,therm}/N_{Fo,diff} = aR^2/DL^2$ (a -thermal diffusivity, D - diffusion coefficient, L -half length of ingot, R - radius of structural element). The magnitude of this ratio thus indicates which of these two factors governs and thus limits the cooling rate during the successive four stages (crystallization - transformation - growth of cementite grains - buildup of special carbides) of the new phase formation process along a given temperature-time cooling curve. In accordance with this criterion has been evaluated the dependence of the concentration of three alloying elements (carbon in cast 015 C steel, nickel in cast alloy steel, sulfur in cast iron) at dendrite boundaries c_b on the rate of transverse dendrite growth v , both variables reduced to dimensionless quantities c_b/c_0 (c - average concentration) and vR/D respectively. Such an analysis is shown to facilitate optimization of casting and heat treatment by control of phase transformations in the design of the technology for a given alloy. Figures 2; tables 1; references 2.

Compound Method of Producing Yokes for Gas Turbines

*937D0025F Moscow LITEYNOYE PROIZVODSTVO
in Russian No 6, Jun 92 pp 20-21*

[Article by A.G. Kovalev, A.N. Lemeshko, and N.V. Levnikov, Industrial Association "Neva Works"; UDC 621.74.002.6:669.14]

[Abstract] A method of casting yokes for gas turbines operating at temperatures up to 800°C has been developed which should reduce both metal waste and labor content, such yokes being made of 30Cr16Ni22V6Nb and now formed by hammer forging. Individual segments of a yoke are to be cast into separate molds and, upon being heated to 900°, integrally cast into a metal mold. Such yoke castings were heat treated as follows: quenching from 1200°C—soaking for 3 h—and water cooling—aging at 800°C for 10 h. The cooling rate after solidification was varied by varying the length of cooling time in the molds and thus the temperature of the castings at the time of their removal from the molds: 900-1000°C after 30 min, 800-900°C after 40 min, 600-750°C after 60 min. The castings were then tested for mechanical properties: 0.2 percent yield and ultimate strength, impact value (J/cm^2), percentage elongation and reduction. They were tested after removal from ceramic molds and after removal from metal molds, at room temperature and at turbine operating temperature. Casting into a metal mold was found to have raised the impact value and the plasticity to levels characteristic of wrought steel without any noticeable anisotropy. Microstructural examination revealed only very little micro-porosity, evidently owing to comminution of austenite grains and removal of the carbide eutectic from the grain boundaries. Neither the mechanical properties nor the microstructure of these castings were found to be significantly sensitive to changes in the cooling rate after solidification. This method of casting should therefore yield more durable turbine yokes and consume 30 percent less metal than forging. Tables 2.

Applying Catastrophic Failure Theory to Quality Control of Castings

*937D0025G Moscow LITEYNOYE PROIZVODSTVO
in Russian No 6, Jun 92 pp 26-28*

[Article by M.A. Yoffe, All-Russian Scientific Research Institute of Machine Building Technology; UDC 621.74.002.6]

[Abstract] In accordance with catastrophic failure theory, the quality of a casting is described by the manner in which an m -dimensional equilibrium manifold fits in an $(n+k)$ -dimensional space $R^k \times R^n$ space, the coordinates in this Euclidean space being the n quality indicators and k controlling technological parameters respectively. As an example is considered a casting with only one quality indicator x , this indicator intricately depending on two technological parameters a, b . The 2-dimensional manifold of and elementary catastrophic

assembly failure is inserted into a 3-dimensional space $R^3 = R^1 R^2$ with coordinate axes x,a,b. Probability represents the potential, its maxima corresponding to the stable states which determine the quality of a casting. The probability function $P(x,a,b)$ is bimodal inside the space which depicts the assembly process and has there three isolated critical points: a maximum indicating a likely "accept" condition, a maximum indicating a likely "reject" condition, and a minimum indicating an extremely unlikely "neither accept nor reject" condition. Outside this space the probability function P either "accept" when on the left-hand side or "reject" when on the right-hand side. The separatrix of the (a,b) space consists of point 0 and a convolution line described by the canonical equation $(a/3)^3 + (b/2)^2 = 0$. As a practical application is considered surface quality control of iron ingots cast in sand-clay molds, where the two key factors on which formation of fall-in flaws depends are the molding pressure and the amount of foundry facing agent in the mold mix. Analysis of the technological process according to that theory supplemented with a cost analysis is an effective method of quality control, as demonstrated on iron end shields for electric motors cast in the Disamatic-2013 machine. It is recommended on the basis of such an analysis to use "graphitol" containing high-disperse ($0.5\text{-}1.0 \mu\text{m}$ grain size) colloidal graphite powder as the foundry facing agent and to regulate the molding pressure within the $1.1\text{-}1.3 \text{ MPa}$ range so as to hold losses in subsequent heat treatment within 1.5-3.0 percent. Figures 3; references 2.

Statistical Models of Production of Low-Porosity Bronze Castings

937D0025H Moscow LITEYNAYE PROIZVODSTVO in Russian No 6, Jun 92 pp 33-34

[Article by A.A. Papirovskiy and G.F. Shemetov, State Technical University; UDC 621.746.58]

[Abstract] Casting of tin bronze is analyzed statistically by the regression method for the dependence of ingot porosity and hermeticity on the thermal parameters of the solidification process. The necessary experimental data were obtained from three batches of 500 mm high and respectively 15 mm, 30 mm, 50 mm thick vertically cast Br010Ts2 brass plates. The temperature profiles were recorded by six Chromel-Aluminel thermocouples at key locations. The solidification process was varied by adjusting the end coolers and changing the riser dimensions. The distribution of porosity R in ingots was determined upon repetitive removal of the solid skin at both ends of an ingot as it kept building up. Hermeticity was measured in terms of the flow rate Q of CO_2 through the same skin specimen under various pressures P from 0.1 MPa to 1.0 MPa . Multivariate regression and correlation analysis of the data has yielded the equation for porosity $R = 4.95 - 2.16 \log G_1 - 0.85 \log G_t - 0.66 \log h$ (temperature gradient G_1 and time gradient G_t at instant of time when the temperature of formation of a continuous solid phase - 950°C for Br010Ts2 bronze - is reached; h - distance from skin specimen to level of melt

in riser) and the equation for CO_2 flow rate $Q = 1.015 + 0.376\Pi + 4.73P - 0.0375t_i - 3.015d_p$ (Π porosity of plate, d_i - thickness of ingot, d_p - thickness of plate). Both equations were tested for significance and adequacy. On their basis it thus possible to determine the maximum permissible porosity at which an ingot will be hermetic under a given pressure and to accordingly control the solidification process. References 1.

Magnetic Properties of Steel 45G17Yu3 Surface Layer After Quenching

937D0048D Yekaterinburg FIZIKA METALLOV I METALLOVEDENIYE in Russian No 2, Feb 92 pp 153-154

[Article by V.A. Zavalishin, A.I. Deryagin, N.D. Zemtsova, V.V. Sagaradze, V.G. Kuleyev, M.B. Rigmant, V.N. Krepyshev, Physics of Metals Institute at the Urals Branch of Russia's Academy of Sciences; UDC 669.15'74'71-194:537.622]

[Abstract] The instability and ferromagnetic transition of paramagnetic steel 45G17Yu3 under aging, plastic deformation, or irradiation which often prevents its use for intended purposes prompted a study of the properties of austenitic steel 45G17Yu3 in the quenched state. The steel composition and magnetic properties are determined by layer-by-layer analysis of 20 mm-thick samples annealed in the air at a $1,100\text{-}1,150^\circ\text{C}$ temperature for 1.5 h and water quenched. Then 0.02 and 0.2 mm-thick shavings are removed for testing. The Mn and C concentration is measured by X-ray diffraction analysis in a VPA-20 instrument since alloying elements may burn out during annealing. The Mn concentration as a function of the distance from the sample surface, the C concentration as a function of the distance from the sample surface, and the dependence of the specific magnetization on the magnetic field strength in various surface layers of the hardened sample are plotted. The magnetic properties are examined in Faraday's magnetic balance with autocompensation. The study shows that the 0.4 mm-thick surface layer is ferromagnetic due to a significant austenite decarburizing and a decrease in the Mn concentration. Below the 0.4 mm depth, the layers remain paramagnetic and preserve the weakly magnetic characteristics. The conclusion is drawn that conventional quenching procedure may lead to the formation of not only ferromagnetic iron oxides but also the development of ferromagnetic cooling and straining α -martensite due to the austenite destabilization and manganese burnout. Figures 3; references 1.

Effect of Straining on Mechanical Properties of Two-Phase Austenitic-Martensitic Steel

937D0048E Yekaterinburg FIZIKA METALLOV I METALLOVEDENIYE in Russian No 2, Feb 92 pp 130-133

[Article by V.G. Serebryakov, E.I. Estrin, Physical Metallurgy and Physics of Metals Institute at the Central

Scientific Research Institute of Ferrous Metallurgy imeni I.P. Bardin; UDC 669.15-194.55/56:539.4.015]

[Abstract] The poor balance of mechanical properties in two-phase martensitic-austenitic, e.g., excessive ductility combined with high strength or a low yield point, prompted attempts to increase the yield strength by plastic deformation. To this end, Cr-Ni steel 50Kh9N5 smelted in a 10 kg induction furnace, forged into squares, cut into blanks, water quenched at 1,200°C with a 30 min exposure, and polished is examined. Tensile tests are carried out at room temperature in an Instron unit. The yield strength, ultimate strength, ductility, hardness after deformation and testing, and martensite concentration after deformation and testing are summarized as a function of the martensite content before straining and the straining degree; the dependence of the yield strength, ultimate strength, elongation, HRC, and strain martensite concentration as a function of the straining degree are plotted. An analysis shows that cold plastic working of two-phase steel with 25-40 percent of martensite simultaneously increases the strength properties and ductility whereby 25-35 percent straining of steel containing 40 percent of martensite attains an optimum range of mechanical properties: an 1,800 N/mm² yield strength, 2,200 N/mm² ultimate strength, and a 20 percent elongation. The high practicability and structural ductility of the two-phase steel are due to the transformation of some austenite into martensite under loading, i.e., the trip effect. Figures 1; tables 1; references 6.

Development of Strength Properties of Ordered Alloys

937D0048F Yekaterinburg FIZIKA METALLOV I METALLOVEDENIYE in Russian No 2, Feb 92 pp 134-146

[Article by V.I. Syutkina, A.Yu. Volkov, Physics of Metals Institute at the Urals Branch of Russia's Academy of Sciences; UDC 548.313:539.4.015]

[Abstract] A report presented to the Fifth All-Union Seminar on the "Dislocation Structure and Mechanical Properties of Metals and Alloys" held in Sverdlovsk in 1991 is reprinted in full. The effect of atomic ordering of solid solutions on their physical and mechanical properties and the outlook for employing these phenomena in commercial alloys are discussed and the need to examine the effect of plastic deformation on the atomic ordering in order to establish the plastic deformation mechanism and identify the causes of frustrated long-range order as well as determine the range of alloy exposure to mechanical factors within which the structure and properties of the ordered state are preserved is stressed. The behavior of the electric resistivity of the Cu+25 percent Au and Cu+19.5 percent Pd alloys on the plastic straining degree is plotted and the dislocation structure of these alloys is examined. The study confirms that the long-range order is violated under plastic deformation in all ordered

alloys, primarily due to an increase in the total dislocation density. It is shown that the structure and properties of ordered alloys can be maintained by preventing the massive emergence and multiplication of dislocations while the yield strength of ordered alloys can be increased by domain wall hardening, by a combination of hardening due to the supersaturated solid solution decay and atomic ordering, by causing a disperse discontinuous decay in the ordered matrix, and by forming an ultrafine-grain structure. Figures 11; references 16: 13 Russian, 3 Western.

Effect of Pressure on Brittle-Ductile Transition and Ductility of Metals With BCC Lattice

937D0048G Yekaterinburg FIZIKA METALLOV I METALLOVEDENIYE in Russian No 2, Feb 92 pp 147-152

[Article by R.V. Churbayev, A.V. Dobromyslov, G.G. Taluts, Physics of Metals Institute at the Urals Branch of Russia's Academy of Sciences; UDC 539.4.015:53.092]

[Abstract] The factors which affect the transition of metals and alloys from the brittle to ductile state jointly and separately and particularly, the effect of pressure and temperature on the brittle-ductile transition (KhPP) are discussed and it is noted that pressure, in turn, affects the temperature of such transition. An attempt is made to study the effect of the pressure in a hydrostatically compressed liquid on the temperature of brittle-ductile transition in W and Mo—metals with a BCC lattice in which the transition occurs at an atmospheric pressure at a high temperature—as well as their ductility at various temperatures. VA grade tungsten and MCh grade molybdenum rods made by hot working are examined. The samples are strained in tension to failure at hydrostatic pressures from 1 atm to 1,150 MPa and temperatures of 180-873K. A formula is derived for determining ductility as the limiting degree of deformation to fracture. The dependence of tensile strength on the straining temperature at an atmospheric pressure, the dependence of the yield strength on the straining temperature at an atmospheric pressure, the behavior of Mo and W tensile strength with pressure at various straining temperatures, the effect of pressure on the transition temperature, and the dependence of the Mo and W ductility on hydrostatic pressure (in logarithmic coordinates) under various loading temperatures are plotted. An analytical law of the transition temperature change under hydrostatic pressure is derived. The lower the overcooling degree relative to the KhPP transition temperature at an atmospheric pressure, the greater the hydrostatic pressure necessary for plastifying the material. The difference between the transition temperatures at atmospheric and high pressures is proportionate to the third power of this pressure. The dependence of the BCC metal ductility on pressure at various temperatures is also described by an exponential law: the maximum ductility margin is proportionate to the temperature and pressure differentials to a certain power. Figures 6; references 10: 7 Russian, 3 Western.

Effect of Alloying on Phase Transitions in Steels With Pearlite Structure During Laser Heating

927D0258D Moscow METALLY in Russian No 3, May-Jun 92 pp 110-114

[Article by D. V. Shtanskiy and I. V. Lyasotskiy; UDC 669.017.3:621.9.048.7:548.526:539.27]

[Abstract] The effect of alloying with silicon, nickel and chromium on the mechanism and kinetics of phase transitions in steels under rapid laser heating was investigated on the basis of electron microscope studies of structural parameters in the heated zone. It was found that alloying significantly alters temperature, kinetic and thermodynamic conditions for recrystallization of ferrite and dissolving of cementite. The main effect of the three alloying elements on the kinetics of phase transitions and on the structure of steel in the zone where hardening is incomplete can be summarized as follows: silicon increases the temperature of the (α - γ)-transition, which increases the probability of a high-temperature phase originating inside pearlite clusters and raises the degree of concentrational and phase inhomogeneity; nickel lowers the transition temperature, which leads to increased depth of the tempered layer and formation of a hardened layer with preserved cementite plates in the martensitic matrix; chromium promotes the metastable disintegration of cementite plates, which leads to formation of structures with a high austenite content; as the percentage content of chromium increases, the amount of the disperse carbide phase increases.

Effect of Temperature on Erosion of Metals Exposed to a Laser Beam

927D0258E Moscow METALLY in Russian No 3, May-Jun 92 pp 115-116

[Article by A. Ye. Chmel and A. M. Kondyrev; UDC 621.785.54]

[Abstract] The relationship between the temperature of specimens of foil made of gold, silver and nickel and how many laser pulses it takes to initiate a plasma flame (spark) on their surface was investigated. A neodymium laser with pulse durations of 60 ns and 0.5 ms was used. It was determined that as the temperature of specimens is increased from room temperature to 170° C, the number of pulses to initiate a plasma flame decreases by two orders of magnitude. The results agree with ideas that the mechanism of destruction of metals by laser pulses is akin to fatigue failure in the field of periodically repeating thermoelastic stresses.

Effect of Heat Treatment on the Structure of Beryllium Foils

927D0258H Moscow METALLY in Russian No 3, May-Jun 92 pp 128-130

[Article by V. P. Krivko, Yu. I. Kokovikhin, and T. G. Kryshab; UDC 548.73; 669.725]

[Abstract] The effect of heat treatment on structural transformations in beryllium foils was investigated to determine what contributes to high strength characteristics in these foils. The subgranular structure of foils and its development in the course of heat treatment was examined using X-ray methods and transmission electron microscopy. Specimens of magnesiothermal beryllium condensate foil were examined directly after rolling (initial state) and then again after annealing. It was found that elastic stresses are removed at an annealing temperature as low as 550° C. Sizes of grains and subgrains virtually do not change after annealings at low temperatures (500-600° C). At higher annealing temperatures, beginning at 650°, there is significant growth of grains. Also, the size of segregations remains the same from the initial state up to 650°. Further increasing the temperature and annealing time leads to intensive growth of grains and to acceleration of ageing processes which are accompanied by increased size of segregations, which increases the level of stresses on interfaces. Thus, to improve strength characteristics of beryllium foils, short-term annealing at 550° C is optimum for removing residual stresses.

Mathematical Model of a Multi-Stand Cold-Rolling Mill for Controlling Strip Thickness

927D0259C Moscow IZVESTIYA VYSSHIKH UCHEBNYKH ZAVEDENIY: CHERNAYA METALLURGIYA in Russian No 6, Jun 1992 pp 12-15

[Article by B. I. Kuznetsov, R. Koziol, and L. B. Kurtseva, Kharkov Institute of Engineering Pedagogy and Krakow Academy of Extractive Metallurgy; UDC 621.771.237:65.811.56]

[Abstract] A mathematical model has been developed to represent a multi-stand cold-rolling mill for controlling strip thickness. The model fully accounts for all disturbances caused by variations in strip thickness and roll eccentricities. The multi-terminal method can be used to find the appropriate transmission coefficients directly in digital form on a computer. The model was used on an IBM PC AT/XT to simulate changes in thickness and tension when cold-rolling 65G steel strip on a 740 NMZ three-stand mill. Strip thickness was reduced from 2.0 to 1.7, 1.55, and 1.5 mm, respectively. The results of the computer simulation closely corresponded to experimental data. Figures 3; references 12: 6 Russian, 6 Polish.

Predicting the Effect of Titanium, Aluminum, and Nitrogen on the Hardenability of Medium Carbon Steels Containing Boron

927D0259E Moscow IZVESTIYA VYSSHIKH UCHEBNYKH ZAVEDENIY: CHERNAYA METALLURGIYA in Russian No 6, Jun 1992 pp 34-36

[Article by V. V. Popov, A. O. Khomenko, G. V. Spirkina, L. B. Yefimova, and I. A. Malov; UDC 669.018.29:620.179.3:669.(295+71+786)]

[Abstract] A thermodynamic model was constructed to predict the effect of titanium, aluminum, and nitrogen on boron concentration in the austenite of medium-carbon engineering steels and to optimize the concentration of these elements in order to enhance the hardenability of these steels. Data on the concentration of these elements was plugged into a series of expressions to obtain a three-equation system with three unknowns. This system was solved numerically using the Newton-Rafson method. The calculations were performed by a program written in Turbo-Pascal and run on IBM-compatible computers. The program was designed to check for all three potential boron nitride compounds. The equilibrium concentration of boron in the austenite at the heat-to-quench temperature was thermodynamically calculated, bearing in mind that an increase in boron concentration in solid solution should increase hardenability, and that this effect would be noticeable at concentrations starting near 0.0008 percent. The results of the thermodynamic calculations were shown to be consistent with hardenability curves derived by end-face quenching per GOST 5657-69. Thus, the data generated by the thermodynamic model can be reliably used to predict and optimize the hardenability of various medium-carbon steels depending on their Ti, Al, and N concentrations and on the concentration of boron in the austenite of these steels. Figures 2, tables 1; references 6: 5 Russian, 1 Western.

Hydrogen Permeability Change in Steel 12Kh18N10T After Nitriding, Oxidation, and H⁺ and N⁺ Ion Irradiation

937D0043A Moscow FIZIKA I KHIMIYA
OBRAZOTKI MATERIALOV in Russian No 5.
Sep-Oct 92 pp 10-15

[Article by V.V. Fedorov, V.I. Pokhmurskiy, Ye.V. Demina, I.V. Semchishin, M.D. Prusakova, L.I. Voloshin, N.A. Makhlin (deceased), Moscow; UDC 669.28]

[Abstract] The materials science problem of hydrogen confinement within the first wall of the nuclear fusion reactor (TYaR) and tritium leakage due to its ability to diffuse through most metals and the shortcomings of the methods of oxidizing or nitriding the high-temperature alloys or group V metals used often for this purpose prompted an analysis of the depth of the protection barrier necessary for arresting the tritium penetration. These analyses show that the hydrogen penetration rate through austenitic steels can be lowered by the surface oxidation or nitriding. Steel 12Kh18N10T is used in the study; its hydrogen permeability is examined by the Dines-Barrer method with an automated MacLeod pressure gauge by measuring the amount of hydrogen penetrating through 1.2 mm-thick membrane samples. The effect of oxide films on the hydrogen penetration and hydrogen flux through the metal and the nitrided layer thickness as a function of the nitriding method are examined. The protective barrier depth is calculated for three different temperatures (773, 973, and 1,173K). The

effect of the implanted nitrogen on the hydrogen penetration rate in samples irradiated with 5 keV N⁺ ions on one or both sides in a Uran unit and the oxide film reduction kinetics after irradiation with 1 MeV H⁺ ions are investigated. The hydrogen permeability of stainless steel after various types of treatment, the effect of the nitrogen ion concentration on the steel permeability, and the effect of irradiation on the permeability are plotted. The dependence of permeability and tritium penetration activation energy on the type of surface treatment is summarized. The findings confirm the possibility of substantially improving the hydrogen resistance and high-temperature strength of austenitic stainless steels by composite treatment with gaseous hydrogen and proton irradiation which result in protective oxide film formation. The study shows that the effect of the surface filling degree with adsorbed nitrogen atoms on the penetration rate at 1,023K is consistent with the predicted 3/2 exponential dependence. Figures 4; tables 2; references 19: 16 Russian, 3 Western.

Effect of Pulsed Laser Radiation on V-Ti Alloys

937D0043D Moscow FIZIKA I KHIMIYA
OBRAZOTKI MATERIALOV in Russian No 5.
Sep-Oct 92 pp 38-45

[Article by S.A. Maslyayev, V.I. Neverov, V.N. Pimenov, Yu.M. Platov, S.Ya. Betsofen, I.P. Sasinovskaya, Moscow; UDC 669.295.873:535.211]

[Abstract] The vulnerability of the first wall materials in nuclear fusion reactors under transient thermal exposures of the plasma stripping or escaping electron type and the most important structural changes as a result of these exposures are discussed and an attempt is made experimentally to check the published theoretical premises of the outlook for using V-Ti alloys as the nuclear fusion reactor confinement wall material and in the international ITER fusion reactor. The thermal factors of plasma stripping is examined under pulsed laser irradiation (LI) in the air and in a vacuum. The samples are irradiated in a GOS-1001 unit in a free lasing mode with a pulse duration of 0.7×10^{-3} s at a 5×10^5 W/sm² pulse energy. The alloy microstructure before and after irradiation is examined by optical and scanning electron microscopy and X-ray diffraction and spectral analyses. The dependence of the damaged and fused layer depth on the pulse duration for pure vanadium and an alloy with 10 percent Ti, the diffraction patterns of alloys with various Ti contents before and after pulse laser irradiation, and the temperature distribution in the sample depth after the exposure are plotted. The lattice constants of the V-Ti alloys and critical liquid phase radius are summarized. An analysis makes it possible to conclude that if a transient thermal exposure of the first wall encompasses a small area and the fusion depth is comparable to the liquid phase diameter, the alloy may run off under the terrestrial gravitational field; this is not likely in the case of large areas. The millisecond pulses in the air form titanium oxides, nitrides, and oxynitrides not only in the recrystallized outer surface layer but also

in the rear side of the samples. The above phenomena must be taken into account in analyzing and predicting the performance of reactor materials. Figures 4; tables 2; references 15: 12 Russian, 3 Western.

Effect of Heating Rate on Thermal Stress Development in Silicon Wafer Under Rapid Annealing

937D0043E Moscow FIZIKA I KHIMIYA OBRABOTKI MATERIALOV in Russian No 5, Sep-Oct 92 pp 46-52

[Article by D.A. Sechenov, A.M. Svetlichnyy, S.I. Solovyev, O.A. Ageyev, Taganrog; UDC 621.785:548.4]

[Abstract] The difficulties of using traditional isothermal processes in VLSI (SBIS) technologies with submicrometer elements and the use of pulsed rapid annealing for minimizing the implanted dopant redistribution as well as the possibility of determining the thermoelastic stresses developing at 40-50 K/cm gradients under such treatment and selecting the optimum conditions with minimal shear stresses are discussed. The thermal stresses developing in a silicon wafer during rapid heating both under controlled and noncontrolled heating rates are investigated theoretically. The temperature field and thermoelastic stress models are formulated; the temperature behavior at the wafer center as a function of the heating duration under controlled and noncontrolled heating rates, the temperature differential between the wafer edge and center as a function of the heating duration under both conditions, the radial temperature and stress distribution in the wafer under both conditions, the crystal lattice slip planes and azimuthal stress distributions, the dependence of the shear stress on the heating time, and the dependence of the critical temperature on the heating rate are plotted. The existence of an optimum condition range which depends on the heating rate is demonstrated and it is shown that the highest temperature can be attained without generating linear defects at a 70-100 K/s heating rate. This analytical procedure makes it possible to optimize the heat treatment conditions under rapid annealing for all heating chamber designs. Figures 6; references 6: 4 Russian, 2 Western.

Properties and Uses of UF₆ Plasma: IV. UF₆ Conversion Mechanism and Kinetics in U-F-O-H Plasma

937D0043H Moscow FIZIKA I KHIMIYA OBRABOTKI MATERIALOV in Russian No 5, Sep-Oct 92 pp 58-66

[Article by Yu.N. Tumanov, K.V. Tsirelnikov, Moscow; UDC 621.039.61]

[Abstract] The discussion of the plasma chemical methods of producing and treating uranium which began

in earlier issues continues; the processes occurring during the UF₆ conversion into uranium oxides in steam plasma are considered from the viewpoint of direct U-235-enriched conversion, making uranium dioxide powder or pellets. F₆ conversion research trends are studied; the dependence of the number of U-F-H-O plasma component moles on temperature and the dependence of the UO₂F₂ condensation time on temperature are plotted. The U-F-O-H plasma composition is examined and the equations describing the UF₆ conversion into uranium oxides, UF₆ conversion reaction kinetics in H-OH plasma, and the results of a comparative analysis of intermediate UF₆ conversion reactions in H-OH plasma and the conversion product condensation processes are discussed. An analysis of data on high-temperature steam conversion shows that the reacting U-F-O-H plasma temperature must exceed the temperature range of 1,020-1,480K thermodynamically necessary for producing U₃O₈ and hydrogen fluoride by at least 200-300K to ensure that the UF₆-U₃O₈ conversion occurs within the characteristic plasma process time of 0.01-0.001. The plasma reactor outlet temperature prior to the uranium oxide and hydrogen fluoride separation must be at least 1,600K in order to prevent the UO₂F₂ condensation and heterophase reaction. Figures 2; tables 3; references 34: 22 Russian, 12 Western.

Properties and Uses of UF₆ Plasma: V. Uranium Reduction Mechanism and Kinetics During UF₆ Mixing With Hydrogen Plasma

937D0043I Moscow FIZIKA I KHIMIYA OBRABOTKI MATERIALOV in Russian No 5, Sep-Oct 92 pp 67-73

[Article by Yu.N. Tumanov, K.V. Tsirelnikov, Moscow; UDC 621.039.61]

[Abstract] The discussion of the plasma chemical methods of producing and treating uranium which began in earlier issues continues; the processes occurring during the UF₆ mixing with hydrogen plasma are outlined. The issues of hydrogen reduction of uranium from uranium hexafluoride used primarily for producing UF₄ which is an intermediate products of metallic uranium production are addressed. The problems of UF₄ sticking to the reactor walls and the need to form a specified granulometric content of the UF₄ powder are discussed and the UF₆ reduction in Ar-H₂ plasma is simulated in order to solve them. The UF₆ interaction kinetics with hydrogen and UF₄ condensation and its granulometric content development are examined. The mass fraction behavior of the UF₆-Ar-H₂ interaction products and temperature variation in the space-time reactor coordinate and the UF₄ particle size spectrum variation during the mixture movement along the reactor are plotted. The conclusion is drawn that the use of U-F plasma may help realize various engineering approaches to producing uranium-bearing substances. It is speculated that the findings will lead to a more deliberate examination of U-F plasma applications and properties. Figures 2; references 11: 9 Russian, 2 Western.

Nitrogen-Niobium Interaction in Molten Steel During Plasma-Arc Welding

927D0258C Moscow METALLY in Russian No 3, May-Jun 92 pp 48-52

[Article by B. L. Bozhenko, V. N. Shalimov, and L. I. Lepekhina; UDC 669.15'293-154:669.046.552.3]

[Abstract] Peculiarities of the interaction of nitrogen with alloying niobium in austenitic steel during plasma-arc welding were investigated. When shielding of the welding zone is not complete, the presence of air leads to intensive saturation of the molten metal with nitrogen. Niobium in the metal is highly reactive with nitrogen. The mechanism of formation of niobium nitride in weld metal during plasma-arc welding with filler wire was demonstrated on the basis of results of thermodynamic analysis. It was found to proceed in two stages: 1) drops of filler metal are actively saturated with nitrogen due to their high temperature and they transport the nitrogen into the weldpool; 2) as the molten steel cools, chemical interaction of nitrogen and niobium takes place in the tail end of the weldpool.

The microstructure and properties of welds with different nitrogen concentrations were examined. Fractured specimens tested for impact strength revealed that the higher the nitrogen concentration in the weld metal, the more inclusions of niobium carbonitride with a rhombic shape there are found in fractures. It is presumed that due to the embrittling effect of carbonitride films and weakening of bonds between grains, impact strength of the weld is decreased to a large degree. Thus, welding of austenitic steels alloyed with elements which are highly reactive with nitrogen demands a high quality of shielding of the arc combustion zone.

Computer Simulation in Determining Weldability and Selecting Welding Parameters for Steels and Alloys

937D0034A Moscow SVAROCHNOYE PROIZVODSTVO in Russian No 8, Aug 92 pp 7-9

[Article by A. N. Khakimov, Doctor of Technical Sciences, State Academy of Oil and Gas im. I. M. Gubkin; UDC 621.791.011]

[Abstract] Developments of the State Academy of Oil and Gas in the field of computerizing the work of engineers who design and make weldments are discussed. A package of applied programs for IBM PC AT computers called "Computerized Optimizer of Properties" makes it possible to determine parameters of efficient technologies for welding carbon and low-alloy steels as well as to predict the structural-phase composition and mechanical and service properties of welds, including parameters of static and cyclical crack resistance. Another development is a computerized dilatometer, KSLD-2, in which specimens are heated by the

radiant energy of lamps and a system of focusing reflectors, permitting plastics, ceramics and glass to be analyzed in addition to metals. Finally, a computer-aided analyzer of pictures of weld structures was developed which consists of a PC, a high-temperature microscope, a TV camera with video control unit, and a metallography microscope. The application software for this system makes it possible to isolate individual components of a structure in black-and-white or color, to separate structural elements, and to perform statistical analyses of the accumulated parameters of structures with generation of corresponding histograms and graphs.

Resistance of Gas Mains to Propagation of Extended Continuous Fractures

937D0034B Moscow SVAROCHNOYE PROIZVODSTVO in Russian No 8, Aug 92 pp 12-14

[Article by G. I. Makarov, Doctor of Technical Sciences, State Academy of Oil and Gas im. I. M. Gubkin; UDC 622.791.4]

[Abstract] A calculation method for evaluating the resistance of gas mains to propagation of extended continuous fractures is presented. It allows determination of parameters which contribute to inhibiting the spread of cracks and localizing damage, such as the toughness of the pipe metal and the depth of backfill covering the main. In cases where safety margins based on these parameters cannot be ensured, length and toughness requirements are calculated for crack-arrester pipes which protect at-risk sections of mains from extended damage.

Higher Durability for Large Welded Metalwork Subject to Corrosive Environments of the Oil and Gas Industry

937D0034D Moscow SVAROCHNOYE PROIZVODSTVO in Russian No 8, Aug 92 pp 20-21

[Article by A. I. Korolev and A. V. Muradov, Candidates of Technical Sciences; UDC 621.791:622.276.05]

[Abstract] Developments of the "Antikor" International Scientific and Training Center at the State Academy of Oil and Gas aimed at improving the corrosion resistance of weldments are reviewed. They include alloyed oxide coatings with a high resistance to a number of corrosive agents for protecting valves and pump and compressor piping, and a composite polymer coating with a titanium filler for protecting lids and bottoms of tanks. With a thickness of 110-120 micrometers, the polymer coating has a hardness of 0.91-0.94 and an adhesive strength of 0.26 MPa. Unlike a number of polymer coatings, it does not accumulate static electricity.

To improve the durability of welds in unalloyed low-carbon steel subject to corrosive environments, research was performed to find ways of making welds less electrochemically heterogeneous. It was found that in aerated environments, this can be achieved by alloying the

weld metal with elements which possess a higher electrochemical potential as compared with iron (e.g., nickel or copper), or which provide a more homogeneous structure (titanium), or which have both effects (molybdenum). In hydrogen sulfide-containing environments, higher corrosion resistance of welds can be achieved by reducing the carbon content in comparison with the primary metal. On the basis of the research and industrial testing of its results, recommendations have been prepared for selecting welding materials which increase the corrosion resistance of pipeline welds at oil and gas fields.

Effect of Laser Treatment on Corrosion Resistance of Steels and Welds

*937D0034F Moscow SVAROCHNOYE
PROIZVODSTVO in Russian No 8, Aug 92 pp 25-28*

[Article by R. D. Radchenko, Candidate of Technical Sciences, State Academy of Oil and Gas im. I. M. Gubkin; UDC 621.791.72:621.375.826]

[Abstract] Laser treatment of low-carbon steels and of welds in them was combined with subsequent heat treatment in a furnace to determine whether surface layers could be produced with enhanced corrosion-mechanical properties in hydrogen sulfide-containing environments. The steels examined were four low-carbon, low-alloy steels of the ferrite-pearlite class, and welds made by automatic arc and electroslag welding in two of these steels were also examined.

It was found that the laser treatment combined with heat treatment forms an optimum structure in surface layers with high corrosion-mechanical properties in hydrogen sulfide-containing environments. In the course of the follow-up heat treatment in a furnace, martensitic structures break up and a layer of recrystallized ferrite is formed with finely dispersed carbides which are uniformly distributed throughout the body of the grain. Laser treatment initiates the recrystallization process as a result of decarburization of the surface. A surface layer with a recrystallized ferrite structure 100-1000 micrometers deep increases corrosion-mechanical strength under static loading in an environment of NACE. The highest stability of properties is found in a surface 500-700 micrometers deep.

It was also found that laser treatment of welds in Cr-Ni steels increases resistance to inter-crystallite corrosion in highly oxidizing environments as a result of austenization of surface layers.

Optimization of Composition of Weld Metal in Arc Welding of 10Kh2M1A-A Steel

*937D0035A Moscow SVAROCHNOYE
PROIZVODSTVO in Russian No 9, Sep 92 pp 5-6*

[Article by Zh. A. Lepilina, V. V. Pankov, N. V. Abashkina, All-Union Research, Design and Technological Institute of Petrochemical Equipment, Yu. N. Semenov,

Scientific and Production Association "Volgograd Oil Industry Equipment", and A. S. Zubchenko, Scientific and Production Association "Central Research Institute of Machine Building Technology"; UDC 621.791:622.242]

[Abstract] The new steel brand 10Kh2M1A-A is of the type 2.25 percent Cr-1 percent Mo which is widely used in reactor equipment for oil refining. A program based on external branching and penalty functions to resolve contradictory requirements was written for an IBM PC AT computer for optimizing the composition of the metal of welds made in this brand of steel. The program helps to reduce laboratory work sharply. An optimum composition of elements (0.08-0.1 C, 0.63 Mn, 0.39-0.42 Si, 0.012-0.017 S+P) was determined for the weld metal which offers high mechanical characteristics: tensile strength approximately 670 MPa, elongation approximately 23 percent, impact strength approximately 130 J/cm².

Calculating Penetration Depth in Electroslag Buildup

*937D0035B Moscow SVAROCHNOYE
PROIZVODSTVO in Russian No 9, Sep 92 pp 8-9*

[Article by V. A. Danilov, Karaganda Polytechnical Institute, and G. G. Chernyshov, Moscow Higher Technical School im. N. E. Bauman; UDC 621.791.92]

[Abstract] It is demonstrated how a diagram of a single flat fixed source of heat in a plate situated in the plane of the surface of a metal bath can be used to calculate the penetration depth in electroslag buildup of gear teeth. A system of equations is presented which makes it possible not only to calculate the depth and area of the penetration zone for prescribed process parameters, but also to assess the effect on the penetration depth of the following parameters separately: width of buildup zone, welding current, voltage in the slag bath, and gap depth of the electrode.

Hydrogen in Metal of Thick-Walled Weldments. Part 1. Hydrogen Cracks in Thick-Walled Weldments

*937D0035C Moscow SVAROCHNOYE
PROIZVODSTVO in Russian No 9, Sep 92 pp 9-11*

[Article by V. I. Panov, Research Institute of Heavy Machine Building of the Production Association "Uralmash"; UDC 621.791.052:620.192.47]

[Abstract] Cracks caused by the presence of hydrogen in heavy machinery weldments are classified on the basis of an analysis of brittle fractures and crack formation in machinery and equipment manufactured by the "Uralmash" production association. Tables are given showing hydrogen contents and mechanical characteristics of six brands of steels which are prone to crack formation, and seven types of heavy machinery weldments in which hydrogen cracks occur, with brands of steels and welding

materials, types of welds, states of stress, and locations and nature of cracks indicated. It is concluded that the character of crack formation and propagation of cracks depend on the level of energy accumulated in the course of welding operations.

Corrosion Cracking of Welds in Low-Carbon Steels in Phosphate Media

937D0035D Moscow SVAROCHNOYE
PROIZVODSTVO in Russian No 9, Sep 92 pp 11-12

[Article by Y. Marcheva and R. Raychev, Higher Chemical Engineering Institute, Sofia, Bulgaria; UDC 621.791.052:620.193.2]

[Abstract] Results of investigations of corrosion cracking of welds in low-carbon steels in phosphate media are presented. Welds made by argon-arc and manual arc welding in 4 mm-thick low-carbon steel with a tensile strength of 440 MPa were examined. Tests on specimens cut out of welded bars were done in conditions where the examined steel demonstrates highest susceptibility to corrosion cracking in a unimolar solution of NaH_2PO_4 ($\text{pH} = 4$) at 20°C . Electrochemical corrosion studies were performed by the potentiodynamic polarization method, and mechanical corrosion tests were done using the method of dynamic tensile deformation at a constant, low rate of deformation.

Metallographic and microscopic studies showed that failure of welds in all cases occurs along the heat-affected zone near the primary metal. Differences in the structure of the primary metal, the metal of the heat-affected zone, and the metal of the weld are described. It was concluded that although the metal of welds made by argon-arc welding is subject to corrosion cracking in an orthophosphate medium, it is less prone to cracking than the primary metal, and this can be explained by differences in structure.

Electric Welding Where Work Is Affected by Industrial Magnetic Fields

937D0035E Moscow SVAROCHNOYE
PROIZVODSTVO in Russian No 9, Sep 92 p 19

[Article by N. Z. Nevyutov, "Sibtsvetmetgazoochistka" Trust; UDC 621.791.75:621.8.038:658.562]

[Abstract] Arc welding of pipes in electrolysis shops is made extremely difficult and even impossible by the presence of strong magnetic fields. Results of testing of the use of backing-strip rings are presented as a simple and practical method for welding of pipe under the

action of industrial magnetic fields. In welding of piping for gas-purification equipment, use of a backing-strip ring offers a shunting effect whereby the ring relieves the butt weld of the external magnetic field and the magnetic field that arises in the weld gap. Because the magnetic permeability of the air gap created at the butt is three to four orders of magnitude less than that of the pipe metal, the magnetic resistance of the gap is correspondingly greater than that of the metal. Moreover, magnetic lines of force in the gap are bent strongly, creating a field gradient which affects conditions of equilibrium during combustion of the welding arc.

Determining Stress Concentration Factors in a Cracked Weld

937D0045A Kiev PROBLEMY PROCHNOSTI
in Russian No 9, Sep 1992 pp 12-18

[Article by N. V. Korikhin, S. N. Evgenson, A. Ya. Aronson, S. V. Ivanov; St. Petersburg; UDC 621.791.001.5]

[Abstract] The photoelastic method of deformation "freezing" was used to study the effect of crack size and location on stress concentration factors in a fillet weld. A model of a fixed-flange I-beam was used for this purpose, making it possible to study two welds with a total of four defects. The beam components were machined from blocks of ED-16 MTGFA epoxy resin and cemented together with epoxy adhesive. Thin polyethylene films of various size were placed in different locations in the adhesive layers to simulate the defects. In a thermostat, a load was applied to the welds while they were subjected to the "freezing" temperature and then gradually cooled. The weld specimens were then sliced into optical sections, three for each crack: one along and two perpendicular to its axis. All the sections were sliced perpendicular to the plane of the crack. The stress concentration factors K_I , K_{II} , and σ_0 were found from the data generated by measuring birefringence parameters at a large number of points and using the least squares method to solve the system of equations used. These results were checked against a theoretical construct of the stress concentration factors. If they did not correspond to one another, the measurements and calculations were repeated. In all, 24 defects were studied. One was a spherical cavity, the others were round or oval one-dimensional cracks. Regression analysis yielded approximate formulas for determining stress concentration factors when designing welded joints with quasi-brittle strength under static and dynamic loading conditions. Figures 2, tables 2; references 6: 5 Russian, Western.

Self-Destruction Causes and Heat Treatment Conditions Ensuring Lumpy Nature Preservation of Manganese Carbonate Concentrates

937D0038A Moscow METALLY in Russian No 5, Sep-Oct 92 pp 5-10

[Article by N.P. Lyakishev, M.I. Gasik, S.G. Grishchenko, Moscow; UDC 669.046.414'74]

[Abstract] The self-destruction of lumpy carbonate manganese concentrate under heat treatment prompted studies of the self-destruction mechanism aimed at developing efficient techniques and heat treatment conditions which either suppress or limit this phenomenon and help maintain the lumpy nature of the heat treated products. The study is conducted allowing for existing notions of the theory of the taut strained state of matter whereby in contrast to earlier researchers, the principal premises of the theory of developed plastic deformation as the most proximate to the phenomenon under study from the physical viewpoint are used. According to the theory, integrity violations in the form submicro- and micropores appear at the earliest plastic deformation events and multiply and increase in size with the formation of microcracks. An algorithm is developed for quantitatively assessing the sample destruction probability during heat treatment. Moreover, plastic deformation termination in destruction is the final event of the submicro-, micro- and macroscopic defect formation and development whereby the probability and severity of fracture are determined by the rate ratio of the microcrack formation and "curing" and is related to the nature of the material and the thermochemical parameters of plastic deformation. Batches of lumpy concentrate are roasted and the roasting indicators of concentrates from four sources are summarized. The findings and analyses attest to the possibility of preserving the lumpy structure of concentrates heat treated at a moderate rate of up to 10°C per minute within an intense dehydration and loosening range of 100-400°C; this confirms a calculation of the raw material destruction probability based on the plastic deformation theory criteria. Figures 1; tables 1; references 10.

Effect of Ore Genesis on Roasting Conditions and Quality of Fluxed Pellets

937D0038B Moscow METALLY in Russian No 5, Sep-Oct 92 pp 11-19

[Article by O.A. Dolitskaya, G.V. Chesnokova, P.N. Dokuchayev, A.A. Klyushin, Moscow; UDC 669.1:622.788.36]

[Abstract] The inadequacy of existing estimates of iron ore concentrates and need for data on the thermal properties of Si-bearing minerals, which are a source of the hardening melt for iron ore pellet production, in order to attain an energy-saving heat treatment process and produce a concentrate with high metallurgical properties prompted an investigation into the effect of the

mineral form of silicon oxide on the hardening mechanisms and pellet heat treatment conditions. The study encompasses the entire range of production, from the mineral ore makeup to the production of fluxed iron ore pellets. The thermal properties of silicate phase monofractions are examined with the help of Derivatograph 3341-Q-1500-D thermal analyzers within a 20-1,300°C range at a 500 mg sample mass, 200 mg/200 mm balance sensitivity, a 500 µV differential thermal analysis voltage, a 1 mV differential thermogravimetric analysis voltage, and a 15 degree/minute heating rate in the air. The porosity, compressive strength, sulfur concentration, and ferrous oxide content behavior within a 600-1,300°C range and the effect of firing on the strength properties of commercial pellets are plotted. The correlations between the temperature-time firing parameters and the properties of the resulting pellets attest to the need to take into account not only the iron and silicon oxide content in the concentrate for developing pellet production practices but also the characteristics of iron ore genesis which makes it possible to determine the physical and chemical properties of the silicon-bearing phases necessary for the liquid-phase hardening of iron ore pellets—the only method of ensuring their requisite mechanical strength. Data on the silicate phase properties can be used to control the firing process and make a ready product with a specified composition and properties. Figures 4; tables 5; references 5.

Phase Transformation During Titanomagnetite Reduction With Hydrogen

937D0038C Moscow METALLY in Russian No 5, Sep-Oct 92 pp 20-30

[Article by G.B. Sadykhov, L.O. Naumova, V.A. Reznichenko, I.A. Karyazin, Moscow; UDC 541.124:669.094.1:669.295]

[Abstract] The unique properties of titanomagnetites as a source of Ti-Fe raw materials and the scarcity of data on their reduction (most sources deal with ilmenite) prompted an examination of the phase transformations during the titanomagnetite reduction with hydrogen. To this end, Kurnakh deposit concentrate is studied, and its chemical and material composition is summarized. The concentrate was reduced in a thermogravimetric unit, and products with a varying reduction degree were produced in order to analyze the phase transformations. The diffraction patterns of the oxide phase of the reduction products at various reduction degrees, the diffraction patterns of the oxide phase of final reduction products made at various temperatures, and the diffraction patterns of the oxide phase of reduction products obtained at an 1,100°C and 1,200°C temperature at the concluding phase at various reduction degrees are plotted. The sequence of reactions occurring during the hydrogen reduction at various temperatures is established. At the concluding phase, iron dititanate reduction is accompanied by chromium reduction from the solid solution, so the final reduction products within a

1,200-1,250°C range are metallic Fe and Cr, M_3O_5 solid solution, and spinel. Figures 4; tables 2; references 18: 1 Russian, 17 Western.

Low-Iron Bauxites of the Vezhayu-Vorykvinskoye Deposit

937D0051F Moscow OGNEUPORY in Russian
No 9-10, Sep-Oct 92 pp 20-24

[Article by N.S. Gayenko, S.G. Dolgikh, A.K. Karklit, and A.V. Kakhmurov, All-Union Refractories Institute; UDC 622.355.14:666.762.1]

[Abstract] Specimens of the low-iron bauxites of the Vezhayu-Vorykvinskoye deposit in Sredniy Timan in the Republic of Komi were subjected to a series of laboratory and technological studies. The study specimens were produced from simple starting mixtures containing 20 percent silica binder and from mixtures with blends of combined millings from different sections of

the deposit. More than 130 different samples were used to produce the study specimens. The compounds tested were selected out of consideration for the commercial processes used to produce types MLS-62 and MKS-72 mullite-silica and mullite-corundum products. Because of their volume fraction of iron oxides, the bauxite refractories produced from the materials of the Vezhayu-Vorykvinskoye do not meet the requirements stipulated in existing specifications (GOST 24704-81) for high-alumina products. The test products made from these bauxites have, however, been confirmed to meet the iron oxide volume fraction indicator established for MLS-62 and MKS-72 products and are thus suitable for use in manufacturing mullite-silica products such as furnaces for annealing anodes, the linings of various high-alumina nonmolded refractories, mortars, compounds, and fillers. Those bauxite samples that contained 70 to 80 percent Al_2O_3 proved to be the most desirable for use in producing mass commercial batches of different types of refractories. Figures 2, tables 6; references 4: 3 Russian, 1 Western.

Principal Radiation Characteristics of Materials of Dust Emission Particles from Waste-Heat Boilers

937D0022B Moscow TYAZHELOYE
MASHINOSTROYENIYE in Russian No 7, Jul 92
 pp 10-12

[Article by M.A. Taymarov, candidate of technical sciences, Kazan Institute of Chemical Engineering; UDC 536.3.]

[Abstract] The infrared radiation characteristics of the materials of dust particles emitted from flue ducts of waste-heat boilers were measured by the Shimon method, this method involving measurement of the specular reflection coefficient for polarized radiation incident at 20° and 70° angles. The apparatus for these measurements included a Specord-80 spectrophotometer, a 12.5 Hz radiation modulator, a polarizer, and an oscillating mirror. This mirror reflected the modulated and polarized radiation beam alternately onto the specimen of dust material with an optically smooth surface and onto a plane aluminum-coated standard reference mirror (0.97 reflection coefficient) through a measurement channel and a comparator channel respectively, both specimen and reference mirror having been placed inside an optical test chamber. The incident radiation beam was polarized so as to make its electric vector oscillate in a plane parallel to the plane of incidence. The reflected radiation beam passed on to a monochromator, a set of plane and spherical mirrors guiding it through the entrance slit to a diffraction grating, and from there through two light filters to a photodetector thermocouple with a CsI lens. The thermocouple output signal was recorded with a digital memory device. The reflection coefficient R of dust material specimen was determined from the relation $R = R_{ref}(I/I_{ref})$ ($R_{ref} = 0.97$; I, I_{ref} intensities of radiation reflected by specimen and by standard reference mirror respectively). The other optical characteristics of a dust material specimen were determined from the relations $R_{20^\circ} = f(10^\circ, n, \kappa)$ and $R_{70^\circ} = f(70^\circ, n, \kappa)$, these relations implicitly involving tabulated Fresnel equations (n - refractive index, κ - absorption coefficient). Three boiler dust materials were tested by this method: UKKS-6/40 calcined zinc dust concentrate, KS-450-VTKU pyrite dust concentrate, and KU-125 Martin process dust. They were tested with radiation at 42 different wavelengths covering the 2.50-28.57 μm region of the spectrum. Figures 1; tables 2; references 2.

**TsKTI (Central Boiler and Turbine Institute)
 Damper Ensuring High Earthquake and Vibration Resistance of Equipment and Pipelines**

937D0022C Moscow TYAZHELOYE
MASHINOSTROYENIYE in Russian No 7, Jul 92
 pp 19-21

[Article by V.V. Kostarev, candidate of technical sciences, and D.Yu. Pavlov, candidate of technical sciences, Scientific-Industrial Association Central Boiler and Turbine Institute; UDC 699.841.002.5]

[Abstract] Following a design and performance analysis of viscous dampers manufactured by Bechtel, EPRI, Gerb, and others for earthquake and vibration protection of nuclear and thermal electric power plant equipment and pipelines, such a damper has been designed at the Central Boiler and Turbine Institute which resembles the Gerb VES 2.5 damper in external appearance but differs from it in internal construction and performance characteristics. It consists of a cylindrical housing filled with a fluid within the 10-1000 Pa.s viscosity range, a hollow plunger around a slug, and a shell around the plunger. Its dynamic stiffness can be varied over a wide range while the viscosity of the working fluid remains constant, not by changing its dimensions but by proper selection of its internal components. The seventh and final version of this damper has a 76 mm in diameter plunger in a 156 mm in diameter housing. The frequency characteristic of its dynamic stiffness in a horizontal direction is flat over a wide range from 20 Hz up at the 7 kN/mm level and droops mildly from 20 Hz down, passing through 4 kN/mm at 3.0 Hz. Field tests have confirmed that this damper very effectively suppresses the seismic and other impact action on plant equipment and pipes as well as their vibration under normal service conditions. It is radiation-resistant and heat-resistant to the extent of being fire-proof, its performance parameters not being appreciably temperature-dependent. It is practically maintenance-free and has a practically unlimited life expectancy exceeding 40 years, in large measure to its high overload capacity and quick recovery speed combined with its ability to compensate for thermal expansion of contiguous metal parts. It is made of nontoxic materials and its manufacturing cost is low. Figures 4; tables 1; references.

Laser Simulation of Radiation-Induced Single Event Upsets in Integrated Circuits

937D0043F Moscow FIZIKA I KHIMIYA
OBRABOTKI MATERIALOV in Russian No 5, Sep-Oct 92 pp 53-55

[Article by A.I. Akishin, E.A. Vitoshkin, L.M. Savelyeva, Yu.I. Tyutrin, Moscow; UDC 537.311.33:539.1.043]

[Abstract] Radiation induced single event upsets (ORs) in satellite RAM (OZU) chips under the effect of heavy cosmic radiation nuclei and ecologically safe laser simulation of SEUs are outlined. The threshold values of the laser radiation energy density at which SEUs appear in 1 kbit static bipolar RAMs are determined by laser simulation. To this end, a focused laser pulse is used, and the simulated effect equivalence is monitored by the voltage change correlations in RAM storage registers under both pulsed laser radiation and the effect of heavy nuclei resulting from Cf-252 source fission. Transmission of heavy charged particles forms conducting channels in semiconductor and insulating RAM structures with electron-hole plasma. SEUs are simulated in 134 RU6 RAM chips in a computer-based test rig which makes it possible to determine the threshold SEU formation energy in the "0" and "1" modes under laser exposure. The data

processing algorithm is described; the study shows that in the "1" coding mode, a SEU appears at an incident energy density of 9.6×10^{-5} J/cm² while in the "0" coding mode— 1.8×10^{-5} J/cm². Under the effect of heavy ions with a 3.7 kBq activity, the SEU cross section in the "1"

coding mode is 1.9×10^{-4} cm² and in the "0" coding mode— 4.5×10^{-4} cm². The method makes it possible to measure the "1" and "0" noise immunity difference of RAM chips made by any method. References: 5 Western.

END OF

FICHE

DATE FILMED

5 FEB 1993